

POLITECNICO DI TORINO

Corso di Laurea Magistrale

in Ingegneria Energetica e Nucleare

Tesi di Laurea Magistrale

**Dynamic modeling and simulation of a power-to-power
energy storage system based on hydrogen**



Relatore

prof. Massimo Santarelli

Co-relatori

ing. Paolo Marocco

dott. Domenico Ferrero

Candidato

Giuseppe Sassone

Anno Accademico 2019/2020

Acknowledgements

I would like to thank my parents first, for their support and their advice in all these years. Another special thank is devoted to Francesca for her patience. I want to mention also all friends known at the Polytechnic of Turin, who have made this “journey” better than I expected. I would like to highlight the great support from prof. Massimo Santarelli, who helped me get in touch with the CEA at Grenoble for a PhD position and whom I thank very much. Last but not least, I want to underline the special role of all professors and assistants in each course, who have inspired me and thanks to them I have developed my passion for energy related topics.

Abstract

The goal of this thesis is to model and evaluate the dynamic behaviour and performances of a power-to-power (P2P) energy storage system installed in remote area, where there is no connection with the electrical grid and power is supplied by renewable energy sources (RES).

The model has been developed in MATLAB-Simulink[®] environment, starting from single components and then constructing the whole system, also introducing control strategies. Single component models have been developed relying on an extensive research in literature, studying mass and energy balance equations, in addition to mass transport, thermal, electrical and electrochemical phenomena. The modelled system is composed by a proton exchange membrane water electrolyzer (PEMWE), a pressurized hydrogen storage tank, a proton exchange membrane fuel cell (PEMFC).

The model has been validated by performing the best fit of PEMWE and PEMFC polarization curves available in literature, using the Simulink[®] Parameter Estimator tool in order to evaluate fitting parameters.

The analysis has been carried out evaluating the dynamic behaviour and performances of such system in different scenarios (i.e. a working day and a non-working day for each month of the year) to observe its response to various power profiles. The results consist of daily power profiles, which show the dynamic response of the system and a table reporting all key performance indicators (KPI) that have been considered for this study. The main result is that such system can increase a lot the self-sufficiency of isolated users supplied by RES, even if certain amount of surplus in energy production from RES needs to be curtailed in most of the cases. Furthermore, in the simulation results, the load is always covered either directly by RES production or by the P2P system. Thus, the consumption associated to the backup system (i.e. diesel generators), which intervenes when the load is totally or partially not covered, is negligible.

In addition to the main simulation results, further analyses have been conducted on the optimal sizing of RES systems, the exploitation of curtailed energy for local hydrogen mobility and the evaluation of the costs related both to different sizes of RES systems and to hydrogen and battery energy storage systems. From such analyses, it has been found that the sizes of the RES systems can be reduced leading to lower costs and that the cheapest energy storage system is the one based on hydrogen.

In conclusion, it can be stated that such system could lead to higher self-sufficiency, higher exploitation of RES and negligible contribution of the backup system, with consequent reduction of greenhouse gases (GHG) emissions. The model developed in this work could be used to simulate and investigate the dynamic response of a P2P system according to different operating conditions in order to predict and optimize its performances.

Contents

Nomenclature	8
Introduction	13
1 Description of the system.....	17
1.1 Electrolyzer.....	19
1.2 Fuel cell	20
1.3 Hydrogen storage tank.....	21
2 Dynamic model.....	22
2.1 Assumptions	22
2.2 Electrolyzer.....	22
2.2.1 Electrochemical model	22
2.2.1.1 Open circuit voltage	23
2.2.1.2 Activation overvoltage.....	24
2.2.1.3 Ohmic overvoltage.....	25
2.2.1.4 Diffusion overvoltage	26
2.2.1.5 Electric double layer effect	26
2.2.2 Mass transport model	27
2.2.2.1 Anode	29
2.2.2.2 Cathode	30
2.2.2.3 Membrane water transport	31
2.2.2.4 Cross-over effect and Faraday's efficiency	33
2.2.3 Thermal model	33
2.3 Fuel cell	34
2.3.1 Electrochemical model	34
2.3.1.1 Open circuit voltage	34
2.3.1.2 Activation overvoltage.....	34
2.3.1.3 Ohmic overvoltage.....	34
2.3.1.4 Diffusion overvoltage	35
2.3.1.5 Electric double layer effect	35
2.3.2 Mass transport model	35
2.3.2.1 Anode	36
2.3.2.2 Cathode	37
2.3.2.3 Membrane water transport	39
2.3.2.4 Condensation.....	39
2.3.3 Thermal model	39

2.4	Hydrogen storage tank.....	39
2.4.1	Mass balance	39
2.4.2	Thermal model	40
2.5	Sizes and parameters of components.....	40
2.5.1	PEMWE and PEMFC stack	41
2.5.2	Storage tank.....	42
2.6	Model control strategies	43
3	Validation.....	45
3.1	PEMWE.....	45
3.2	PEMFC	46
4	Results.....	48
4.1	Main simulation results	50
4.1.1	Working day in January	51
4.1.2	Non-working day in January	52
4.1.3	Working day in February	53
4.1.4	Non-working day in February	54
4.1.5	Working day in March	55
4.1.6	Non-working day in March.....	56
4.1.7	Working day in April	57
4.1.8	Non-working day in April.....	58
4.1.9	Working day in May	59
4.1.10	Non-working day in May	60
4.1.11	Working day in June	61
4.1.12	Non-working day in June	62
4.1.13	Working day in July	63
4.1.14	Non-working day in July.....	64
4.1.15	Working day in August	65
4.1.16	Non-working day in August.....	66
4.1.17	Working day in September.....	67
4.1.18	Non-working day in September	68
4.1.19	Working day in October	69
4.1.20	Non-working day in October.....	70
4.1.21	Working day in November.....	71
4.1.22	Non-working day in November.....	72
4.1.23	Working day in December	73

4.1.24	Non-working day in December	74
4.2	Comments	75
4.3	Further analyses	76
4.3.1	Optimization of RES sizes	76
4.3.2	Curtailed power to hydrogen mobility	78
4.3.3	Comparison between different RES sizes	81
4.3.4	Comparison between hydrogen and battery energy storage systems	84
5	Conclusions	88
	References	89

Nomenclature

Acronym	Description
AC	Alternating current
DC	Direct current
GHG	Greenhouse gases
KPI	Key Performance Indicators
O&M	Operational and maintenance cost
PEM	Proton exchange membrane
PEMFC	Proton exchange membrane fuel cell
PEMWE	Proton exchange membrane water electrolyzer
PV	Photovoltaic
P2P	Power-to-power
RES	Renewable energy sources

Symbol	Description	Unit of measure
a	Water activity	–
A	Surface	m^2
ASR	Area specific resistance	$\Omega \text{ cm}^2$
c	Specific cost	€/kW, €/kWh, €/kg
c_s	Specific consumption	kg/km
c_p	Specific heat	$\text{J mol}^{-1} \text{ K}^{-1}$
C	Concentration	mol/m^3
C_{el}	Electric double layer capacitance	F
C_{th}	Thermal capacitance	J/K
$CAPEX$	Capital expenditures	€
d	Real discount rate	%
D	Diffusion coefficient	m^2/s
D	Diameter	m
F	Faraday's constant	C/mol
e^-	Electron	–

continue in the next page

Symbol	Description	Unit of measure
E	Energy	J
h	Enthalpy	J/mol
h_{th}	Heat transfer coefficient	$W m^{-2} K^{-1}$
H	Height	m
i	Current density	A/cm^2
i_0	Exchange current density	A/cm^2
k_O	Outlet flow coefficient	$mol Pa^{-1} s^{-1}$
K_{darcy}	Membrane permeability to water	m^2
L	Length	m
LHV	Low heating value	J/kg
MM	Molar mass	kg/mol
n	Cost exponent	–
n	Number of moles	mol
\dot{n}	Molar flow rate	mol/s
n_{cell}	Number of cells	–
n_{rack}	Number of battery racks	–
NPC	Net present cost	€
OCV	Open circuit voltage	V
$OPEX$	Operational and maintenance costs	€
p	Pressure	Pa
P	Power	W
R	Universal gas constant	$J mol^{-1} K^{-1}$
RC	Replacement costs	€
RH	Relative humidity	%
s	Entropy	$J mol^{-1} K^{-1}$
S	Generic size	kW, kWh, kg
SOC	State of charge	%
t	Time	s
t	Thickness	m
T	Temperature	K
V	Voltage	V

continue in the next page

Symbol	Description	Unit of measure
V	Volume	m ³
W	Weight	kg
y	Molar fraction	—
ΔG	Gibbs free energy of the reaction	J/mol
ΔH	Enthalpy of the reaction	J/mol
ΔS	Entropy of the reaction	J mol ⁻¹ K ⁻¹
α	Charge transfer coefficient	—
Φ	Heat flux	W
ϵ	Porosity	—
λ_{H_2}	Excess of hydrogen	—
λ_{air}	Excess of air	—
λ	Water content (or degree of humidification)	—
μ	Dynamic viscosity	Pa s
η_{act}	Activation overvoltage	V
η_{diff}	Diffusion overvoltage	V
η_{ohm}	Ohmic overvoltage	V
η_{far}	Faraday's efficiency	—
σ	Conductivity	$\Omega^{-1} \text{ cm}^{-1}$
ν	Stoichiometric coefficient	—

Subscript	Description
amb	Ambient condition
A	Anode
ch	Channel
cons	Consumed
cond	Condensed
C	Cathode
diff	Diffusion
el	Electrical
eod	Electro-osmotic drag

continue in the next page

Subscript	Description
E	Electrode
gen	Generated
in	Inlet
ion	Ionic
max	Maximum
me	Membrane
min	Minimum
n	Rated
out	Outlet
pr	Pressure effect (Darcy's law)
ref	Reference
th	Thermal

Superscript	Description
0	Standard conditions
*	Modified conditions

Introduction

European Commission's policies on energy and environment [1] highlights the need for electrification, decarbonisation and reduction of greenhouse gases (GHG) emissions, in addition to the need to increase the energy efficiency and the use of technologies related to renewable energy sources (RES). More in detail, according to key targets for 2030 [1], RES share in both production and final consumption have to increase. In other words, a transition to a more sustainable energy system not more relying on fossil fuels is needed.

Therefore, in the prospect of future energy systems, in which RES will have a larger share in the energy mix, technologies related to energy storage will play a key role, since there are issues related to intermittent nature of such sources (e.g. solar and wind) that makes them unpredictable and non-dispatchable. Indeed, energy storage is essential to match energy demand and production as well as solve problems related to self-sufficiency and grid stability.

A possible solution could be to store electrical energy in the form of hydrogen by means of the so-called power-to-hydrogen technology. Hydrogen is produced by electrolysis exploiting electrical energy from RES, it can be stored in several form (e.g. compressed gas, liquified hydrogen or in solid matrices) and used to produce again electricity when it is needed. In general, technologies exploiting RES to produce hydrogen could lead to more sustainable, affordable and secure energy systems and contribute to the economic development and the reduction of GHG emissions, in addition to create new work placement. Therefore, synergy between hydrogen and RES could have a key role in transition to future energy systems.

Moreover, in the context of a transition from centralized (i.e. characterized by unidirectional energy flows) to distributed (i.e. bidirectional energy flows) power generation, due to the presence of RES systems at user side, power-to-X technologies (e.g. power-to-heat, power-to-power, power-to-fuels, etc.) are gaining more interest because of the need to increase flexibility of energy systems and synergy among energy carriers associated to different energy networks (e.g. natural gas network, district heating and cooling, power grid). This kind of technology is based on the conversion of electrical energy to a different form of energy either to cover the demand associated to other energy vectors or for energy storage purposes.

In this work, power-to-power (P2P) technology based on hydrogen storage has been investigated. This technology exploits electricity produced by RES to supply local users in a more stable and continuous manner, without using fossil fuels. Generally, the aim of P2P technologies is to store electricity in an intermediate form of energy (e.g. methane, hydrogen, etc.) when there is a surplus in the electricity production from RES compared to the energy demand and then convert it newly to power in the case of deficit.

There are many studies related to this kind of system, but the number of real-scale installations that gives the opportunity to evaluate the real behaviour of such system is still small. For this reason, projects that will make it possible to remedy this shortcoming are needed. An example is REMOTE [2], a European Horizon 2020 funded project "aimed to demonstrate the technical and economic feasibility" of P2P systems based on hydrogen energy storage, "installed in isolated micro-grids or off-grid remote areas supplied by renewable electricity, in order to guarantee the complete self-sustainability of the site, without any need for fossil fuels" [2]. REMOTE consists of four installation sites, which are different from each other in terms of energy sources, energy demand and production, business cases and system configurations

(see figure 0.1). These various situations allow to demonstrate the feasibility of such systems in different conditions.

This thesis is related to the context of REMOTE [2]. More in detail, simulations performed in this thesis are focused on DEMO 4 of the REMOTE project, the installation located in Froan/Rye Islands in Norway. In this case, it is an isolated micro grid, where the supplied electricity comes from photovoltaic (PV) and wind generators and it is characterized by residential loads and fish industry available on-site. The business case is related to the avoided costs for new sub-marine power line. In this site, almost complete substitution of fossil fuels is performed, indeed, only less than 5% of the load is covered by the backup system, consisting of diesel generators [2].

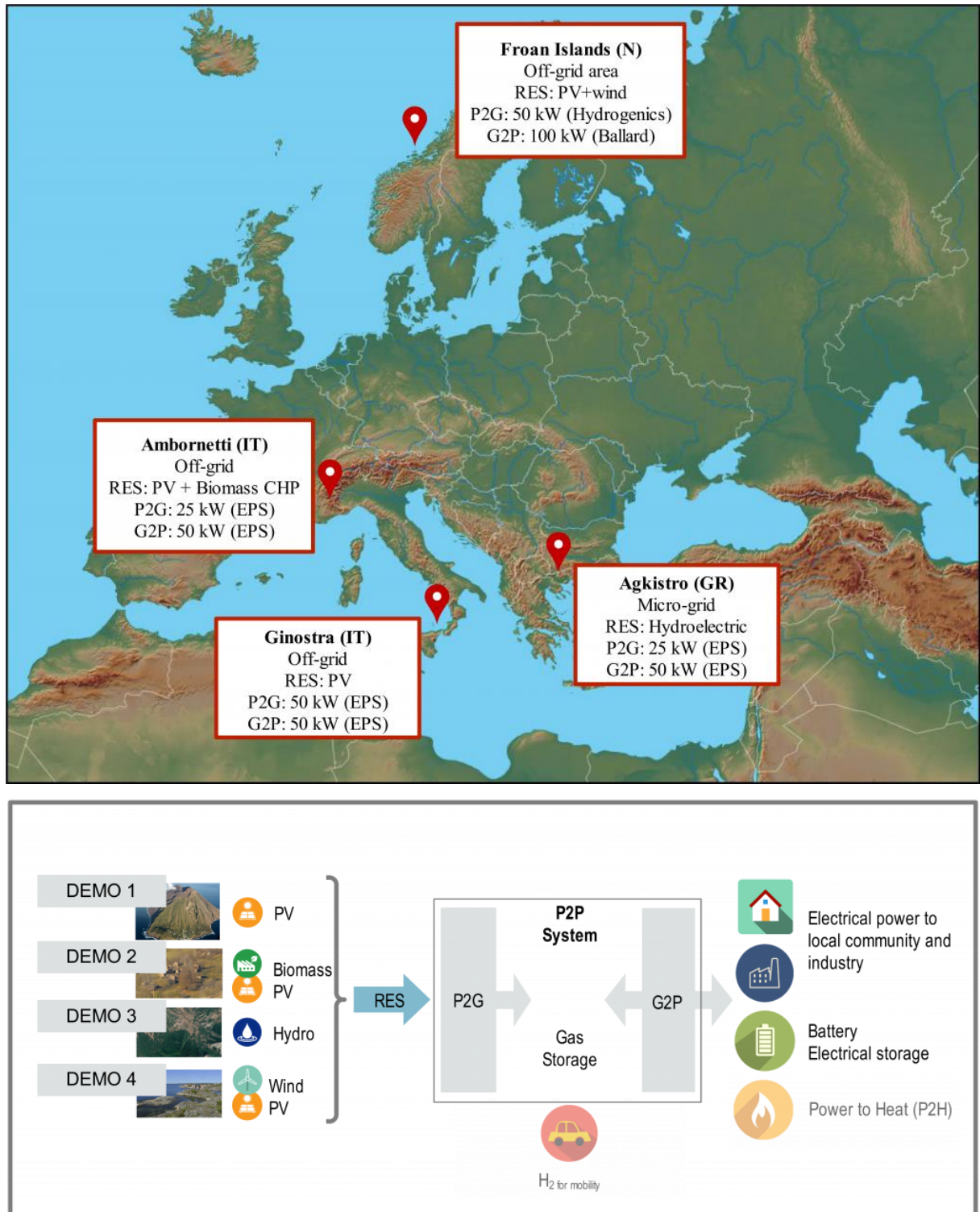


Figure 0.1 REMOTE project pictures taken from the website [2]

The goal of this work is to better understand the dynamic behaviour and evaluate the performances of a P2P system by means of a flexible dynamic model developed in the

MATLAB-Simulink[®] environment and performing an analysis on simulations results, based on different scenarios.

The thesis has been organized in the following sections:

- Description of the whole system and its components;
- Development of the dynamic model;
- Model validation according to data available in literature;
- Analysis of main simulation results and further analyses;
- Conclusions and recommendations for further works.

1 Description of the system

In general, main components of a P2P system are the electrolyzer and fuel cell stacks and the hydrogen storage. The real system is also composed by several auxiliaries which affect the dynamic response. In figure 1.1, different possible system configurations have been shown. In general, the components for the real system are:

- Power converters;
- Electrolyzer and fuel cell stacks;
- Hydrogen storage tank;
- Water-gas separators;
- Pumps and blowers;
- Compressor (if the electrolyzer works at pressure lower than the hydrogen storage tank);
- Heat exchangers;
- Expansion valve;
- Humidifiers.

In the model have been considered a proton exchange membrane electrolyzer (PEMWE) and a proton exchange membrane fuel cell (PEMFC), according to DEMO 4 of the REMOTE project, namely the installation in Froan/Rye Islands.

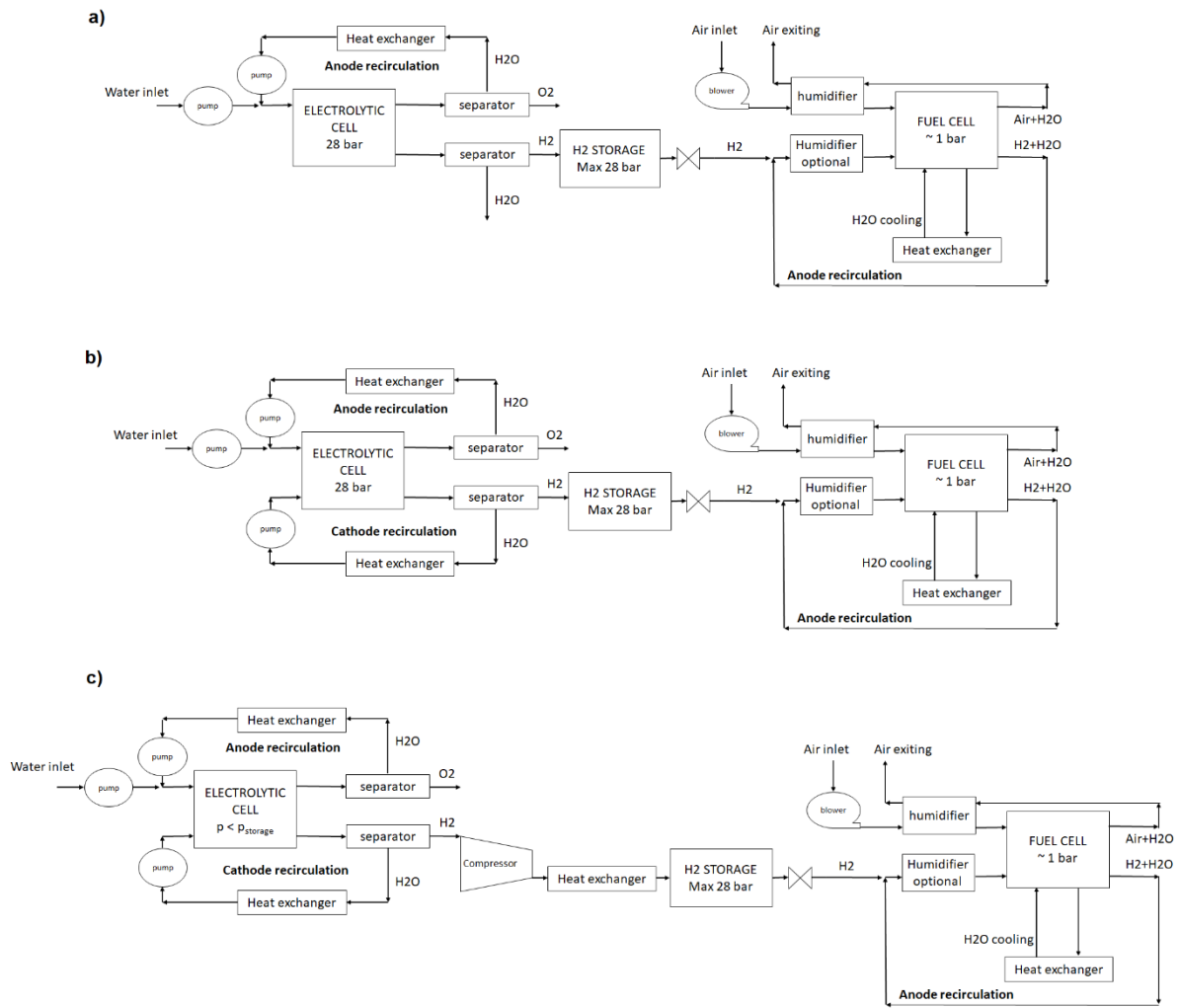


Figure 1.1 Different configurations of the real system: a) without cathode recirculation for the electrolyzer and without compressor, b) with cathode recirculation for the electrolyzer and without compressor, c) with cathode recirculation for the electrolyzer and compressor.

In the charging phase, surplus electricity from RES goes to power converters (AC/DC and DC/DC), which adjust electrical parameters before reaching the electrolyzer stack. A pump supplies water to the electrolyzer, where oxygen and hydrogen are produced by electrolysis. Water-gas separators are needed to separate water from gases (i.e. oxygen and hydrogen) and recirculate it through two separated circuits for the two electrodes of the electrolyzer (i.e. water exiting from cathode is recirculated at the cathode and water exiting from anode recirculated at the anode) to avoid the risk of formation of possible explosive mixture between residual oxygen and hydrogen in the recirculated streams. In both circuits are present heat exchangers to control the feed water temperature and pumps to overcome the pressure drops in the pipes. Usually, water exiting from cathode, after being separated from hydrogen, is simply drained without recirculate it to the cathode inlet (see figure 1.1.a). Once the hydrogen has been separated it is sent to a compressor before reaching the hydrogen storage tank if the working pressure of the

electrolyzer is lower than the pressure in the storage tank or directly sent to the storage tank if the working pressure of the electrolyzer is higher than the pressure in the storage tank. If the compressor is needed, then a cooling system should be installed to reduce the temperature that would be too high at the inlet of the storage tank. In the scheme in figure 1.1c, for the sake of simplicity, the compressor and the cooling system are represented as a heat exchanger in series to the compressor, but in reality the compression would consist of more stages with intercooling. If the compressor is not needed, then the temperature reduction due to heat transfer losses in the pipes is enough to bring hydrogen exiting from electrolyzer close to the target temperature without the need of a cooler, before reaching the storage tank.

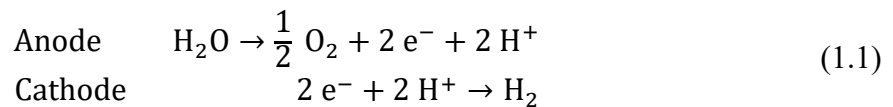
In the discharging phase, hydrogen required by the fuel cell stack is sent from the storage tank to an expansion valve to reduce the pressure up to a value which allows to overcome pressure drops in the pipe and reach the fuel cell stack working at a pressure slightly higher than ambient pressure. Air blower is needed to supply air taken from environment to the fuel cell stack. Before entering the fuel cell stack, air and hydrogen must be correctly humidified by means of humidifiers. In the fuel cell, oxygen from air and hydrogen react to produce water. Air and hydrogen are sent in excess to ensure the complete reaction in all the cells of the stack. Cathode outlet (i.e. water and air excess) is sent to the air humidifier to humidify the air at the cathode inlet, while anode outlet is recirculated to the anode inlet before the optional hydrogen humidifier, according to Bao et al. [3]. The fuel cell stack temperature is controlled by means of a heat exchanger. Electricity produced by the fuel cell stack is sent to power converters (DC/DC and DC/AC) and finally to the local grid and users.

However, the modelled system does not account for all auxiliaries, but it is focused on main components:

- PEMWE, working in pressure;
- Pressurized hydrogen storage tank;
- PEMFC.

1.1 Electrolyzer

The electrolyzer considered in the modelled system is a PEMWE. Water splitting reaction occurs during electrolysis and half-reactions at the electrodes are [4]:



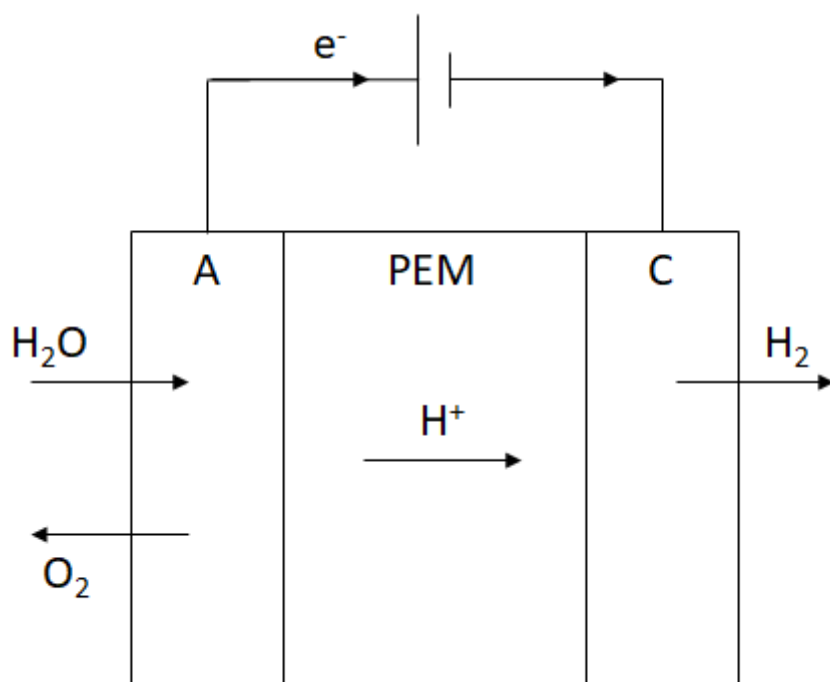


Figure 1.2 Ideal scheme of a PEMWE [4]

The name of the PEMWE derives from the material of the electrolyte, that is a proton exchange membrane (PEM). This membrane is made of a material called Nafion, a fluoro-sulfonated polymer [4]. This material is produced starting from ethylene which is processed to produce poly-tetra-fluorine-ethylene (PTFE) also called Teflon, by means of perfluorination. This hydrophobic polymer is then sulfonated with the hydrogen sulphite, by means of sulphonation. The result is a hydrophobic polymer characterized by hydrophilic regions due to the presence of the hydrogen sulphite along polymeric chains, where hydrogen ions can move.

This type of electrolyzer is characterized by the need of humidification, since the hydrogen ions conducted in the Nafion membrane are hydrated ions, according to Grotthuss mechanism [4]. Thus, the operating temperature must be lower than the boiling temperature, usually below about 85°C. Since kinetic phenomena are not favoured at such low temperatures, precious catalyst (i.e. Platinum, Pt) is needed to sustain the reaction. The main problem of such precious catalyst is that it suffers carbon deposition. For this reasons, co-electrolysis (i.e. electrolysis of both H₂O and CO₂) is not possible in a PEMWE.

1.2 Fuel cell

Similarly to the PEMWE, the fuel cell studied is a PEM type and therefore it is also affected by the problems related to low operating temperatures. Indeed, only hydrogen can be used as fuel (99,99% purity) to avoid carbon deposition. Half-reactions at the electrodes are [4]:

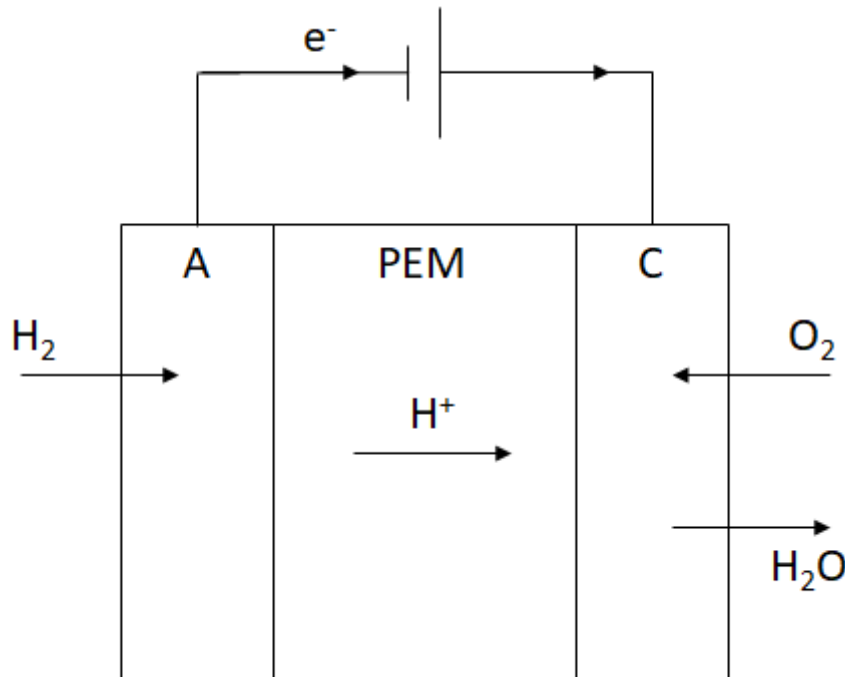
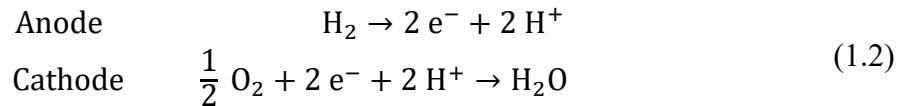


Figure 1.3 Ideal scheme of a PEMFC [4]

1.3 Hydrogen storage tank

Hydrogen can be stored in different ways. This energy vector is characterized by a very high specific energy (i.e. in terms of mass), but its energy density (i.e. in terms of volume) is very low. The kind of storage system must handle with this problem. For this reason, it needs to be stored in a more energy dense state. Main hydrogen storage solutions are:

- Compressed gas;
- Liquified;
- Adsorbed in solid matrices.

In the modelled system, the hydrogen produced by the electrolyzer is stored in a pressurized vessel, which can allow a maximum pressure of 28 bar. When such pressure is reached it means that the tank is full of hydrogen, thus the excess power from RES is curtailed. The minimum pressure in the tank is 3 bar, designed to allow the flow of hydrogen to reach the PEMFC considering pressure drops in the pipes. During the discharge, if the pressure reaches the minimum value, then the hydrogen flow exiting from the storage tank is stopped by acting on a valve and the load is covered by the backup system, which consists of diesel generators.

2 Dynamic model

The model has been developed in MATLAB-Simulink® environment. Simulink is a tool integrated in the MATLAB environment, used for modelling, design and analysis of dynamic systems. In this tool, only time evolution of computed quantities can be performed, without any information about spatial distributions. Thus, lumped parameter models have been developed for each component, which have been treated as zero-dimensional objects.

The dynamic model has been developed for each component separately and, then, for the global system, connecting all main components and implementing control strategies. Model equations have been defined according to models available in literature. The dynamic model is based on mass and energy balance equations considering mass transport, thermal, electrical and electrochemical phenomena. More in detail, slowest and dominant transients are due to mass transport phenomena, while thermal and, lastly, electrical phenomena are characterized by faster response.

Once the system to be modelled has been defined, differential equations related to dynamic phenomena derived from models available in literature have been implemented in the tool, according to the software language.

2.1 Assumptions

Main assumptions in the model are the following:

- Components treated like zero-dimensional objects (i.e. low Biot number [5, 6]);
- Temperature at the outlet is equal to the temperature of the component itself;
- Gases and water vapour have been considered as ideal gases;
- Initial temperatures and pressures for PEMWE and PEMFC are set equal to ambient conditions;
- Anode and cathode temperatures for PEMWE and PEMFC are the same;
- Products and reactants excess start exiting the stack only if the operating pressure of the stack is reached.

2.2 Electrolyzer

2.2.1 Electrochemical model

In the PEMWE, the water splitting redox reaction takes place:



Water is fed at the anode, while oxygen forms at the anode and hydrogen forms at the cathode.

The electrochemical model includes both electric and electrochemical phenomena. The result of the electrochemical model is the voltage of the cell. The equation for the cell voltage is [4]:

$$V_{\text{cell}} = \text{OCV} + \eta_{\text{act}} + \eta_{\text{ohm}} + \eta_{\text{diff}} \quad (2.2)$$

where:

- OCV is the open circuit voltage;
- η_{act} is the activation overvoltage;
- η_{ohm} is the ohmic overvoltage;
- η_{diff} is the diffusion (or concentration) overvoltage.

2.2.1.1 Open circuit voltage

The open circuit voltage (OCV) is given by the Nernst equation for an electrolytic cell:

$$OCV = \frac{\Delta G}{z \cdot F} + \frac{R \cdot T}{z \cdot F} \cdot \ln \left(\frac{\prod_{i=1}^P p_i^{v_i}}{\prod_{j=1}^R p_j^{v_j}} \right) \quad (2.3)$$

where:

- R is the universal gas constant;
- F is the Faraday's constant;
- z is the charge number;
- ΔG is the Gibbs free energy of the reaction.
- p_i is the partial pressure of the chemical species i .

This Gibbs free energy element is given by:

$$\Delta G = \Delta H - T \cdot \Delta S \quad (2.4)$$

where ΔH and ΔS are respectively the molar enthalpy and molar entropy of the reaction. These two terms are defined as the difference between products and reactants molar enthalpies and molar entropies weighted on stoichiometric coefficients:

$$\Delta H = \sum_{i=1}^P v_i \cdot h_i - \sum_{j=1}^R v_j \cdot h_j \quad (2.5)$$

$$\Delta S = \sum_{i=1}^P v_i \cdot s_i - \sum_{j=1}^R v_j \cdot s_j \quad (2.6)$$

where:

- h and s are respectively the molar enthalpies and molar entropies associated to products (P) and reactants (R);
- v are the stoichiometric coefficients.

Thus, for water splitting reaction, the enthalpy and entropy variations are:

$$\Delta H = 1 \cdot h_{H_2} + \frac{1}{2} \cdot h_{O_2} - 1 \cdot h_{H_2O} \quad (2.7)$$

$$\Delta S = 1 \cdot s_{H_2} + \frac{1}{2} \cdot s_{O_2} - 1 \cdot s_{H_2O} \quad (2.8)$$

Usually, molar enthalpy and entropy are expressed in form of a polynomial in literature [7]:

$$h^0 - h_{298,15}^0 = A \cdot t + \frac{1}{2} \cdot B \cdot t^2 + \frac{1}{3} \cdot C \cdot t^3 + \frac{1}{4} \cdot D \cdot t^4 - \frac{E}{t} + F - H \quad (2.9)$$

$$s^0 = A \cdot \ln(t) + B \cdot t + \frac{1}{2} \cdot C \cdot t^2 + \frac{1}{3} \cdot D \cdot t^3 - \frac{E}{2 \cdot t^2} + G \quad (2.10)$$

where:

- h^0 is the standard molar enthalpy in kJ/mol;
- s^0 is the standard molar entropy in J mol⁻¹ K⁻¹;
- t is the temperature in K divided by 1000.

Table 2.1 Coefficients for fluid properties relations [7]

	H₂O	H₂	O₂	N₂
	298-500 K	298-1000 K	100-700 K	100-500 K
A	-203,6060	33,066178	31,32234	28,98641
B	1523,290	-11,363417	-20,23531	1,853978
C	-3196,413	11,432816	57,86644	-9,647459
D	2474,455	-2,772874	-36,50624	16,63537
E	3,855326	-0,158558	-0,007374	0,000117
F	-256,5478	-9,980797	-8,903471	-8,671914
G	-488,71	172,707974	246,7945	226,4168
H	-285,8304	0,0	0,0	0,0

Thus, the Nernst equation for the PEMWE is:

$$OCV = \frac{\Delta G}{z \cdot F} + \frac{R \cdot T}{z \cdot F} \cdot \ln \left(\frac{p_{H_2} \cdot p_{O_2}^{\frac{1}{2}}}{p_{H_2O}} \right) \quad (2.11)$$

2.2.1.2 Activation overvoltage

This term is related to losses caused by the activation of the reaction. It is defined as [8, 9]:

$$\eta_{act} = \frac{R \cdot T}{\alpha_A \cdot F} \cdot \operatorname{arsinh} \left(\frac{i}{2 \cdot i_{0,A}} \right) + \frac{R \cdot T}{\alpha_C \cdot F} \cdot \operatorname{arsinh} \left(\frac{i}{2 \cdot i_{0,C}} \right) \quad (2.12)$$

where:

- i is the current density in A/cm².
- $i_{0,A}$ and $i_{0,C}$ are the exchange current densities for anode and cathode;
- α_A and α_C are the charge transfer coefficients for anode and cathode.

2.2.1.3 Ohmic overvoltage

Ohmic overvoltage can be defined by the Ohm's law:

$$\eta_{\text{ohm}} = ASR \cdot i \quad (2.13)$$

where, ASR is the area specific resistance in $\Omega \text{ cm}^2$. In general, the ASR includes both electronic and ionic contributions:

$$ASR = ASR_{\text{el}} + ASR_{\text{ion}} \quad (2.14)$$

where, ASR_{el} and ASR_{ion} are the electronic and ionic area specific resistance. However, the term associated to electrical losses is often neglected in literature [10, 9, 11], so the main contribute is given by the ionic term. Thus, the area specific resistance can be written as:

$$ASR = ASR_{\text{ion}} = \frac{t_{\text{me}}}{\sigma_{\text{me}}} \quad (2.15)$$

where:

- t_{me} is the thickness of the membrane;
- σ_{me} is the ionic conductivity of the membrane.

According to literature [9, 11, 12] the ionic conductivity of the membrane can be defined as:

$$\sigma_{\text{me}} = (0.005139 \cdot \lambda_{\text{me}} - 0.00326) \cdot \exp \left[1268 \cdot \left(\frac{1}{303} - \frac{1}{T} \right) \right] \quad (2.16)$$

where, σ_{me} is given in $\Omega^{-1} \text{ cm}^{-1}$ and λ_{me} is the membrane water content calculated as the arithmetic mean between anode and cathode water content [13]:

$$\lambda_{\text{me}} = \frac{\lambda_{\text{A}} + \lambda_{\text{C}}}{2} \quad (2.17)$$

Water content depends on the electrode water activity [14]:

$$\lambda = \begin{cases} 0,043 + 17,81 \cdot a - 39,85 \cdot a^2 + 36 \cdot a^3 & 0 < a \leq 1 \\ 14 + 1,4 \cdot (a - 1) & 1 < a \leq 3 \\ 16,8 & a > 3 \end{cases} \quad (2.18)$$

where, a is the water activity, defined as [15]:

$$a = \frac{p_{\text{H}_2\text{O}}}{p_{\text{sat}}} \quad (2.19)$$

where:

- p_{sat} is the saturation pressure of water;
- $p_{\text{H}_2\text{O}}$ is the water partial pressure.

The saturation pressure of water is given by [15]:

$$\log_{10}(p_{\text{sat}}) = -2,1794 + 0,02953 \cdot T - 9,1837 \times 10^{-5} \cdot T^2 + 1,4454 \times 10^{-7} \cdot T^3 \quad (2.20)$$

where:

- T is given in $^{\circ}\text{C}$;
- p_{sat} is given in atm.

2.2.1.4 Diffusion overvoltage

In this model also diffusion overvoltage has been considered. It can be written as [16]:

$$\eta_{\text{diff}} = -\frac{R \cdot T}{z \cdot F} \cdot \ln\left(\frac{C_{\text{me}}}{C_{\text{ch}}}\right) \quad (2.21)$$

where, C_{me} and C_{ch} are respectively the concentrations at the channel and at the membrane of species involved in the reaction. The total diffusion overvoltage is composed by anode and cathode contributions, as for the activation overvoltage. Thus, the final relation for total diffusion overvoltage is:

$$\eta_{\text{diff}} = \eta_{\text{diff,A}} + \eta_{\text{diff,C}} \quad (2.22)$$

For the PEMWE, anode and cathode contributions are defined as:

$$\eta_{\text{diff,A}} = \left| \frac{R \cdot T}{4 \cdot F} \cdot \ln\left(\frac{C_{\text{O}_2,\text{me}}}{C_{\text{O}_2,\text{ch}}}\right) \right| \quad (2.23)$$

$$\eta_{\text{diff,C}} = \left| \frac{R \cdot T}{2 \cdot F} \cdot \ln\left(\frac{C_{\text{H}_2,\text{me}}}{C_{\text{H}_2,\text{ch}}}\right) \right| \quad (2.24)$$

2.2.1.5 Electric double layer effect

In the electrochemical submodel, according to many authors [16, 17, 18, 19, 20], also capacitive phenomena are considered. According to literature [16, 17], this phenomenon is related to a charge distribution at the interface between the electrode and the membrane, which leads to the formation of two layers of opposite polarity able to store electrical energy and behave like a supercapacitor. Thus, the equivalent circuit is shown in figure 2.1.

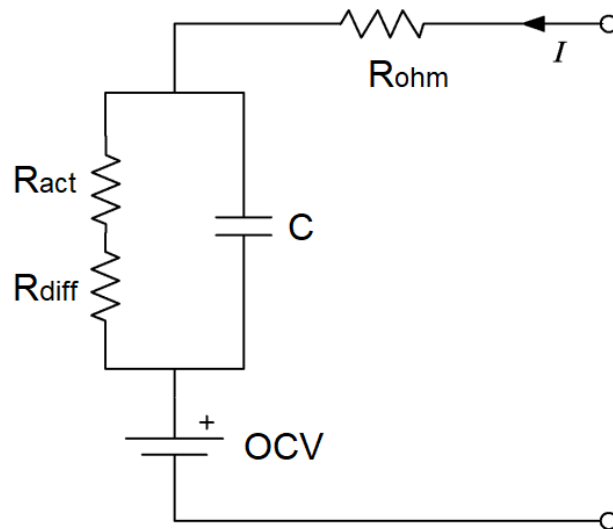


Figure 2.1 Equivalent electrical circuit of the PEMWE [16, 18, 19, 20]

The differential equation associated to this phenomenon is [16]:

$$V_{C_{el}} = \left(I - C_{el} \cdot \frac{dV_{C_{el}}}{dt} \right) \cdot \frac{\eta_{act} + \eta_{diff}}{I} \quad (2.25)$$

where, $V_{C_{el}}$ is the voltage across the electric double layer capacitance C_{el} . Thus, final equation for the cell voltage is:

$$V_{cell} = OCV + \eta_{ohm} + V_{C_{el}} \quad (2.26)$$

2.2.2 Mass transport model

In this section, mass transport submodel for the PEMWE has been described, including mass balance differential equations and mass transport phenomena.

Chemical species involved in the reaction have been treated as ideal gases. Thus, molar fractions y_i , molar concentrations at the channel $C_{ch,i}$, partial pressures p_i for the i -th species and total pressure at the electrode p_E (i.e. anode or cathode) have been defined as:

$$y_i = \frac{p_i}{p_E} \quad (2.27)$$

$$C_{ch,i} = \frac{n_i}{V_E} \quad (2.28)$$

$$p_i = \frac{n_i \cdot R \cdot T_E}{V_E} \quad (2.29)$$

$$p_E = \sum_{i=1}^n p_i \quad (2.30)$$

where:

- n_i is the number of moles of the species i ;
- V_E and T_E are respectively the volume and the temperature at the electrode (anode or cathode).

In the PEMWE, water concentration at the channel has been defined as follow, according to Marangio et al. [8]:

$$C_{H_2O, ch} = \frac{\rho_{H_2O}}{MM_{H_2O}} \quad (2.31)$$

where, ρ_{H_2O} is the water density given by [21]:

$$\rho_{H_2O} = 1000 \cdot \left[1 - \frac{T + 288,9414}{508929,2 \cdot (T + 68,12963)} \cdot (T - 3,9863)^2 \right] \quad (2.32)$$

where, T is given in °C and ρ_{H_2O} in kg/m³.

Concentrations at the membrane have been computed according to Fick's law, considering the minus sign in case of molar flow rate from the channel to the membrane, or the plus sign vice versa:

$$C_{me} = C_{ch} \pm \frac{t_{me} \cdot \dot{n}}{D_{eff,E} \cdot A_{cell}} \quad (2.33)$$

where:

- \dot{n} is the molar flow moving from the channel to the membrane, or vice versa;
- $D_{eff,E}$ is the effective binary diffusion coefficient at the electrode [8, 9].

The effective binary diffusion coefficient has been defined as [8, 9]:

$$D_{eff} = D_{AB} \cdot \epsilon \cdot \left(\frac{\epsilon - \epsilon_p}{1 - \epsilon_p} \right)^\alpha \quad (2.34)$$

where:

- D_{AB} in cm^2/s is the binary diffusion coefficient of the mixture of the substances A and B;
- ϵ is the porosity of the electrode;
- ϵ_p is percolation threshold, whose value is 0,11 [8];
- α is an empirical coefficient, whose value is 0,785 [8].

The binary diffusion coefficient has been defined as [8]:

$$D_{AB} = a \cdot \left(\frac{T}{\sqrt{T_{crit,A} \cdot T_{crit,B}}} \right)^b \cdot (p_{crit,A} \cdot p_{crit,B})^{\frac{1}{3}} \cdot (T_{crit,A} \cdot T_{crit,B})^{\frac{5}{12}} \cdot \sqrt{\frac{1}{MM_A} + \frac{1}{MM_B}} \quad (2.35)$$

where:

- p_{crit} in atm and T_{crit} in K are the critical pressure and temperature reported in table 2.2;
- a and b are empirical coefficients, whose values are reported in table 2.3.

Table 2.2 Critical temperature and pressure [8]

	H₂O	H₂	O₂
p_{crit} [atm]	218,3	12,8	49,7
T_{crit} [K]	647,3	33,3	154,4

Table 2.3 Empirical coefficients in the binary diffusion coefficient equation [8]

	Pairs of two non-polar gases	Pairs of H₂O and a non-polar gas
a	$2,745 \times 10^{-4}$	$3,640 \times 10^{-4}$
b	1,823	2,334

In the model, pairs of water and non-polar gas have been considered.

2.2.2.1 Anode

Chemical species involved in the anode of the PEMWE are oxygen formed during the reaction and water entering the PEMWE involved in the reaction. Thus, the total pressure at the anode has been defined as:

$$p_A = p_{O_2} + p_{H_2O} \quad (2.36)$$

Oxygen

The mass balance equation for oxygen at the anode is:

$$\frac{dn_{O_2}}{dt} = \dot{n}_{O_2,gen} - \dot{n}_{O_2,out} \quad (2.37)$$

where:

- $\dot{n}_{O_2,gen}$ is the oxygen molar flow generated at the anode;
- $\dot{n}_{O_2,out}$ is the oxygen molar flow at the anode outlet.

Oxygen generation term is given by the Faraday's law:

$$\dot{n}_{O_2,gen} = \eta_{far} \cdot \frac{I \cdot n_{cell}}{4 \cdot F} \quad (2.38)$$

where:

- η_{far} is the Faraday's efficiency [22];
- n_{cell} is the number of cells.

The outlet flow of oxygen has been defined as:

$$\dot{n}_{O_2,out} = y_{O_2} \cdot \dot{n}_{out,A} \quad (2.39)$$

where, $\dot{n}_{out,A}$ is the molar flow exiting from the anode has been evaluated as [13, 17]:

$$\dot{n}_{out,A} = (p_A - p_{out}) \cdot k_{O,A} \quad (2.40)$$

- $k_{O,A}$ is the anode outlet flow coefficient [17];
- p_{out} is the pressure downstream the component.

The oxygen concentration at the membrane has been defined according to Fick's law:

$$C_{O_2,me} = C_{O_2,ch} + \frac{t_{me} \cdot \dot{n}_{O_2}}{D_{eff} \cdot A_{cell}} \quad (2.41)$$

where:

$$\dot{n}_{O_2} = \dot{n}_{O_2,gen} \quad (2.42)$$

Water

Mass balance equation for water at the anode is:

$$\frac{dn_{\text{H}_2\text{O}}}{dt} = \dot{n}_{\text{H}_2\text{O},\text{in}} - \dot{n}_{\text{H}_2\text{O},\text{me}} - \dot{n}_{\text{H}_2\text{O},\text{cons}} - \dot{n}_{\text{H}_2\text{O},\text{out}} \quad (2.43)$$

where:

- $\dot{n}_{\text{H}_2\text{O},\text{in}}$ is the molar flow of water at the anode inlet;
- $\dot{n}_{\text{H}_2\text{O},\text{out}}$ is the molar flow of water at the anode outlet;
- $\dot{n}_{\text{H}_2\text{O},\text{cons}}$ is the molar flow of water consumed by the reaction at the anode;
- $\dot{n}_{\text{H}_2\text{O},\text{me}}$ is the molar flow of water through the membrane.

The inlet flow rate is controlled by a PID to have enough water for the reaction and to control the temperature of the stack, preventing to go above a target limit. It has been computed as:

$$\dot{n}_{\text{H}_2\text{O},\text{in}} = \lambda_{\text{H}_2\text{O}} \cdot \dot{n}_{\text{H}_2\text{O},\text{cons}} + \dot{n}_{\text{H}_2\text{O},\text{cool}}$$

where:

- $\lambda_{\text{H}_2\text{O}}$ is the excess of water considered equal to 2;
- $\dot{n}_{\text{H}_2\text{O},\text{cool}}$ is the water added when the temperature of the stack reach a certain value. When the temperature is below the target value this term is set equal to zero.

Water consumption is evaluated with the Faraday's law:

$$\dot{n}_{\text{H}_2\text{O},\text{cons}} = \frac{I \cdot n_{\text{cell}}}{2 \cdot F} \quad (2.44)$$

The outlet flow rates are determined by:

$$\dot{n}_{\text{H}_2\text{O},\text{out}} = y_{\text{H}_2\text{O}} \cdot \dot{n}_{\text{out},\text{A}} \quad (2.45)$$

Water transport through the membrane has been defined in section 2.2.2.3.

Water concentration at the membrane is given by:

$$C_{\text{H}_2\text{O},\text{me},\text{A}} = C_{\text{H}_2\text{O},\text{ch},\text{A}} - \frac{t_{\text{A}} \cdot \dot{n}_{\text{H}_2\text{O},\text{A}}}{D_{\text{eff},\text{A}} \cdot A_{\text{cell}}} \quad (2.46)$$

where:

$$\dot{n}_{\text{H}_2\text{O},\text{A}} = \dot{n}_{\text{H}_2\text{O},\text{cons}} + \dot{n}_{\text{H}_2\text{O},\text{me}} \quad (2.47)$$

2.2.2.2 Cathode

Chemical species involved in the cathode of the PEMWE are hydrogen formed during the reaction and water passed through the membrane. Thus, the total pressure at the cathode has been defined as:

$$p_{\text{C}} = p_{\text{H}_2} + p_{\text{H}_2\text{O}} \quad (2.48)$$

Hydrogen

The differential equation for hydrogen at the cathode is:

$$\frac{dn_{\text{H}_2}}{dt} = \dot{n}_{\text{H}_2,\text{gen}} - \dot{n}_{\text{H}_2,\text{out}} \quad (2.49)$$

where:

- $\dot{n}_{\text{H}_2,\text{gen}}$ is the molar flow of hydrogen generated at the cathode;
- $\dot{n}_{\text{H}_2,\text{out}}$ is the molar flow of hydrogen at the cathode outlet.

The hydrogen formed during the reaction is given by the Faraday's law:

$$\dot{n}_{\text{H}_2,\text{gen}} = \eta_{\text{far}} \cdot \frac{I \cdot n_{\text{cell}}}{2 \cdot F} \quad (2.50)$$

The outlet flow of hydrogen is:

$$\dot{n}_{\text{H}_2,\text{out}} = y_{\text{H}_2} \cdot \dot{n}_{\text{out,C}} \quad (2.51)$$

Molar flow exiting from the cathode has been evaluated as [13, 17]:

$$\dot{n}_{\text{out,C}} = (p_{\text{C}} - p_{\text{out}}) \cdot k_{\text{O,C}} \quad (2.52)$$

where, $k_{\text{O,C}}$ is the cathode outlet flow coefficient [17].

The hydrogen concentration at the membrane has been calculated according to Fick's law:

$$C_{\text{H}_2,\text{me}} = C_{\text{H}_2,\text{ch}} + \frac{t_{\text{me}} \cdot n_{\text{H}_2}}{D_{\text{eff}} \cdot A_{\text{cell}}} \quad (2.53)$$

where:

$$\dot{n}_{\text{H}_2} = \dot{n}_{\text{H}_2,\text{gen}} \quad (2.54)$$

Water

Mass balance equation for water at the cathode is:

$$\frac{dn_{\text{H}_2\text{O}}}{dt} = \dot{n}_{\text{H}_2\text{O},\text{me}} - \dot{n}_{\text{H}_2\text{O},\text{out}} \quad (2.55)$$

Outlet molar flow rate of water is:

$$\dot{n}_{\text{H}_2\text{O},\text{out}} = y_{\text{H}_2\text{O}} \cdot \dot{n}_{\text{out,C}} \quad (2.56)$$

Water transport through the membrane has been defined in section 2.2.2.3.

At cathode side, concentration of water at the membrane is given by:

$$C_{\text{H}_2\text{O},\text{me,C}} = C_{\text{H}_2\text{O},\text{ch,C}} + \frac{t_{\text{C}} \cdot \dot{n}_{\text{H}_2\text{O},\text{C}}}{D_{\text{eff,C}} \cdot A_{\text{cell}}} \quad (2.57)$$

where:

$$\dot{n}_{\text{H}_2\text{O},\text{C}} = \dot{n}_{\text{H}_2\text{O},\text{me}} \quad (2.58)$$

2.2.2.3 Membrane water transport

Some water can cross the membrane due to different transport phenomena. According to many authors in literature [4, 8, 9, 13], the water through the membrane has been calculated considering three main phenomena:

- Diffusion;

- Electro-osmotic drag;
- Effect of pressure.

Water transport from anode to cathode is given by [8]:

$$\dot{n}_{\text{H}_2\text{O,me}} = \dot{n}_{\text{H}_2\text{O,diff}} + \dot{n}_{\text{H}_2\text{O,eod}} - \dot{n}_{\text{H}_2\text{O,pr}} \quad (2.59)$$

Mass transport of water due to diffusion depends on concentration gradient across the membrane. In the case of PEMWE, having larger concentration of water at the anode, the water diffuses from anode to cathode. This phenomenon has been evaluated with the Fick's law [8, 9, 13]:

$$\dot{n}_{\text{H}_2\text{O,diff}} = A_{\text{cell}} \cdot D_{\text{H}_2\text{O}} \cdot \frac{(C_{\text{H}_2\text{O,me,A}} - C_{\text{H}_2\text{O,me,C}})}{t_{\text{me}}} \quad (2.60)$$

where:

- $C_{\text{H}_2\text{O,me,C}}$ and $C_{\text{H}_2\text{O,me,A}}$ are the concentrations of water at the membrane, respectively at cathode and anode side;
- $D_{\text{H}_2\text{O}}$ is the water diffusion coefficient.

The water diffusion coefficient $D_{\text{H}_2\text{O}}$ is function of the temperature and a diffusion coefficient D_λ given in m^2/s which is function of the water content of the membrane [13, 17]:

$$D_{\text{H}_2\text{O}} = D_\lambda \cdot \exp \left[2416 \cdot \left(\frac{1}{303} - \frac{1}{T_{\text{cell}}} \right) \right] \quad (2.61)$$

where, the term D_λ is defined as [13, 17]:

$$D_\lambda = \begin{cases} 10^{-10} & \lambda_{\text{me}} < 2 \\ 10^{-10} \cdot [1 + 2 \cdot (\lambda_{\text{mem}} - 2)] & 2 \leq \lambda_{\text{me}} < 3 \\ 10^{-10} \cdot [3 - 1,67 \cdot (\lambda_{\text{mem}} - 3)] & 3 \leq \lambda_{\text{me}} < 4,5 \\ 1,25 \times 10^{-10} & \lambda_{\text{me}} \geq 4,5 \end{cases} \quad (2.62)$$

The electro-osmotic drag is linked to the migration of hydrogen ions through the membrane. Thus, water molecules are dragged from anode to cathode. It can be evaluated as [13]:

$$\dot{n}_{\text{H}_2\text{O,eod}} = n_d \cdot \frac{I}{F} \quad (2.63)$$

where, n_d is the electro-osmotic drag coefficient, which depends on water content of the membrane [23]:

$$n_d = \begin{cases} 1 & \lambda_{\text{me}} \leq 14 \\ \frac{1,5}{8} \cdot (\lambda_{\text{me}} - 14) + 1 & \lambda_{\text{me}} > 14 \end{cases} \quad (2.64)$$

The last term in equation (2.59) is associated to pressure gradient across the membrane. In the case of larger pressure at the cathode, then this term imposes a mass transport of water from the cathode to the anode. This phenomenon is governed by Darcy's law [9]:

$$\dot{n}_{\text{H}_2\text{O,pr}} = \frac{K_{\text{darcy}} \cdot A_{\text{cell}} \cdot \rho_{\text{H}_2\text{O}} \cdot (p_C - p_A)}{t_{\text{me}} \cdot \mu_{\text{H}_2\text{O}} \cdot \text{MM}_{\text{H}_2\text{O}}} \quad (2.65)$$

where:

- K_{darcy} is the membrane permeability to water;
- $\rho_{\text{H}_2\text{O}}$ and $\mu_{\text{H}_2\text{O}}$ are density and dynamic viscosity of water.

Both density and viscosity are function of temperature. Water density is defined in equation (2.32). The water viscosity is given by [24]:

$$\mu_{\text{H}_2\text{O}} = 0,6612 \cdot (T - 229)^{-1,562} \quad (2.66)$$

where, T is given in K and $\mu_{\text{H}_2\text{O}}$ in Pa s.

2.2.2.4 Cross-over effect and Faraday's efficiency

In the PEMWE has been considered the cross-over effect which cause a reduction of the molecules involved in the reaction, since some of them could cross the membrane. According to many authors in literature [11, 13, 22], this phenomenon can be considered as an efficiency which multiplies the ideal flow rate of oxygen and hydrogen generated by the reaction, according to the Faraday's law:

$$\dot{n}_{\text{gen}} = \eta_{\text{far}} \cdot \frac{I \cdot n_{\text{cell}}}{z \cdot F} \quad (2.67)$$

The faraday's efficiency is given by [22]:

$$\eta_{\text{far}} = f_2 \cdot \frac{i^2}{f_1 + i^2} \quad (2.68)$$

where, f_1 and f_2 are empirical coefficients [22], defined in table 2.6.

2.2.3 Thermal model

Assuming the single component like a zero-dimensional object, the lumped thermal capacitance model has been considered for the thermal sub-model, since it is used by many authors in literature [6, 10, 11]. Thus, the energy balance equation for the PEMWE is:

$$C_{\text{th}} \cdot \frac{dT}{dt} = P_{\text{el}} - \Phi_{\text{loss}} + \sum_{i=1}^n \pm \dot{n}_i \cdot h_i \quad (2.69)$$

The terms in the equation (2.69) have been defined as:

$$P_{\text{el}} = V_{\text{cell}} \cdot I \cdot n_{\text{cell}} \quad (2.70)$$

$$\Phi_{\text{loss}} = h_{\text{th}} \cdot A_{\text{th}} \cdot \Delta T = h_{\text{th}} \cdot A_{\text{th}} \cdot (T - T_{\text{amb}}) \quad (2.71)$$

$$\sum_{i=1}^n \pm \dot{n}_i \cdot h_i = \dot{n}_{\text{H}_2\text{O},\text{in}} \cdot h_{\text{H}_2\text{O},\text{in}} - \dot{n}_{\text{H}_2\text{O},\text{out}} \cdot h_{\text{H}_2\text{O},\text{out}} - \dot{n}_{\text{H}_2,\text{out}} \cdot h_{\text{H}_2,\text{out}} - \dot{n}_{\text{O}_2,\text{out}} \cdot h_{\text{O}_2,\text{out}} \quad (2.72)$$

where:

- C_{th} is the thermal capacitance;
- P_{el} is the electric power in input to the electrolyzer;

- Φ_{loss} is the thermal flux towards the environment;
- \dot{n} is the molar flow rate;
- A_{th} is the heat transfer area;
- h_{th} is the heat transfer coefficient.

2.3 Fuel cell

2.3.1 Electrochemical model

The redox reaction occurring in the PEMFC is:



Humidified hydrogen enters at the anode and oxygen contained in humidified air enters at the cathode, while water forms at the cathode.

The equation for the cell voltage is [4]:

$$V_{\text{cell}} = \text{OCV} - \eta_{\text{act}} - \eta_{\text{ohm}} - \eta_{\text{diff}} \quad (2.74)$$

Open circuit voltage and overvoltage have been calculated in a similar way like has been done for the PEMWE. Formulations for each term are summarized in sections 2.3.1.1, 2.3.1.2, 2.3.1.3 and 2.3.1.4.

2.3.1.1 Open circuit voltage

The Nernst equation for the PEMFC is:

$$\text{OCV} = -\frac{\Delta G}{z \cdot F} + \frac{R \cdot T}{z \cdot F} \cdot \ln\left(\frac{\prod_{i=1}^R p_i^{v_i}}{\prod_{j=1}^P p_j^{v_j}}\right) = -\frac{\Delta G}{z \cdot F} + \frac{R \cdot T}{z \cdot F} \cdot \ln\left(\frac{p_{\text{H}_2} \cdot p_{\text{O}_2}^{\frac{1}{2}}}{p_{\text{H}_2\text{O}}}\right) \quad (2.75)$$

For water formation reaction, the enthalpy and entropy variations used to calculate the Gibbs free energy of the reaction are defined as:

$$\Delta H = 1 \cdot h_{\text{H}_2\text{O}} - 1 \cdot h_{\text{H}_2} - \frac{1}{2} \cdot h_{\text{O}_2} \quad (2.76)$$

$$\Delta S = 1 \cdot s_{\text{H}_2\text{O}} - 1 \cdot s_{\text{H}_2} - \frac{1}{2} \cdot s_{\text{O}_2} \quad (2.77)$$

2.3.1.2 Activation overvoltage

This term is defined exactly like it has been done for the PEMWE in equation (2.12).

2.3.1.3 Ohmic overvoltage

Even for the PEMFC as for the PEMWE, the electrical resistance can be neglected and the ohmic overvoltage can be defined as it has been done for the PEMWE in section 2.2.1.3.

2.3.1.4 Diffusion overvoltage

The diffusion overvoltage can be written as it has been done in section 2.2.1.4, equation (2.21) and (2.22). For the PEMFC, anode and cathode contributions have been defined as:

$$\eta_{\text{diff,A}} = \left| \frac{R \cdot T}{2 \cdot F} \cdot \ln \left(\frac{C_{\text{H}_2,\text{me}}}{C_{\text{H}_2,\text{ch}}} \right) \right| \quad (2.78)$$

$$\eta_{\text{diff,C}} = \left| \frac{R \cdot T}{4 \cdot F} \cdot \ln \left(\frac{C_{\text{O}_2,\text{me}}}{C_{\text{O}_2,\text{ch}}} \right) \right| \quad (2.79)$$

2.3.1.5 Electric double layer effect

Even for the PEMFC as it has been done for the PEMWE, also capacitive phenomena have been included in the electrochemical model, according to literature [16, 17, 18]. The equivalent circuit is shown in figure 2.2.

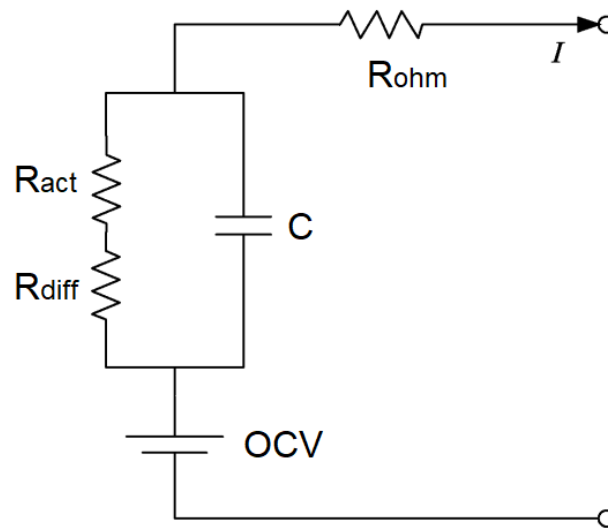


Figure 2.2 Equivalent circuit of the PEMFC [16, 18]

Thus, the differential equation associated to this phenomenon has been define as in equation (2.25). The final equation for the cell voltage is:

$$V_{\text{cell}} = OCV - \eta_{\text{ohm}} - V_{\text{Cel}} \quad (2.80)$$

2.3.2 Mass transport model

In the PEMFC the sub-model associated with mass transport and mass balance equation has been developed similarly to the PEMWE. Same considerations made for the PEMWE, regarding species involved in the reaction, are also valid for the PEMFC. More in detail, molar

fractions, molar concentrations at the channel, partial pressures, total pressure, molar concentrations at the membrane and diffusion coefficients have been defined as it has been done for the PEMWE in section 2.2.2.

In the PEMFC, unlike the PEMWE, the water concentration at the channel has been defined considering water vapour as an ideal gas:

$$C_{H_2O,ch} = \frac{n_{H_2O}}{V_E} \quad (2.81)$$

2.3.2.1 Anode

Chemical species involved in the anode of the PEMFC are hydrogen involved in the reaction and water contained in the humidified hydrogen flow at the anode inlet. Thus, the total pressure at the anode has been defined as:

$$p_A = p_{H_2} + p_{H_2O} \quad (2.82)$$

Hydrogen

Mass balance equation for hydrogen at the anode is:

$$\frac{dn_{H_2}}{dt} = \dot{n}_{H_2,in} - \dot{n}_{H_2,out} - \dot{n}_{H_2,cons} \quad (2.83)$$

Hydrogen consumed by the reaction is:

$$\dot{n}_{H_2,cons} = \frac{I \cdot n_{cell}}{2 \cdot F} \quad (2.84)$$

Hydrogen at the anode inlet is:

$$\dot{n}_{H_2,in} = \lambda_{H_2} \cdot \dot{n}_{H_2,cons} \quad (2.85)$$

where, λ_{H_2} is the hydrogen excess [25]. Hydrogen exiting from the anode is:

$$\dot{n}_{H_2,out} = y_{H_2} \cdot \dot{n}_{out,A} \quad (2.86)$$

where, the term $\dot{n}_{out,A}$ has been defined as it has been done in equation (2.40).

The hydrogen concentration at the membrane has been calculated by using Fick's law:

$$C_{H_2,me} = C_{H_2,ch} - \frac{t_A \cdot \dot{n}_{H_2}}{D_{eff,A} \cdot A_{cell}} \quad (2.87)$$

where:

$$\dot{n}_{H_2} = \dot{n}_{H_2,cons} \quad (2.88)$$

Water

Mass balance equation for water at the anode is:

$$\frac{dn_{H_2O}}{dt} = \dot{n}_{H_2O,in} - \dot{n}_{H_2O,out} - \dot{n}_{H_2O,me} \quad (2.89)$$

The water inlet flow can be written as:

$$\dot{n}_{\text{H}_2\text{O},\text{A},\text{in}} = y_{\text{H}_2\text{O},\text{A},\text{in}} \cdot \frac{\dot{n}_{\text{H}_2,\text{in}}}{y_{\text{H}_2,\text{in}}} = y_{\text{H}_2\text{O},\text{A},\text{in}} \cdot \frac{\dot{n}_{\text{H}_2,\text{in}}}{1 - y_{\text{H}_2\text{O},\text{A},\text{in}}} \quad (2.90)$$

where, the inlet water molar fraction is defined as [3, 18, 26]:

$$y_{\text{H}_2\text{O},\text{A},\text{in}} = \frac{p_{\text{H}_2\text{O},\text{A},\text{in}}}{p_{\text{A}}} = \frac{\text{RH}_{\text{A},\text{in}} \cdot p_{\text{sat}}(T)}{p_{\text{A}}} \quad (2.91)$$

Thus, the water molar flow at the anode inlet can be defined as:

$$\dot{n}_{\text{H}_2\text{O},\text{A},\text{in}} = \dot{n}_{\text{H}_2,\text{in}} \cdot \frac{\text{RH}_{\text{A},\text{in}} \cdot p_{\text{sat}}(T)}{p_{\text{A}} - \text{RH}_{\text{A},\text{in}} \cdot p_{\text{sat}}(T)} \quad (2.92)$$

The water exiting from the anode is:

$$\dot{n}_{\text{H}_2\text{O},\text{out}} = y_{\text{H}_2\text{O}} \cdot \dot{n}_{\text{out},\text{A}} \quad (2.93)$$

Water through the membrane is defined in section 2.3.2.3.

The water concentration at the membrane is:

$$C_{\text{H}_2\text{O},\text{me},\text{A}} = C_{\text{H}_2\text{O},\text{ch},\text{A}} - \frac{t_{\text{A}} \cdot \dot{n}_{\text{H}_2\text{O},\text{A}}}{D_{\text{eff},\text{A}} \cdot A_{\text{cell}}} \quad (2.94)$$

where:

$$\dot{n}_{\text{H}_2\text{O},\text{A}} = \dot{n}_{\text{H}_2\text{O},\text{me}} \quad (2.95)$$

2.3.2.2 Cathode

Chemical species involved in the cathode of the PEMFC are oxygen involved in the reaction, contained in the air entering the cathode together with nitrogen and water, in addition to water formed during the reaction. Thus, the total pressure at the cathode has been defined as:

$$p_{\text{C}} = p_{\text{O}_2} + p_{\text{N}_2} + p_{\text{H}_2\text{O}} \quad (2.96)$$

Oxygen

Mass balance equation for the oxygen at the cathode is:

$$\frac{dn_{\text{O}_2}}{dt} = \dot{n}_{\text{O}_2,\text{in}} - \dot{n}_{\text{O}_2,\text{out}} - \dot{n}_{\text{O}_2,\text{cons}} \quad (2.97)$$

Oxygen consumed by the reaction has been defined as:

$$\dot{n}_{\text{O}_2,\text{cons}} = \frac{I \cdot n_{\text{cell}}}{4 \cdot F} \quad (2.98)$$

Oxygen entering the cathode is:

$$\dot{n}_{\text{O}_2,\text{in}} = \lambda_{\text{air}} \cdot \dot{n}_{\text{O}_2,\text{cons}} \quad (2.99)$$

where, λ_{air} is the air excess [25]. Oxygen exiting from the cathode has been calculated as:

$$\dot{n}_{\text{O}_2,\text{out}} = y_{\text{O}_2} \cdot \dot{n}_{\text{out},\text{C}} \quad (2.100)$$

Molar flow exiting from the cathode $\dot{n}_{\text{out,C}}$ has been evaluated as it has been done in equation (2.52).

Concentration of oxygen at the membrane is given by Fick's law:

$$C_{\text{O}_2,\text{me}} = C_{\text{O}_2,\text{ch}} - \frac{t_{\text{C}} \cdot \dot{n}_{\text{O}_2}}{D_{\text{eff,C}} \cdot A_{\text{cell}}} \quad (2.101)$$

where:

$$\dot{n}_{\text{O}_2} = \dot{n}_{\text{O}_2,\text{cons}} \quad (2.102)$$

Nitrogen

Mass balance equation for nitrogen is:

$$\frac{dn_{\text{N}_2}}{dt} = \dot{n}_{\text{N}_2,\text{in}} - \dot{n}_{\text{N}_2,\text{out}} \quad (2.103)$$

Nitrogen molar flow at the cathode inlet has been computed starting from dry air from the environment which is known to be composed of approximately 79% nitrogen and 21% oxygen in molar fractions [18, 27]. Thus, nitrogen at the cathode inlet has been defined as:

$$\dot{n}_{\text{N}_2,\text{in}} = 0,79 \cdot \dot{n}_{\text{air,in}} \quad (2.104)$$

where, $\dot{n}_{\text{air,in}}$ is the dry air molar flow rate at the inlet, defined as:

$$\dot{n}_{\text{air,in}} = \frac{\dot{n}_{\text{O}_2,\text{in}}}{0.21} \quad (2.105)$$

Water

Mass balance equation for water at the cathode is:

$$\frac{dn_{\text{H}_2\text{O}}}{dt} = \dot{n}_{\text{H}_2\text{O},\text{in}} - \dot{n}_{\text{H}_2\text{O},\text{out}} + \dot{n}_{\text{H}_2\text{O},\text{me}} + \dot{n}_{\text{H}_2\text{O},\text{gen}} \quad (2.106)$$

Water formed at the cathode during the reaction has been defined according to Faraday's law:

$$\dot{n}_{\text{H}_2\text{O},\text{gen}} = \frac{I \cdot n_{\text{cell}}}{2 \cdot F} \quad (2.107)$$

Water entering at the cathode has been computed similarly to equation (2.92):

$$\dot{n}_{\text{H}_2\text{O},\text{C},\text{in}} = \dot{n}_{\text{air,in}} \cdot \frac{\text{RH}_{\text{C},\text{in}} \cdot p_{\text{sat}}(T)}{p_{\text{C}} - \text{RH}_{\text{C},\text{in}} \cdot p_{\text{sat}}(T)} \quad (2.108)$$

Water exiting from the cathode has been computed as:

$$\dot{n}_{\text{H}_2\text{O},\text{out}} = y_{\text{H}_2\text{O}} \cdot \dot{n}_{\text{out,C}} \quad (2.109)$$

Water concentration at the membrane has been defined according to Fick's law:

$$C_{\text{H}_2\text{O},\text{me}} = C_{\text{H}_2\text{O},\text{ch}} + \frac{t_{\text{C}} \cdot \dot{n}_{\text{H}_2\text{O},\text{C}}}{D_{\text{eff,C}} \cdot A_{\text{cell}}} \quad (2.110)$$

where:

$$\dot{n}_{\text{H}_2\text{O},\text{C}} = \dot{n}_{\text{H}_2\text{O},\text{me}} + \dot{n}_{\text{H}_2\text{O},\text{gen}} \quad (2.111)$$

2.3.2.3 Membrane water transport

As for PEMWE, water transport through the membrane take place also in the PEMFC and it has been defined like in equation (2.59). Each term is defined exactly like in section 2.2.2.3.

2.3.2.4 Condensation

In the fuel cell, condensation phenomenon has been considered. Condensation occurs when partial pressure of water at the electrode is higher than saturation pressure. Condensed water is defined as [18, 26]:

$$n_{\text{H}_2\text{O},\text{cond}} = \begin{cases} 0 & p_{\text{H}_2\text{O}} < p_{\text{sat}} \\ \frac{(p_{\text{H}_2\text{O}} - p_{\text{sat}}) \cdot V}{R \cdot T} & p_{\text{H}_2\text{O}} \geq p_{\text{sat}} \end{cases} \quad (2.112)$$

2.3.3 Thermal model

Applying first law of thermodynamics to the PEMFC stack [17]:

$$C_{\text{th}} \cdot \frac{dT}{dt} = -P_{\text{el}} - \Phi_{\text{cooling}} - \Phi_{\text{loss}} + \sum_{i=1}^n \pm \dot{n}_i \cdot h_i \quad (2.113)$$

where P_{el} and Φ_{loss} have been defined as it has been done for the PEMWE in section 2.2.3, while the heat flux exiting from the stack, associated the cooling system, is:

$$\Phi_{\text{cooling}} = \dot{n}_{\text{cool}} \cdot (h_{\text{H}_2\text{O},\text{cool},\text{out}} - h_{\text{H}_2\text{O},\text{cool},\text{in}}) \quad (2.114)$$

The coolant flow rate \dot{n}_{cool} is controlled to have the temperature below a certain target value, by using a PID control block in the model. When the target temperature is reached water starts flowing to cool down the stack.

The term associated to enthalpy fluxes in equation (2.113) has been defined as:

$$\begin{aligned} \sum_{i=1}^n \pm \dot{n}_i \cdot h_i &= \dot{n}_{\text{H}_2\text{O},\text{A},\text{in}} \cdot h_{\text{H}_2\text{O},\text{A},\text{in}} + \dot{n}_{\text{H}_2\text{O},\text{C},\text{in}} \cdot h_{\text{H}_2\text{O},\text{C},\text{in}} + \dot{n}_{\text{H}_2,\text{in}} \cdot h_{\text{H}_2,\text{in}} \\ &+ \dot{n}_{\text{O}_2,\text{in}} \cdot h_{\text{O}_2,\text{in}} - \dot{n}_{\text{H}_2\text{O},\text{out}} \cdot h_{\text{H}_2\text{O},\text{out}} - \dot{n}_{\text{H}_2,\text{out}} \cdot h_{\text{H}_2,\text{out}} \\ &- \dot{n}_{\text{O}_2,\text{out}} \cdot h_{\text{O}_2,\text{out}} \end{aligned} \quad (2.115)$$

The term $\dot{n}_{\text{H}_2\text{O},\text{out}}$ considers water exiting from both anode and cathode:

$$\dot{n}_{\text{H}_2\text{O},\text{out}} = \dot{n}_{\text{H}_2\text{O},\text{A},\text{out}} + \dot{n}_{\text{H}_2\text{O},\text{C},\text{out}} \quad (2.116)$$

2.4 Hydrogen storage tank

2.4.1 Mass balance

The mass balance equation for the hydrogen storage tank is:

$$\frac{dn_{H_2}}{dt} = \dot{n}_{H_2,in} - \dot{n}_{H_2,out} \quad (2.117)$$

where, hydrogen entering the tank is the hydrogen exiting from the PEMWE stack, while the hydrogen outlet flow is equals to the hydrogen required by the PEMFC stack.

2.4.2 Thermal model

The energy balance equation accounts for inlet and outlet contributions and heat losses:

$$C_{th} \cdot \frac{dT}{dt} = \dot{n}_{H_2,in} \cdot h_{H_2,in} - \dot{n}_{H_2,out} \cdot h_{H_2,out} - h_{th} \cdot A_{th} \cdot (T - T_{amb}) \quad (2.118)$$

The thermal capacitance is defined as:

$$C_{th} = n \cdot c_p \quad (2.119)$$

where c_p is the specific heat of hydrogen, given by [7]:

$$c_p^0 = A + B \cdot t + C \cdot t^2 + D \cdot t^3 + \frac{E}{t^2} \quad (2.120)$$

The parameter in the equation (2.120) are the same defined in table 2.1.

The pressure in the storage tank has been defined considering the hydrogen as an ideal gas [12, 22]:

$$p = \frac{n \cdot R \cdot T}{V} \quad (2.121)$$

2.5 Sizes and parameters of components

In this section, component sizes and model parameters have been defined according to an extensive literature review. Data about component sizes have been derived from real sizes available in previous work related to DEMO 4 of the REMOTE project [28]. These values are defined in table 2.4.

Table 2.4 Model components sizes [28]

Symbol	Description	Value
$P_{n,PEMWE}$	PEMWE stack rated power	50 kW
$P_{n,PEMFC}$	PEMFC stack rated power	100 kW
$m_{H_2,max}$	Maximum storable hydrogen	100 kg
p_{max}	Maximum operating pressure in the storage	28 bar
p_{min}	Minimum operating pressure in the storage	3 bar

The number of cells of PEMWE and PEMFC stacks have been computed as:

$$n_{\text{cell}} = \frac{P_n}{P_{\text{cell,max}}} \quad (2.122)$$

where, P_n is the rated power of the stack and $P_{\text{cell,max}}$ is the maximum power of the cell. The number of cells for the PEMWE stack is resulted to be equal to 115, while for the PEMFC stack is equal to 2377.

Model parameters have been defined in sections 2.5.1 and 2.5.2. For all components, heat losses to the environment are assumed to be dominated by natural convection. Thus, the heat transfer coefficient has been considered to be equal to $5 \text{ W m}^{-2} \text{ K}^{-1}$.

2.5.1 PEMWE and PEMFC stack

Parameters for PEMWE and PEMFC, derived from an extensive research in literature, are defined in table 2.5, table 2.6 and table 2.7.

Table 2.5 Common parameters for PEMWE and PEMFC derived from literature

Symbol	Description	Value	Reference
C_{el}	Electric double layer capacitance	6,6218 F	[17]
$k_{\text{O,A}}$	Outlet flow coefficient at the anode	$5,965 \times 10^{-6} \text{ mol Pa}^{-1} \text{ s}^{-1}$	[17]
$k_{\text{O,C}}$	Outlet flow coefficient at the cathode	$8,547 \times 10^{-6} \text{ mol Pa}^{-1} \text{ s}^{-1}$	[17]
K_{darcy}	Membrane permeability to water	$1,58 \times 10^{-18} \text{ m}^2$	[8, 9]
A_{cell}	Area of the cell	110 cm^2	[27]
A_{th}	Heat transfer area	110 cm^2	[27]
V_{A}	Volume of anode	$7,59 \times 10^{-4} \text{ m}^3$	[27]
V_{C}	Volume of cathode	$7,59 \times 10^{-4} \text{ m}^3$	[27]
t_{A}	Thickness of anode	$3,65 \times 10^{-4} \text{ m}$	[29]
t_{C}	Thickness of cathode	$3,65 \times 10^{-4} \text{ m}$	[29]
t_{me}	Thickness of membrane	$175 \mu\text{m}$	[29, 30]

Table 2.6 PEMWE parameters derived from literature

Symbol	Description	Value	Reference
C_{th}	Thermal capacitance	8232 J/K	[6]
f_1	Faraday's efficiency empirical coefficient	2 000 A ² /m ⁴	[22]
f_2	Faraday's efficiency empirical coefficient	0,93	[22]
ϵ	Porosity of electrodes	0,3	[8]

Table 2.7 PEMFC parameters derived from literature

Symbol	Description	Value	Reference
C_{th}	Thermal capacity	11 005 J/K	[22]
ϵ	Porosity of electrodes	0,4	[25]
$RH_{A,in}$	Relative humidity at the anode inlet	100%	[25]
$RH_{C,in}$	Relative humidity at the cathode inlet	100%	[25]
λ_{H_2}	Excess of hydrogen	2	[25]
λ_{air}	Excess of air	2	[25]

2.5.2 Storage tank

The dimensions of the storage tank have been estimated by using data from previous work on REMOTE project [28] (see table 2.4). The volume of the tank has been estimated considering the maximum amount of hydrogen that can be stored in the condition of fully charge tank, at the maximum operating pressure. It has been evaluated as follow:

$$V = \frac{m_{H_2,max}}{\rho_{H_2}(p_{max})} \quad (2.123)$$

Once the volume needed for fully charge tank has been evaluated, actual dimensions have been calculated. More in detail, it has been assumed a cylindrical tank with dimensions defined in table 2.8. Thus, actual volume and heat transfer area of the tank has been computed as:

$$V = \frac{\pi}{4} \cdot D^2 \cdot H \quad (2.124)$$

$$A_{th} = \pi \cdot D \cdot H + 2 \cdot \frac{\pi}{4} \cdot D^2 \quad (2.125)$$

Table 2.8 Storage tank parameters

Symbol	Description	Value
D	Diameter	2,5 m
H	Height	9,5 m
A_{th}	Heat transfer area	84,43 m ²
V	Volume of the tank	46,633 m ³

2.6 Model control strategies

Different control strategies have been implemented in order to simulate also particular conditions (i.e. curtailment and possible backup system intervention).

As told in sections 2.2.2.1 and 2.3.3, temperature controls for PEMWE and PEMFC stacks have been included using PID control blocks in the model, in order to quantify the flow rate of coolant needed to avoid the temperature to go beyond a certain target value, which has been set to be equal to 60 °C.

Curtailment of surplus power can occur in two different situations during the charging phase and it can be either total or partial curtailment. Total curtailment takes place when the pressure in the storage tank reach the maximum value, while partial curtailment occurs when surplus power is higher than rated power of the PEMWE stack. In the case of total curtailment, the curtailed power is equals to surplus power, while for partial curtailment it is equal to the difference between surplus power and rated power of the PEMWE stack (see table 2.9).

Table 2.9 Control strategies in case of curtailment

Case	Condition	Curtailed power
Total curtailment	$p_{storage} > p_{max}$	$P_{curtailed} = P_{surplus}$
Partial curtailment	$P_{surplus} > P_{n,PEMWE}$	$P_{curtailed} = P_{surplus} - P_{n,PEMWE}$

When the P2P system is not able to cover either partially or totally the load during discharging phase, the backup system (i.e. diesel generators) comes into operation. The load is totally covered by the backup system when the pressure in the storage tank reach the minimum value, while there is only a partial contribution of the backup when the power deficit required by the load is higher than the rated power of the PEMFC stack. In the case of load totally covered by the backup system the power supplied by the backup is equal to the power deficit, while it is equal to the difference between power deficit and rated power of the PEMFC stack in case of partial contribution of the backup system (see table 2.10).

Table 2.10 Control strategy in the case of backup system intervention

Case	Condition	Backup power
Load totally covered by backup	$p_{\text{storage}} < p_{\text{min}}$	$P_{\text{backup}} = P_{\text{deficit}}$
Load partially covered by backup	$P_{\text{deficit}} > P_{\text{n,PEMFC}}$	$P_{\text{backup}} = P_{\text{deficit}} - P_{\text{n,PEMFC}}$

Even if this last condition is very rare, it has been considered to have a more flexible model able to simulate also less frequent behaviour of the system.

3 Validation

Since experimental data were not available, the validation has been done considering validated results from literature. The validation has been performed for the PEMWE and the PEMFC. More in detail, the validation has been performed by using polarization curves of both PEMWE and PEMFC from validated models available in literature [15, 31], evaluated at operating conditions similar to those considered in this work. Temperature at which these curves have been evaluated is 60 °C, while the pressure is about 28 bar for the PEMWE and about ambient pressure for the PEMFC.

The validation is performed by using the Simulink Design Optimization Toolbox, more precisely the Simulink Parameter Estimator tool. This tool is used to minimize a certain cost function, namely the so-called sum squared error (SSE) defined as [32]:

$$SSE = \sum_{i=1}^n (x_{\text{ref},i} - x_{\text{sim},i})^2 \quad (3.1)$$

where:

- x_{ref} is the reference value taken from literature;
- x_{sim} is the value obtained by the model simulation.

The cost function minimization is performed at each iteration by varying the values of fitting parameters considered for the validation, that are:

- Anode and cathode exchange current densities;
- Anode and cathode charge transfer coefficients.

3.1 PEMWE

The polarization curve considered for the PEMWE is derived according to the polarization curve computed by Frensch et al. [31] (see figure 3.1). Values of fitting parameters have been defined in table 3.1.

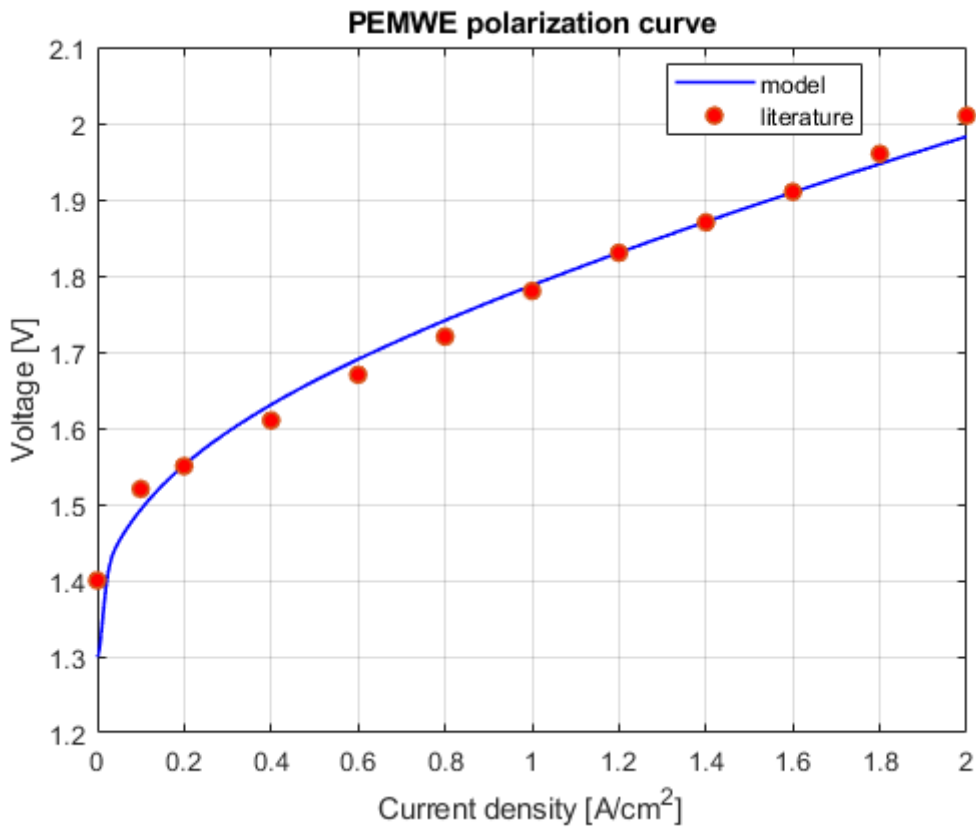


Figure 3.1 Validation of PEMWE polarization curve evaluated at 28 bar and 60 °C

Table 3.1 PEMWE fitting parameters estimated by the tool

Symbol	Description	Value
α_A	Charge transfer coefficient at the anode	2,491
α_C	Charge transfer coefficient at the cathode	0,445
$i_{0,A}$	Exchange current density at the anode	$1,634 \times 10^{-5} \text{ A/cm}^2$
$i_{0,C}$	Exchange current density at the cathode	$5,445 \times 10^{-2} \text{ A/cm}^2$

The value of the minimized cost function is 0,003 250 6.

3.2 PEMFC

The polarization curve considered for the PEMFC is derived according to the polarization curve computed by Musio et al. [15] (see figure 3.2). Values of fitting parameters have been defined in table 3.2.

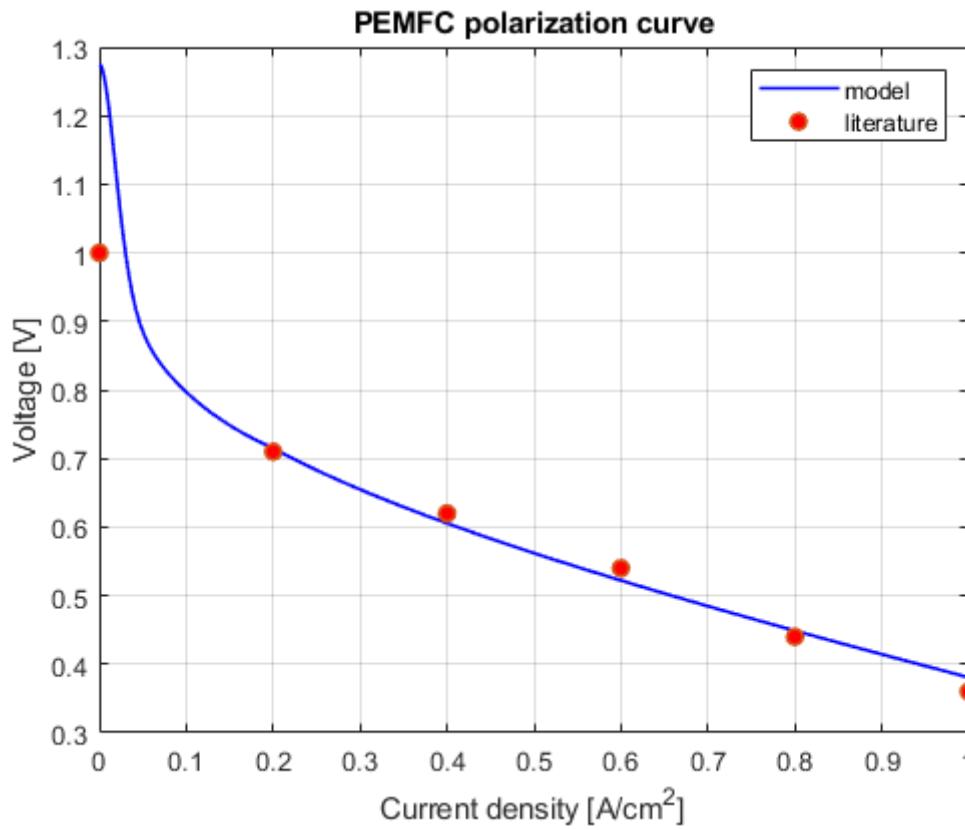


Figure 3.2 Validation of PEMFC polarization curve evaluated at ambient pressure and 60 °C

Table 3.2 PEMFC fitting parameters estimated by the tool

Symbol	Description	Value
α_A	Charge transfer coefficient at the anode	0,507
α_C	Charge transfer coefficient at the cathode	0,846
$i_{0,A}$	Exchange current density at the anode	$2,277 \times 10^{-2} \text{ A/cm}^2$
$i_{0,C}$	Exchange current density at the cathode	$2,121 \times 10^{-6} \text{ A/cm}^2$

The value of the minimized cost function is 0,076 956.

4 Results

The results analysis has been carried out by evaluating the behaviour of such system on several days throughout the year to evaluate the system response to different power profiles associated to both demand and production. More in detail, it has been considered an analysis based on two days per month (i.e. working day and non-working day). In addition to the main simulation results, further analyses have been performed concerning the optimal sizing of RES systems, the evaluation of the use of curtailed energy for local hydrogen mobility, the assessment of costs related to different sizes of RES systems and the comparisons of volumes, weights and costs associated to hydrogen and battery energy storage systems.

Power profiles used in the simulations have been taken from data related to RES production and energy load of the DEMO 4 of the REMOTE project, namely the installation located in Froan/Rye Islands in Norway. As told in the introduction, this is the installation considered for the model simulation this work.

In order to evaluate the performance of P2P system, useful quantities have been calculated by post-processing the simulation results. Such quantities are the Key Performance Indicators (KPI), which have been derived from deliverables of the REMOTE project available on the website [2] and defined in table 4.1.

Table 4.1 List of KPI

KPI	Description	Definition
KPI 1	Load directly covered by RES	$\frac{E_{\text{RES-to-Load}}}{E_{\text{Load,tot}}}$
KPI 2	Load covered by the fuel cell	$\frac{E_{\text{PEMFC}}}{E_{\text{Load,tot}}}$
KPI 3	Load covered by the backup system	$\frac{E_{\text{Backup}}}{E_{\text{Load,tot}}}$
KPI 4	RES directly sent to the load	$\frac{E_{\text{RES-to-Load}}}{E_{\text{RES,tot}}}$
KPI 5	RES sent to the electrolyzer	$\frac{E_{\text{PEMWE}}}{E_{\text{RES,tot}}}$
KPI 6	RES to curtailment	$\frac{E_{\text{Curtailed}}}{E_{\text{RES,tot}}}$
KPI 7	Surplus RES to electrolyzer	$\frac{E_{\text{PEMWE}}}{E_{\text{Surplus}}}$
KPI 8	Surplus RES to curtailment	$\frac{E_{\text{Curtailed}}}{E_{\text{Surplus}}}$

KPI are energy related parameters. The energy terms have been computed by integrating in time the power profiles resulted from the model simulation. Such integration has been performed as follow:

$$E = \sum_{i=1}^{n-1} \frac{P_{i+1} + P_i}{2} \cdot (t_{i+1} - t_i) \quad (4.1)$$

where, n is the number of seconds in a day and t represent the time expressed in s. Each energy term is defined in table 4.2.

Table 4.2 Description of the energy terms

Symbol	Description
$E_{RES,tot}$	Total energy produced by RES
$E_{Load,tot}$	Total energy required by load
$E_{RES-to-Load}$	Energy directly sent from RES to load
$E_{Surplus}$	Energy surplus
E_{PEMWE}	Energy to PEMWE
E_{PEMFC}	Energy from PEMFC
$E_{Curtailed}$	Curtailed energy
E_{Backup}	Energy from backup generators

4.1 Main simulation results

In this section, the main results of the simulations have been reported. More in detail, for each simulation, the results consist of a figure showing the evolution over time of power profiles and the pressure in the storage tank and a table showing the computed KPI.

4.1.1 Working day in January

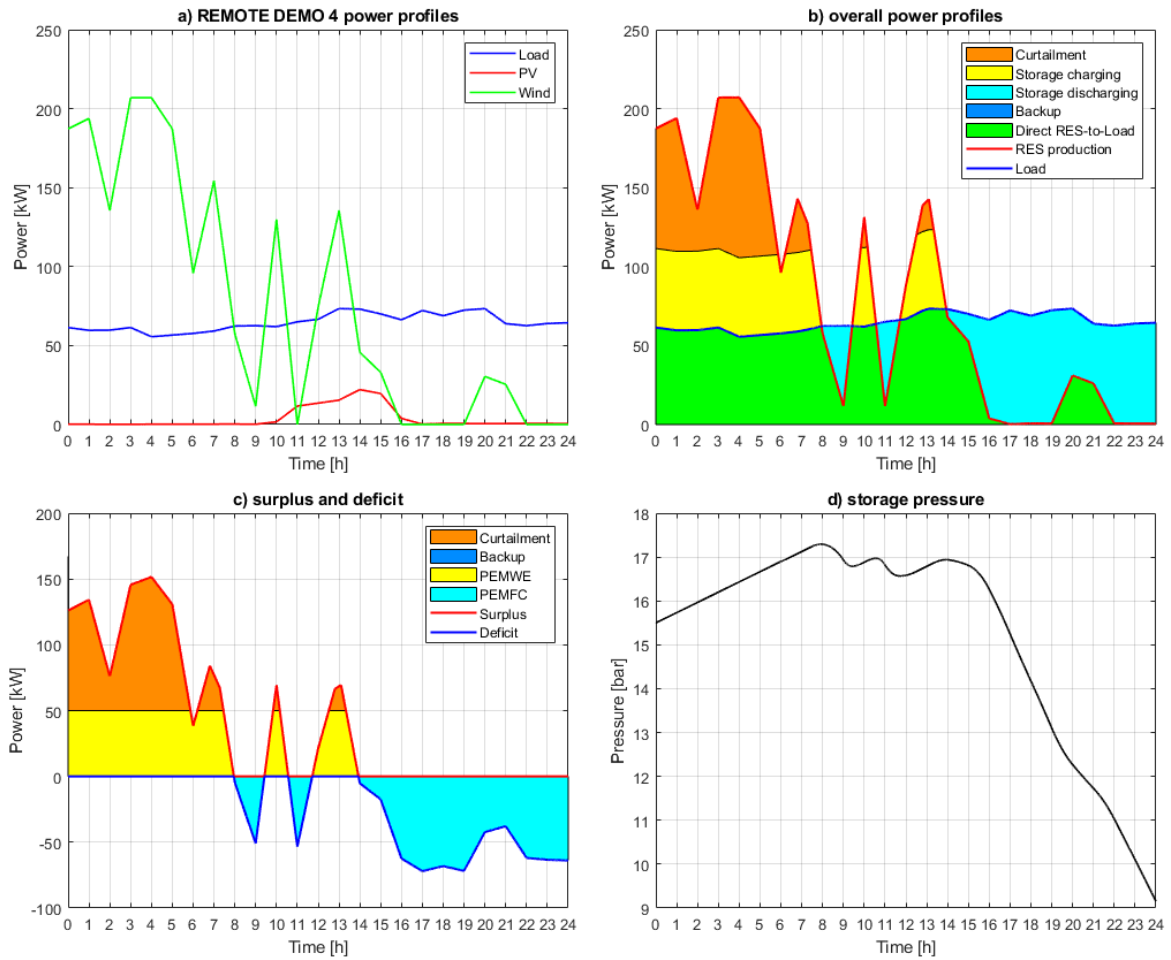


Figure 4.1 Simulation results on a working day in January: a) RES and load power profiles b) overall power profiles, c) surplus and deficit, d) storage pressure.

Table 4.3 KPI values on a working day in January

KPI	Description	Value
KPI 1	Load directly covered by RES	61%
KPI 2	Load covered by the fuel cell	39%
KPI 3	Load covered by the backup system	0%
KPI 4	RES directly sent to the load	50%
KPI 5	RES sent to the electrolyzer	26%
KPI 6	RES to curtailment	24%
KPI 7	Surplus RES to electrolyzer	52%
KPI 8	Surplus RES to curtailment	48%

4.1.2 Non-working day in January

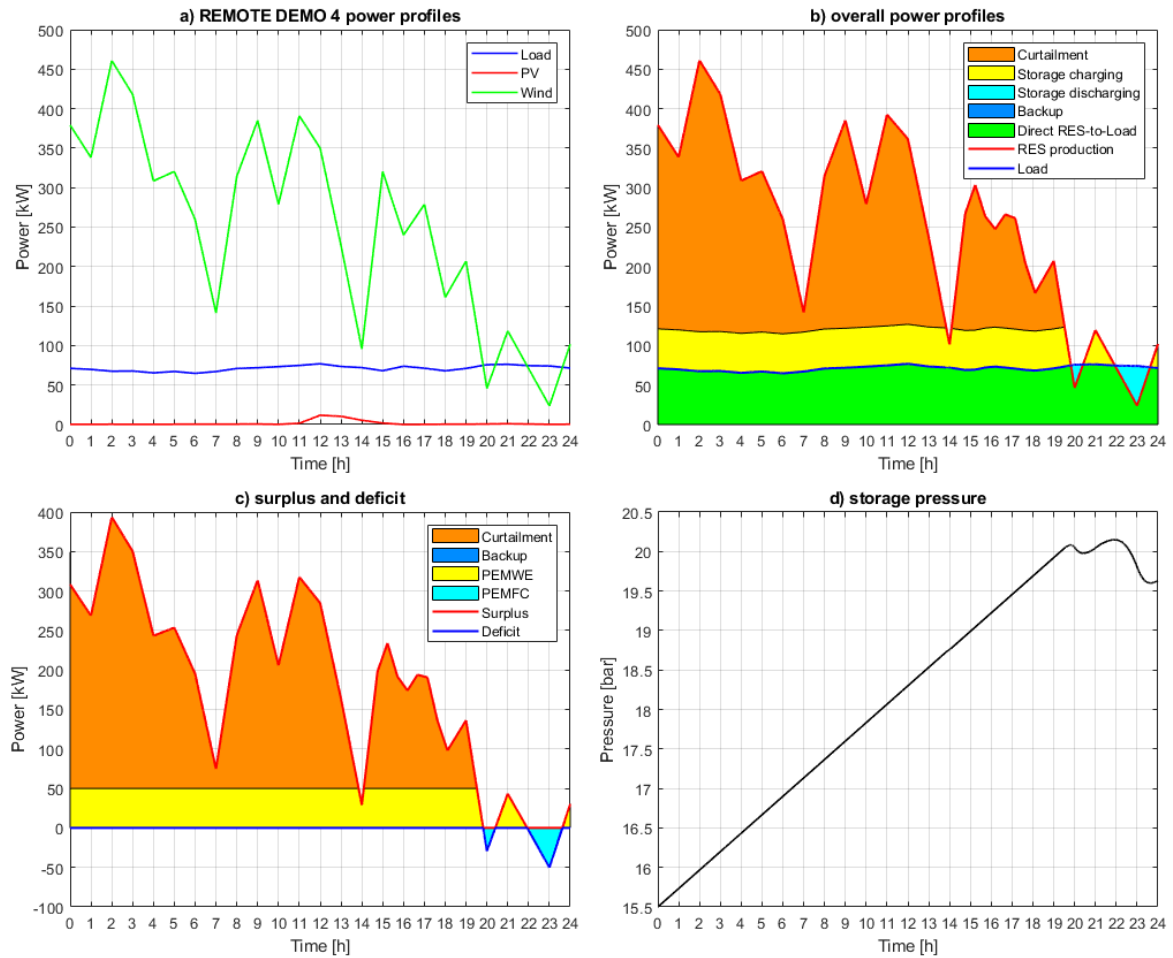


Figure 4.2 Simulation results on a non-working day in January: a) RES and load power profiles b) overall power profiles, c) surplus and deficit, d) storage pressure.

Table 4.4 KPI values on a non-working day in January

KPI	Description	Value
KPI 1	Load directly covered by RES	97%
KPI 2	Load covered by the fuel cell	3%
KPI 3	Load covered by the backup system	0%
KPI 4	RES directly sent to the load	27%
KPI 5	RES sent to the electrolyzer	17%
KPI 6	RES to curtailment	56%
KPI 7	Surplus RES to electrolyzer	23%
KPI 8	Surplus RES to curtailment	77%

4.1.3 Working day in February

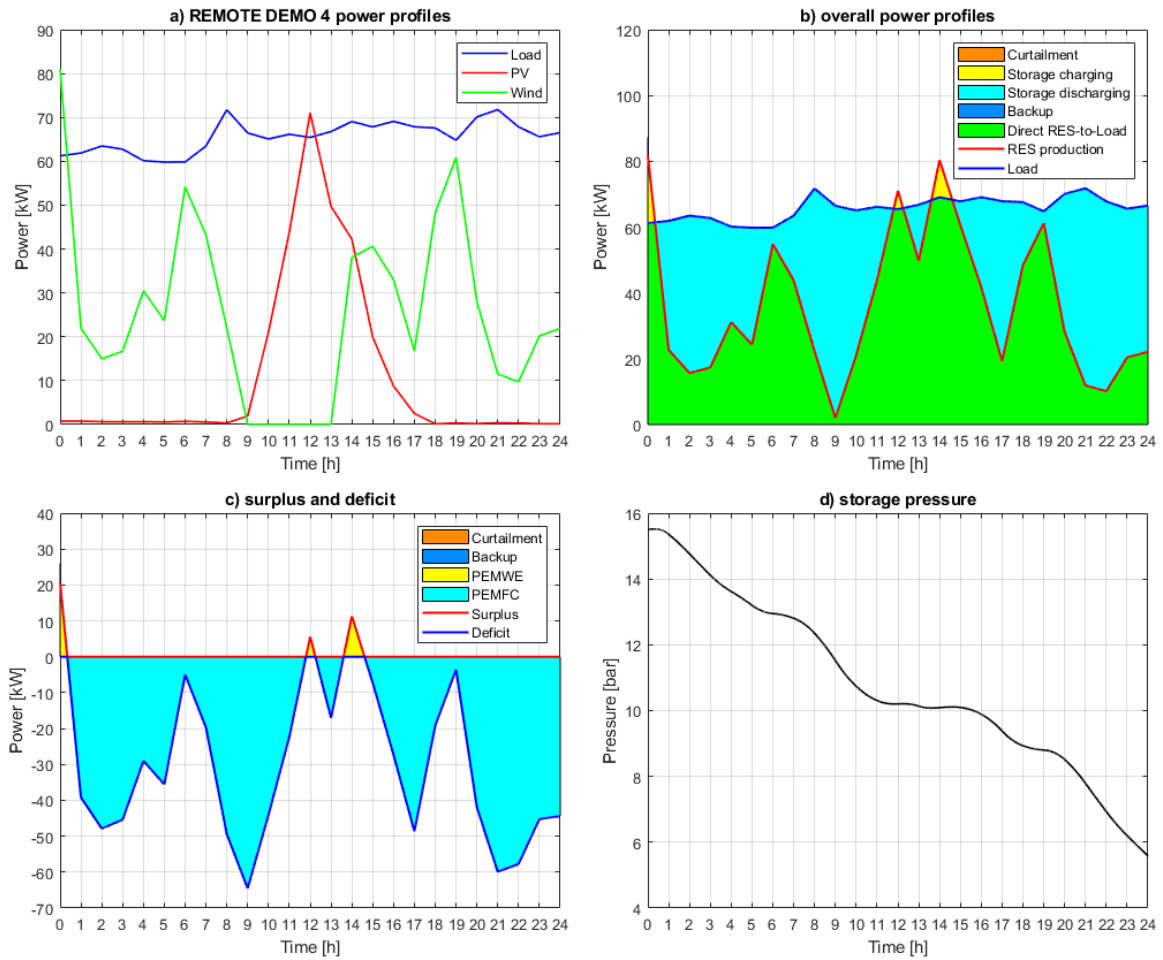


Figure 4.3 Simulation results on a working day in February: a) RES and load power profiles b) overall power profiles, c) surplus and deficit, d) storage pressure.

Table 4.5 KPI values on a working day in February

KPI	Description	Value
KPI 1	Load directly covered by RES	53%
KPI 2	Load covered by the fuel cell	47%
KPI 3	Load covered by the backup system	0%
KPI 4	RES directly sent to the load	99%
KPI 5	RES sent to the electrolyzer	1%
KPI 6	RES to curtailment	0%
KPI 7	Surplus RES to electrolyzer	100%
KPI 8	Surplus RES to curtailment	0%

4.1.4 Non-working day in February

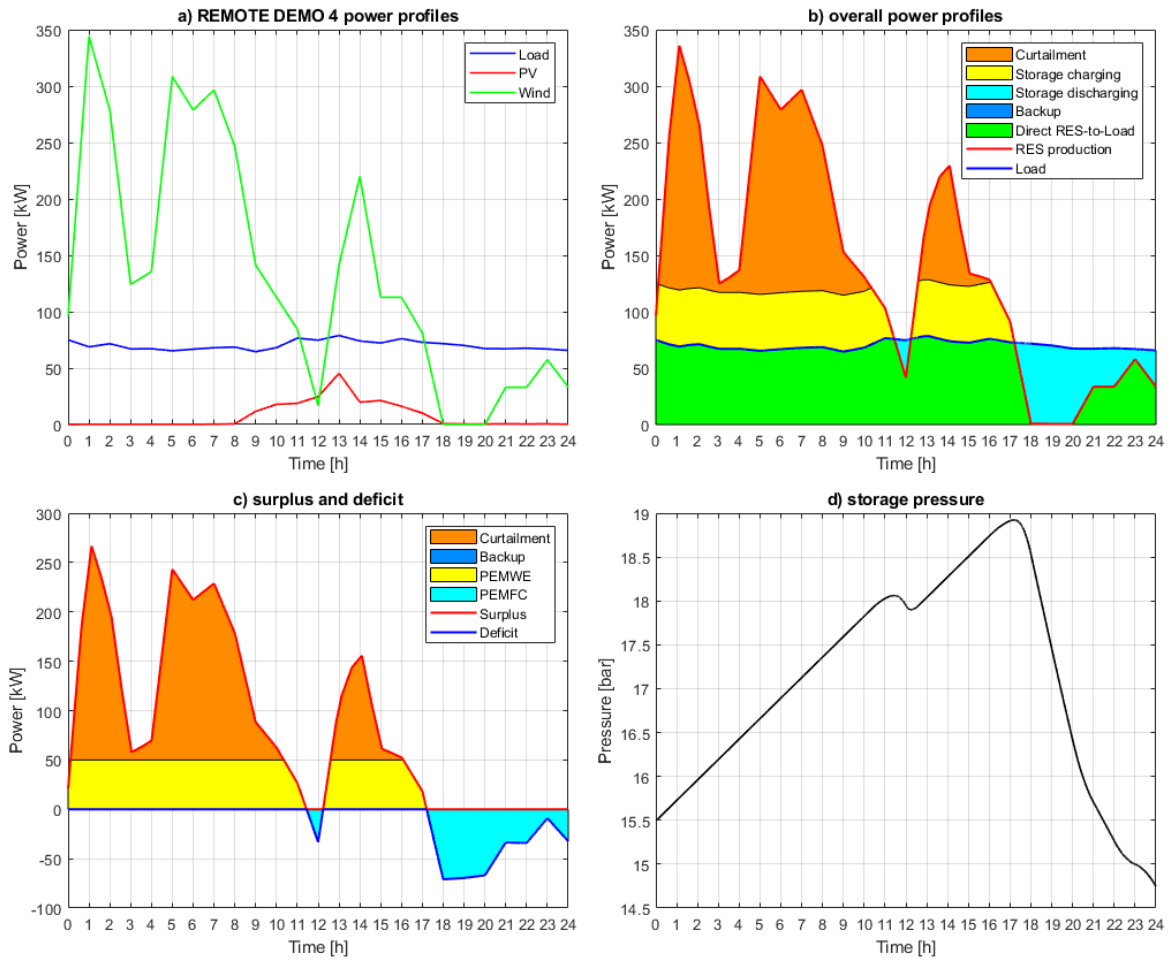


Figure 4.4 Simulation results on a non-working day in February: a) RES and load power profiles b) overall power profiles, c) surplus and deficit, d) storage pressure.

Table 4.6 KPI values on a non-working day in February

KPI	Description	Value
KPI 1	Load directly covered by RES	82%
KPI 2	Load covered by the fuel cell	18%
KPI 3	Load covered by the backup system	0%
KPI 4	RES directly sent to the load	40%
KPI 5	RES sent to the electrolyzer	23%
KPI 6	RES to curtailment	37%
KPI 7	Surplus RES to electrolyzer	38%
KPI 8	Surplus RES to curtailment	62%

4.1.5 Working day in March

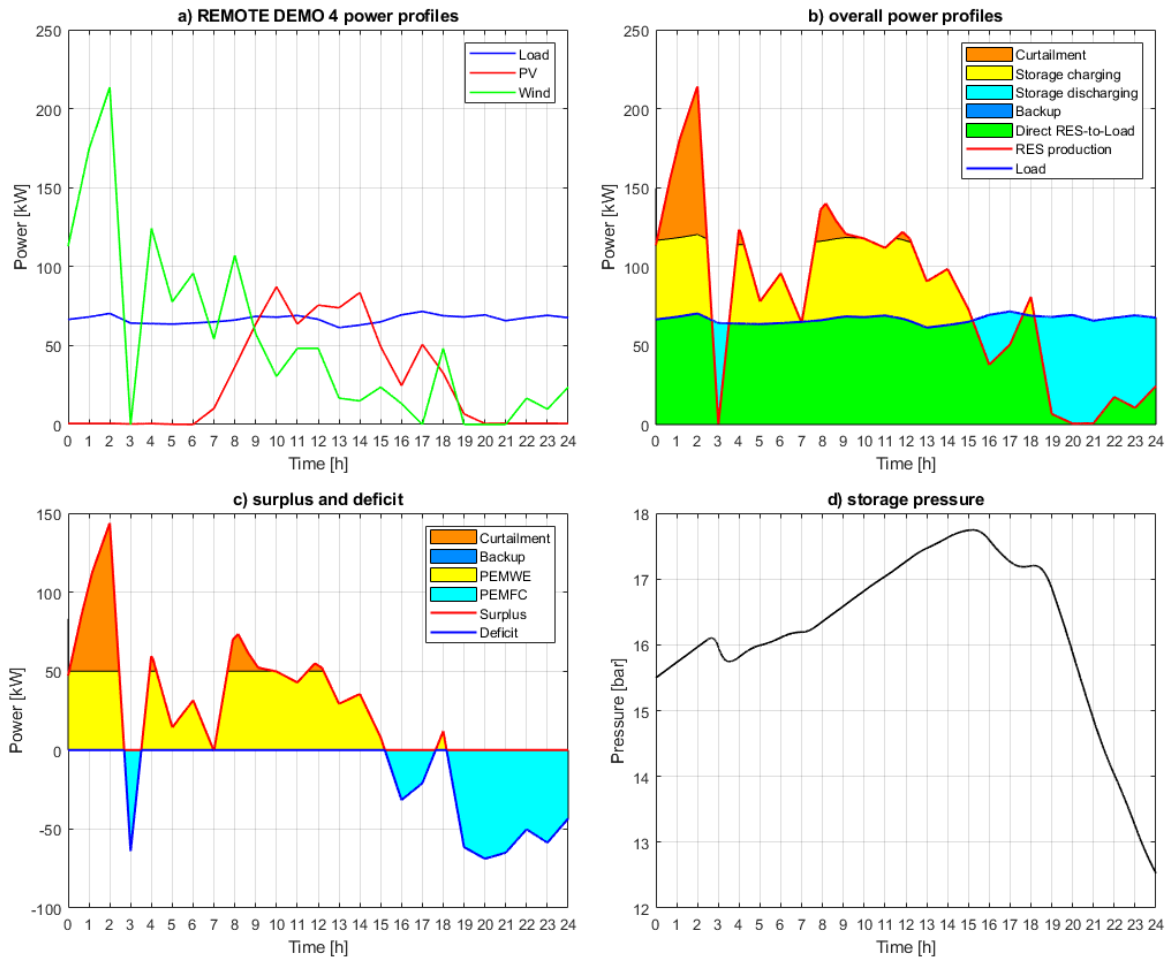


Figure 4.5 Simulation results on a working day in March: a) RES and load power profiles b) overall power profiles, c) surplus and deficit, d) storage pressure.

Table 4.7 KPI values on a working day in March

KPI	Description	Value
KPI 1	Load directly covered by RES	76%
KPI 2	Load covered by the fuel cell	24%
KPI 3	Load covered by the backup system	0%
KPI 4	RES directly sent to the load	63%
KPI 5	RES sent to the electrolyzer	29%
KPI 6	RES to curtailment	8%
KPI 7	Surplus RES to electrolyzer	79%
KPI 8	Surplus RES to curtailment	21%

4.1.6 Non-working day in March

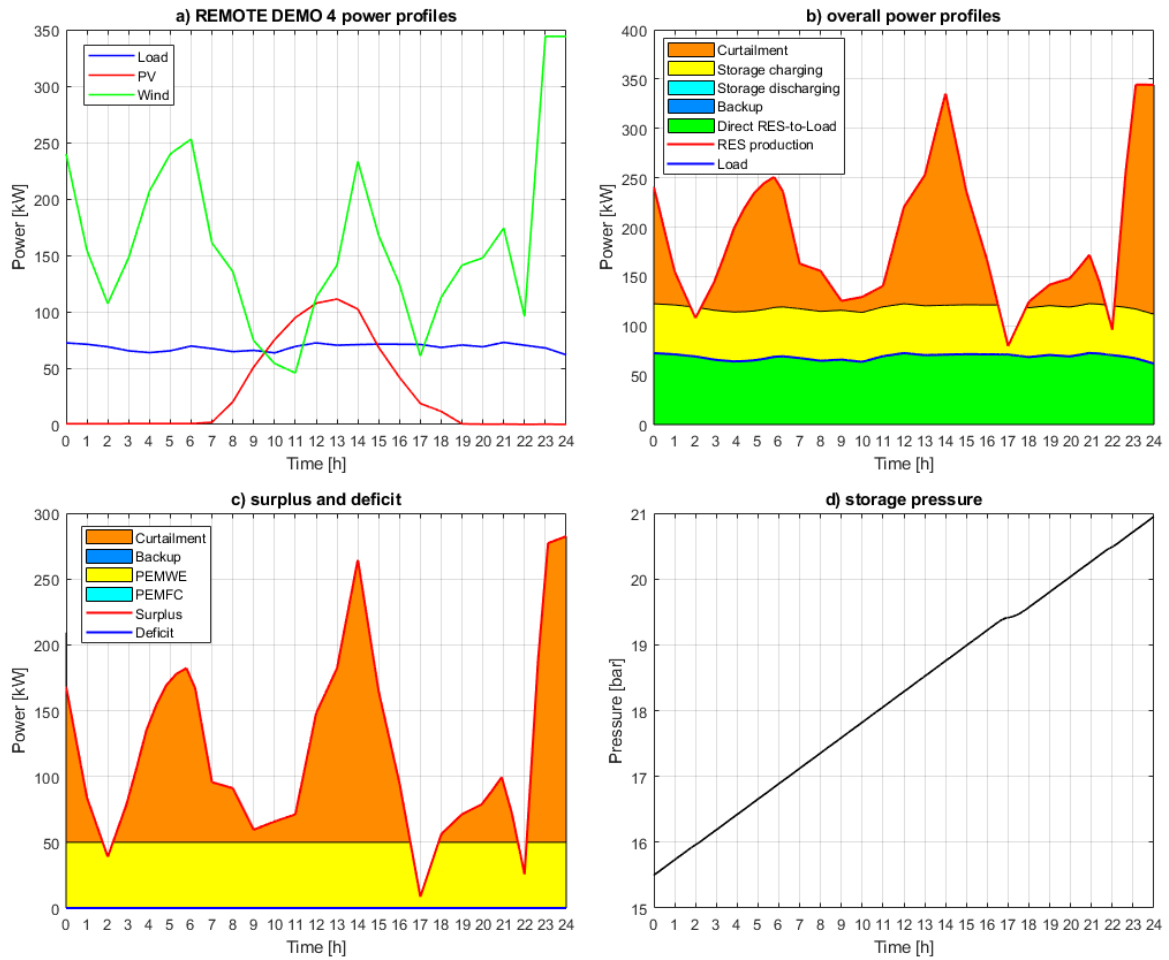


Figure 4.6 Simulation results on a non-working day in March: a) RES and load power profiles, b) overall power profiles, c) surplus and deficit, d) storage pressure.

Table 4.8 KPI values on a non-working day in March

KPI	Description	Value
KPI 1	Load directly covered by RES	100%
KPI 2	Load covered by the fuel cell	0%
KPI 3	Load covered by the backup system	0%
KPI 4	RES directly sent to the load	37%
KPI 5	RES sent to the electrolyzer	26%
KPI 6	RES to curtailment	37%
KPI 7	Surplus RES to electrolyzer	42%
KPI 8	Surplus RES to curtailment	58%

4.1.7 Working day in April

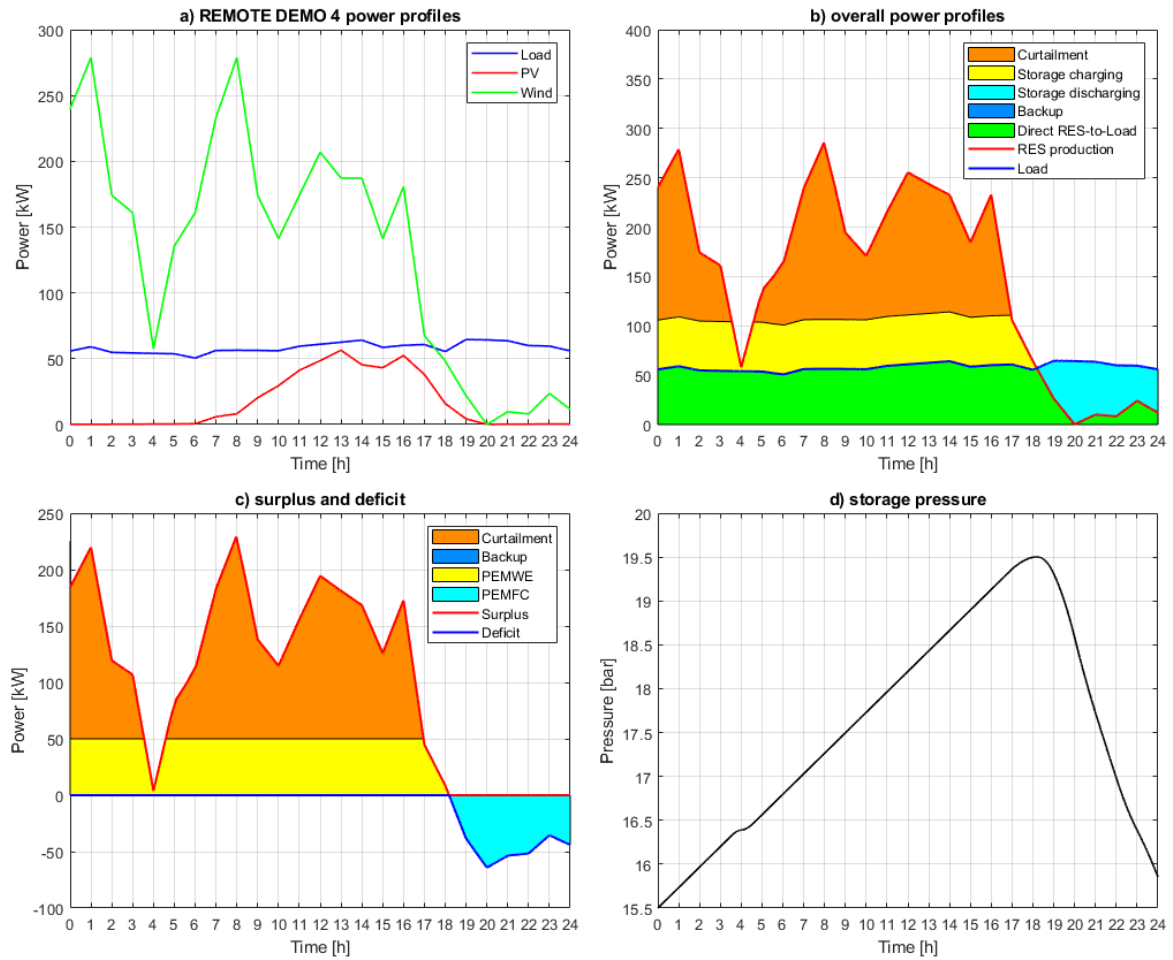


Figure 4.7 Simulation results on a working day in April: a) RES and load power profiles b) overall power profiles, c) surplus and deficit, d) storage pressure.

Table 4.9 KPI values on a working day in April

KPI	Description	Value
KPI 1	Load directly covered by RES	81%
KPI 2	Load covered by the fuel cell	19%
KPI 3	Load covered by the backup system	0%
KPI 4	RES directly sent to the load	32%
KPI 5	RES sent to the electrolyzer	24%
KPI 6	RES to curtailment	44%
KPI 7	Surplus RES to electrolyzer	35%
KPI 8	Surplus RES to curtailment	65%

4.1.8 Non-working day in April

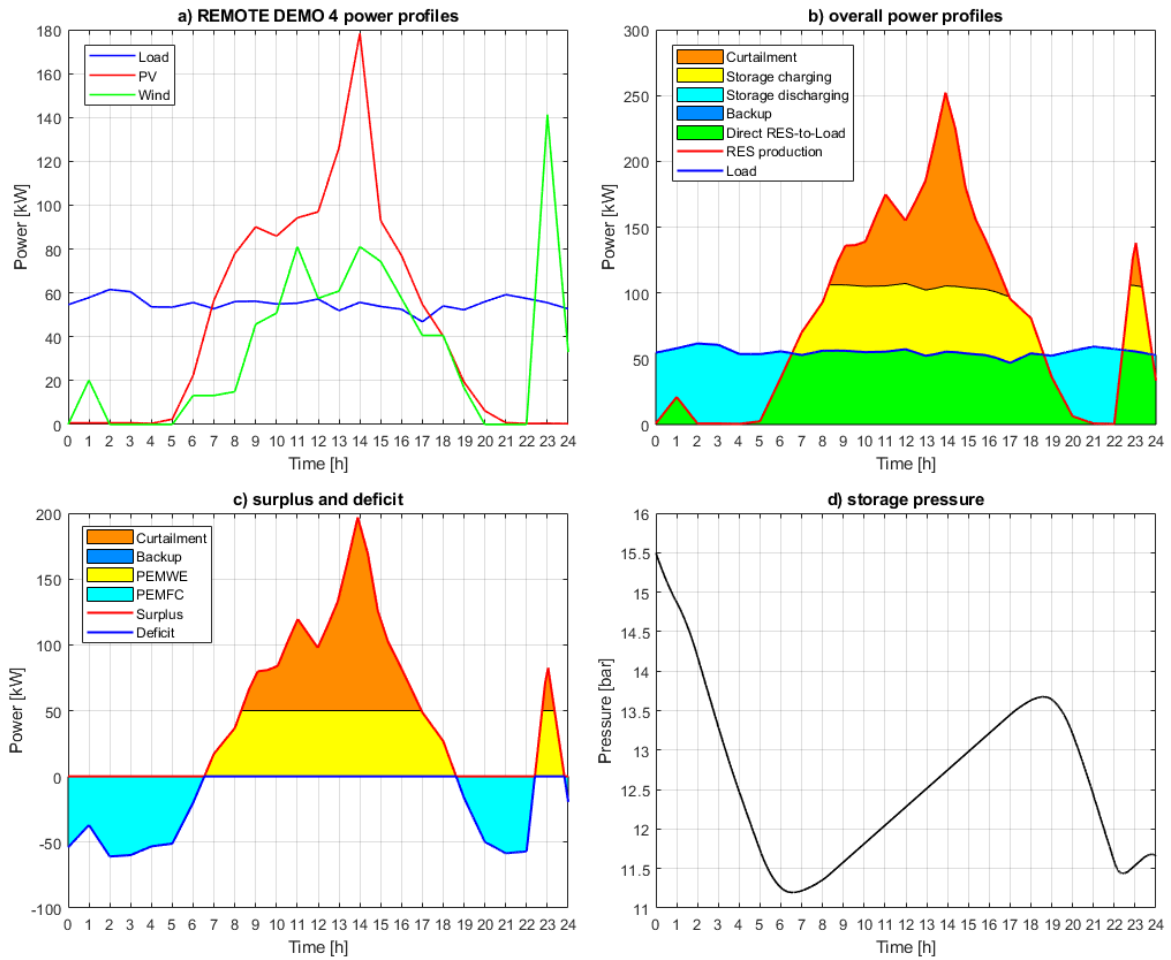


Figure 4.8 Simulation results on a non-working day in April: a) RES and load power profiles, b) overall power profiles, c) surplus and deficit, d) storage pressure.

Table 4.10 KPI values on a non-working day in April

KPI	Description	Value
KPI 1	Load directly covered by RES	65%
KPI 2	Load covered by the fuel cell	35%
KPI 3	Load covered by the backup system	0%
KPI 4	RES directly sent to the load	44%
KPI 5	RES sent to the electrolyzer	30%
KPI 6	RES to curtailment	26%
KPI 7	Surplus RES to electrolyzer	53%
KPI 8	Surplus RES to curtailment	47%

4.1.9 Working day in May

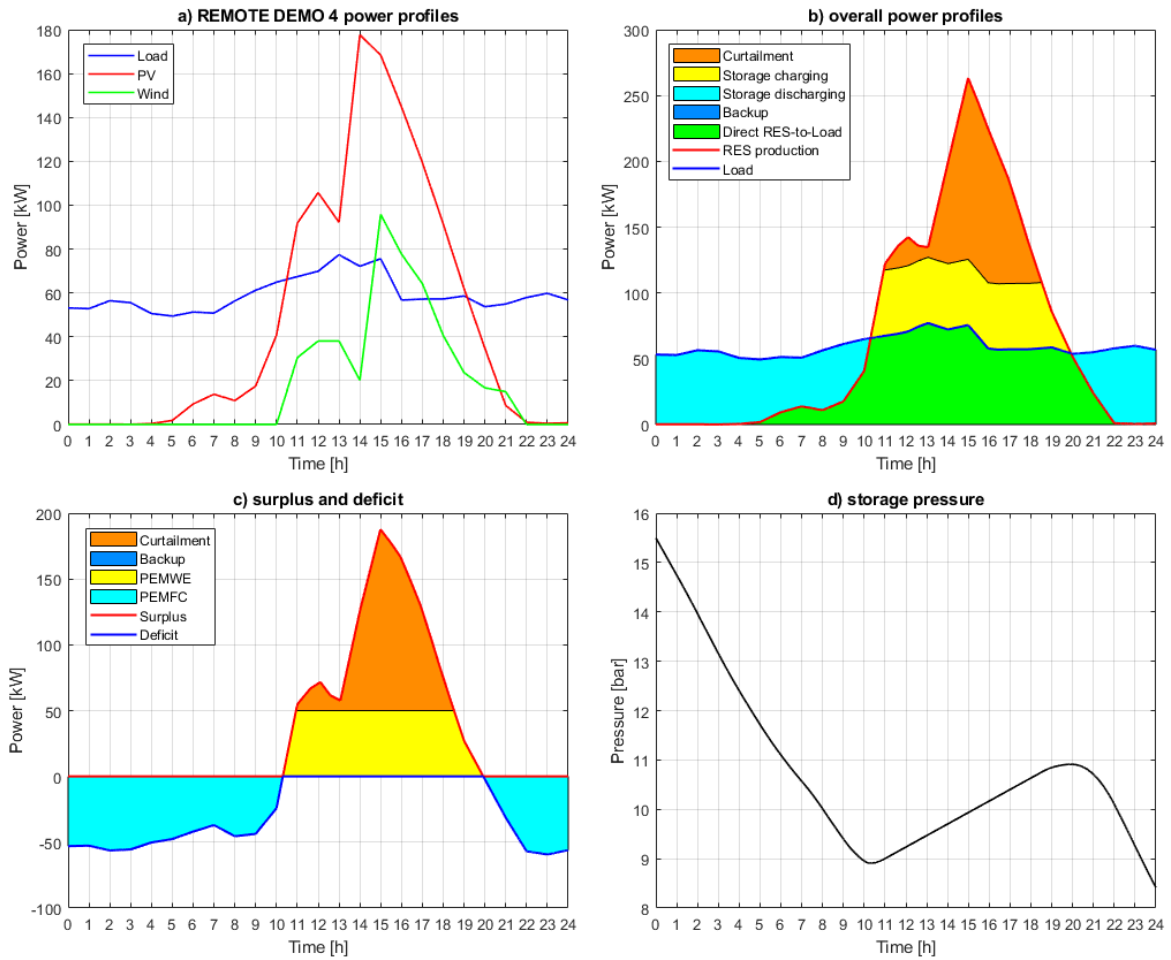


Figure 4.9 Simulation results on a working day in May: a) RES and load power profiles b) overall power profiles, c) surplus and deficit, d) storage pressure.

Table 4.11 KPI values on a working day in May

KPI	Description	Value
KPI 1	Load directly covered by RES	54%
KPI 2	Load covered by the fuel cell	46%
KPI 3	Load covered by the backup system	0%
KPI 4	RES directly sent to the load	47%
KPI 5	RES sent to the electrolyzer	26%
KPI 6	RES to curtailment	27%
KPI 7	Surplus RES to electrolyzer	48%
KPI 8	Surplus RES to curtailment	52%

4.1.10 Non-working day in May

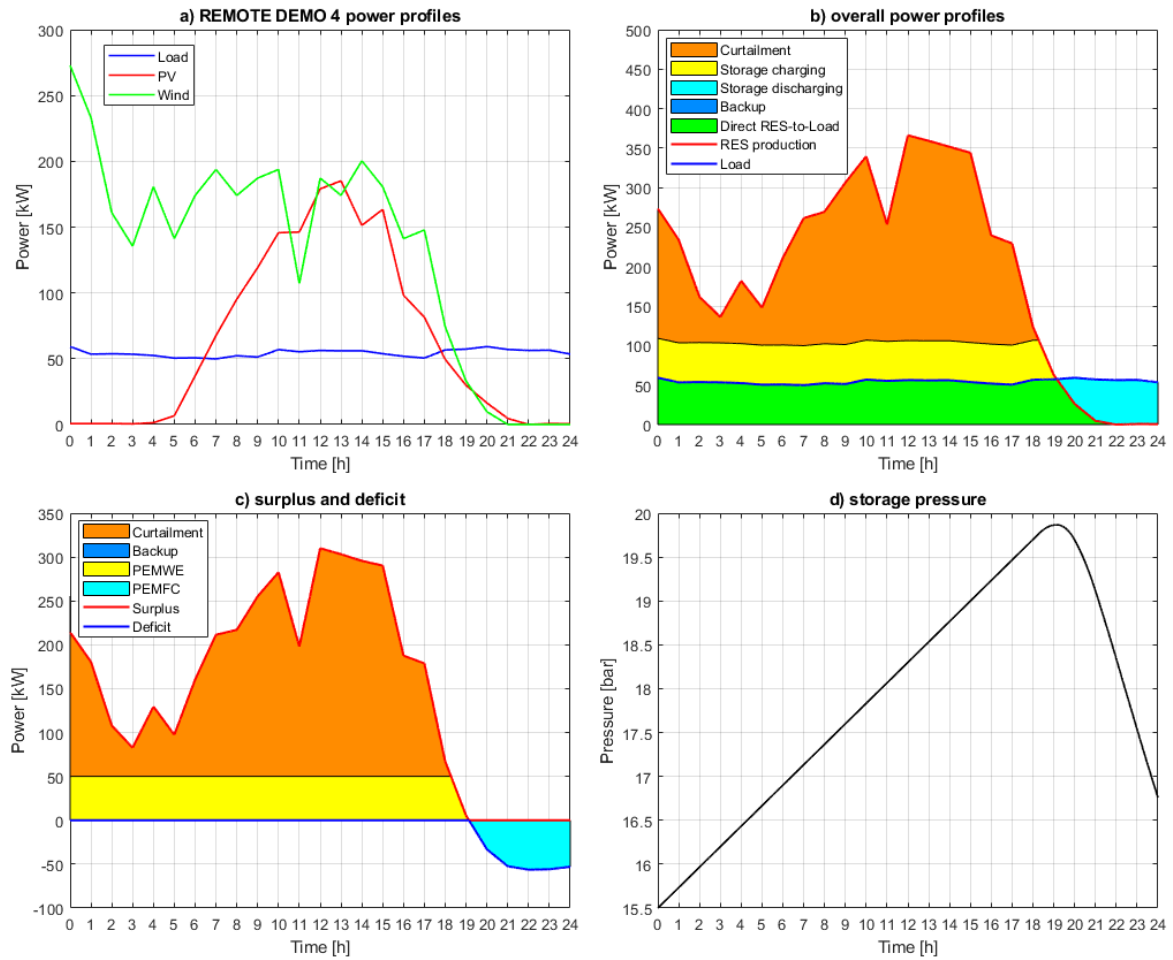


Figure 4.10 Simulation results on a non-working day in May: a) RES and load power profiles, b) overall power profiles, c) surplus and deficit, d) storage pressure.

Table 4.12 KPI values on a non-working day in May

KPI	Description	Value
KPI 1	Load directly covered by RES	83%
KPI 2	Load covered by the fuel cell	17%
KPI 3	Load covered by the backup system	0%
KPI 4	RES directly sent to the load	23%
KPI 5	RES sent to the electrolyzer	20%
KPI 6	RES to curtailment	57%
KPI 7	Surplus RES to electrolyzer	25%
KPI 8	Surplus RES to curtailment	75%

4.1.11 Working day in June

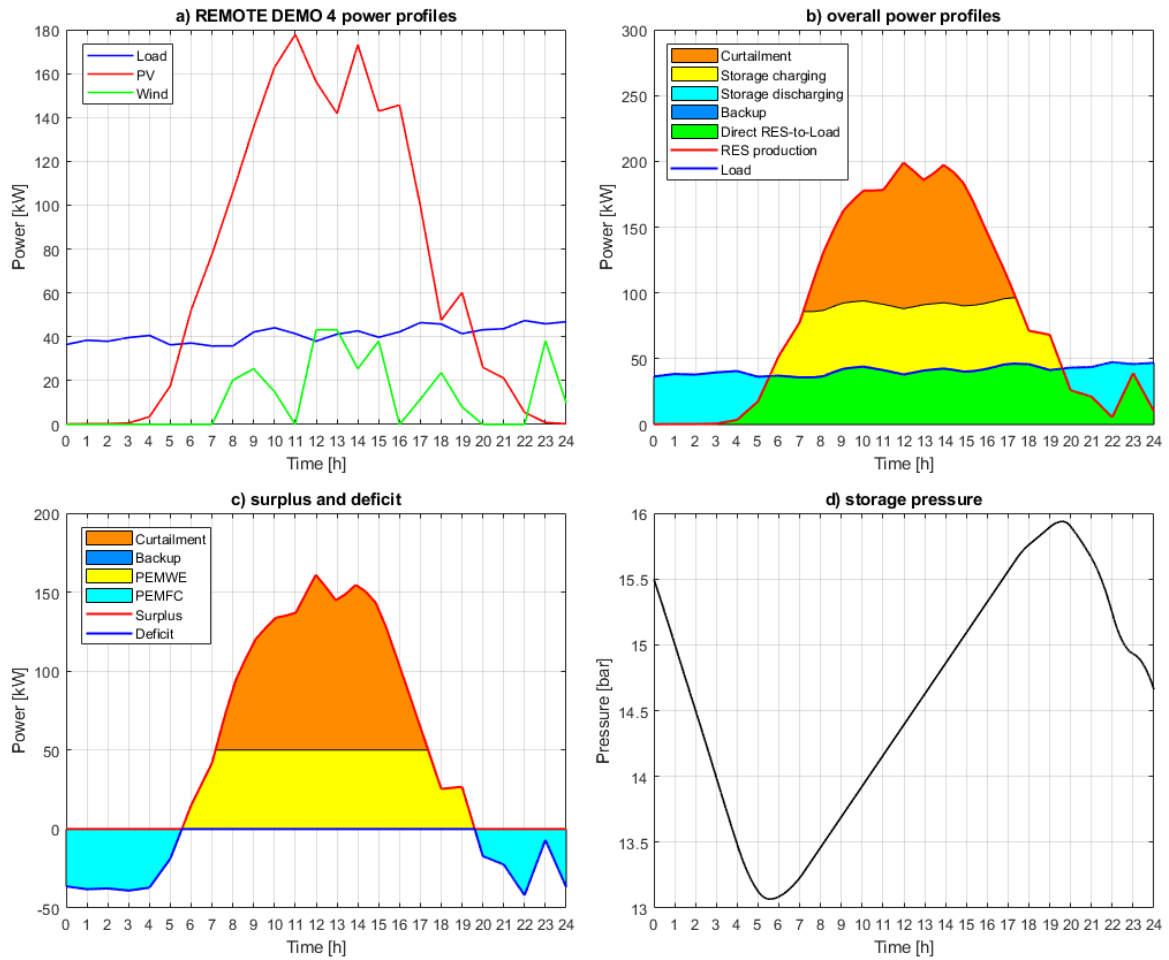


Figure 4.11 Simulation results on a working day in June: a) RES and load power profiles b) overall power profiles, c) surplus and deficit, d) storage pressure.

Table 4.13 KPI values on a working day in June

KPI	Description	Value
KPI 1	Load directly covered by RES	71%
KPI 2	Load covered by the fuel cell	29%
KPI 3	Load covered by the backup system	0%
KPI 4	RES directly sent to the load	34%
KPI 5	RES sent to the electrolyzer	30%
KPI 6	RES to curtailment	36%
KPI 7	Surplus RES to electrolyzer	45%
KPI 8	Surplus RES to curtailment	55%

4.1.12 Non-working day in June

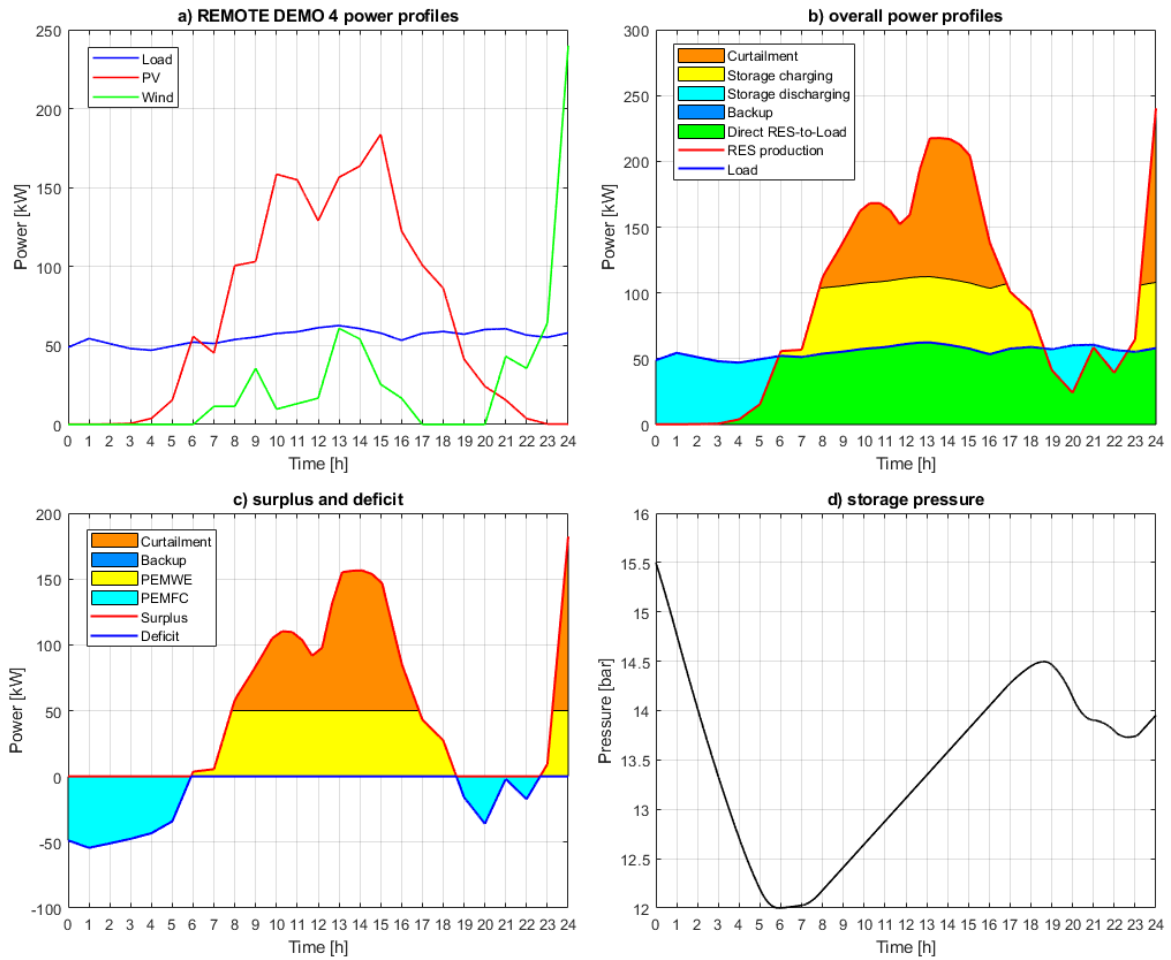


Figure 4.12 Simulation results on a non-working day in June: a) RES and load power profiles b) overall power profiles, c) surplus and deficit, d) storage pressure.

Table 4.14 KPI values on a non-working day in June

KPI	Description	Value
KPI 1	Load directly covered by RES	76%
KPI 2	Load covered by the fuel cell	24%
KPI 3	Load covered by the backup system	0%
KPI 4	RES directly sent to the load	47%
KPI 5	RES sent to the electrolyzer	26%
KPI 6	RES to curtailment	27%
KPI 7	Surplus RES to electrolyzer	49%
KPI 8	Surplus RES to curtailment	50%

4.1.13 Working day in July

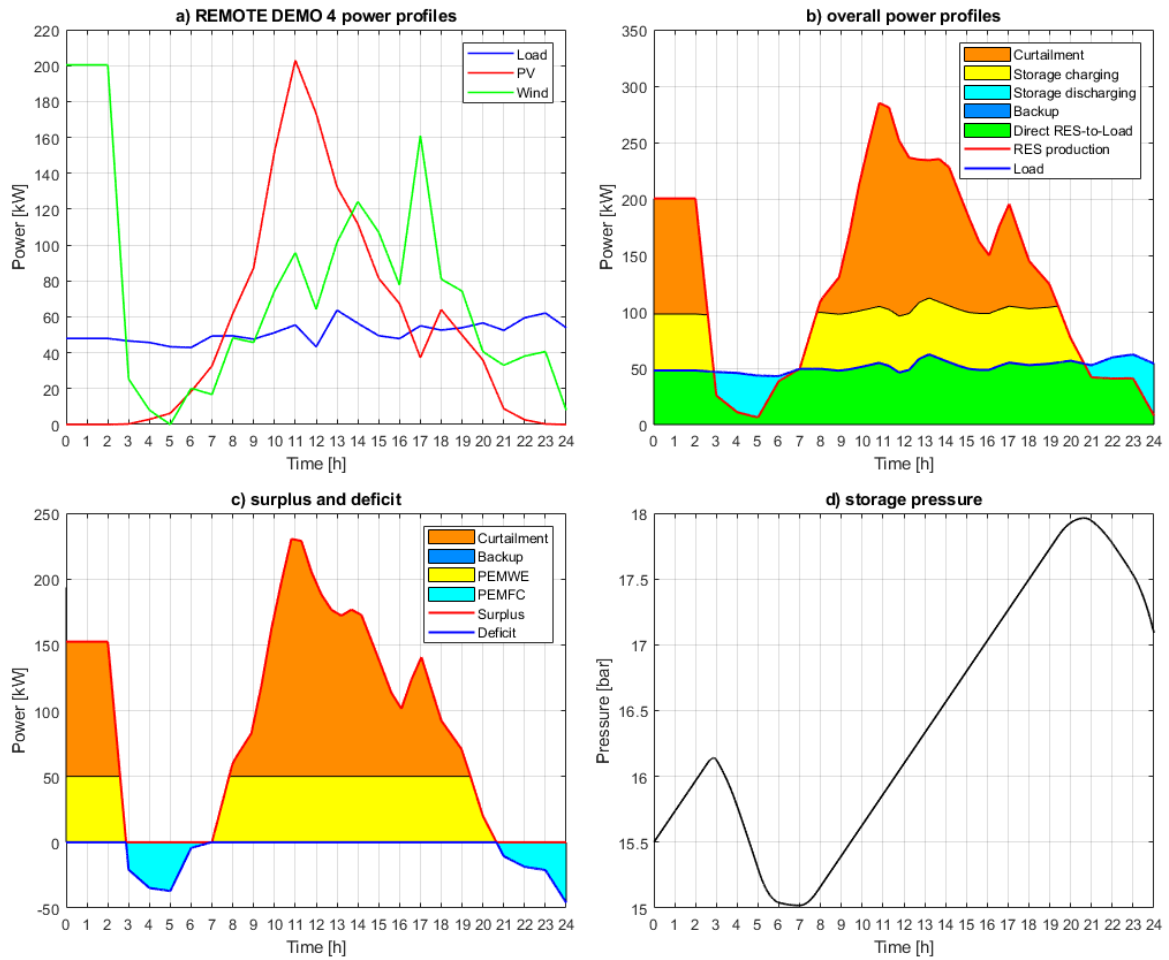


Figure 4.13 Simulation results on a working day in July: a) RES and load power profiles b) overall power profiles, c) surplus and deficit, d) storage pressure.

Table 4.15 KPI values on a working day in July

KPI	Description	Value
KPI 1	Load directly covered by RES	87%
KPI 2	Load covered by the fuel cell	13%
KPI 3	Load covered by the backup system	0%
KPI 4	RES directly sent to the load	34%
KPI 5	RES sent to the electrolyzer	25%
KPI 6	RES to curtailment	41%
KPI 7	Surplus RES to electrolyzer	38%
KPI 8	Surplus RES to curtailment	62%

4.1.14 Non-working day in July

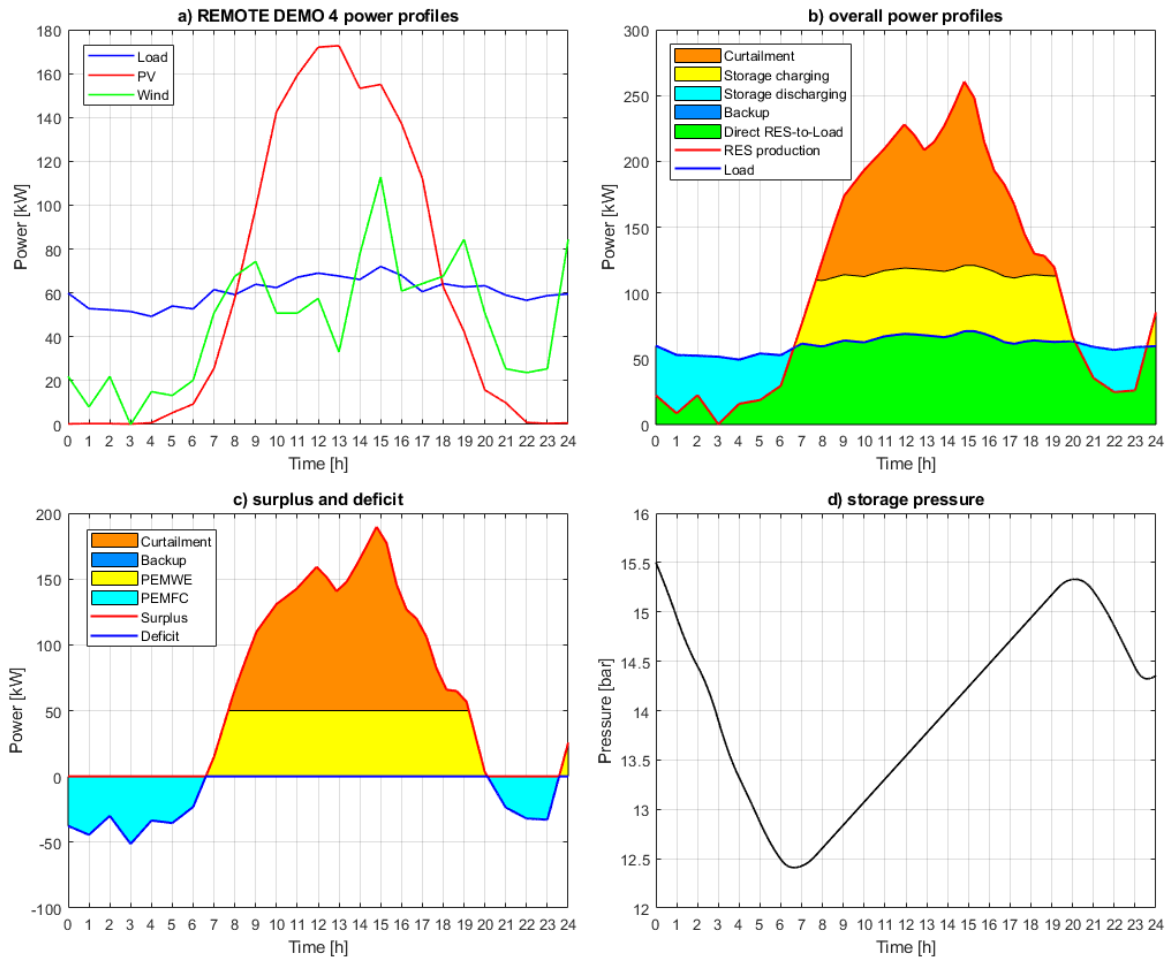


Figure 4.14 Simulation results on a non-working day in July: a) RES and load power profiles b) overall power profiles, c) surplus and deficit, d) storage pressure.

Table 4.16 KPI values on a non-working day in July

KPI	Description	Value
KPI 1	Load directly covered by RES	79%
KPI 2	Load covered by the fuel cell	21%
KPI 3	Load covered by the backup system	0%
KPI 4	RES directly sent to the load	43%
KPI 5	RES sent to the electrolyzer	24%
KPI 6	RES to curtailment	33%
KPI 7	Surplus RES to electrolyzer	42%
KPI 8	Surplus RES to curtailment	58%

4.1.15 Working day in August

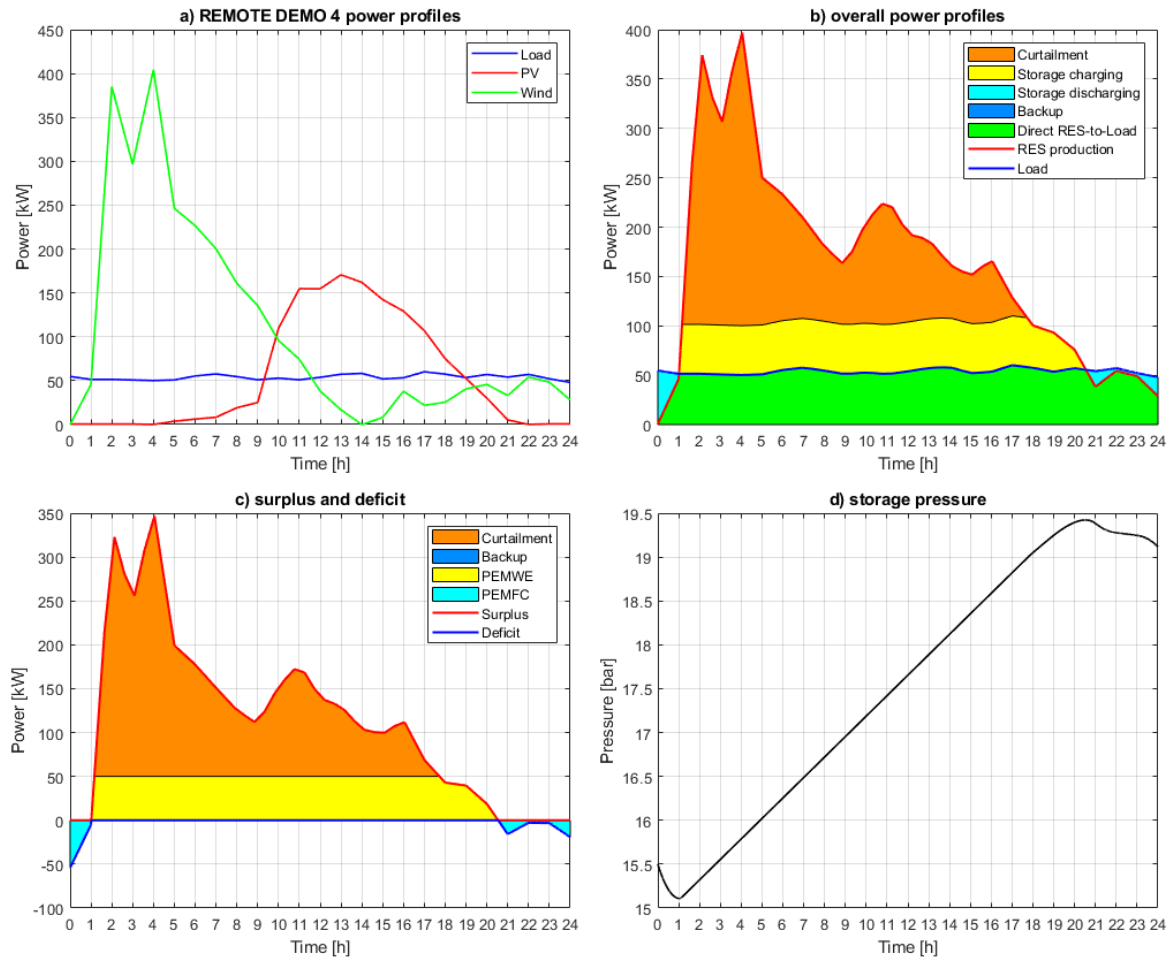


Figure 4.15 Simulation results on a working day in August: a) RES and load power profiles b) overall power profiles, c) surplus and deficit, d) storage pressure.

Table 4.17 KPI values on a working day in August

KPI	Description	Value
KPI 1	Load directly covered by RES	96%
KPI 2	Load covered by the fuel cell	4%
KPI 3	Load covered by the backup system	0%
KPI 4	RES directly sent to the load	31%
KPI 5	RES sent to the electrolyzer	23%
KPI 6	RES to curtailment	46%
KPI 7	Surplus RES to electrolyzer	33%
KPI 8	Surplus RES to curtailment	67%

4.1.16 Non-working day in August

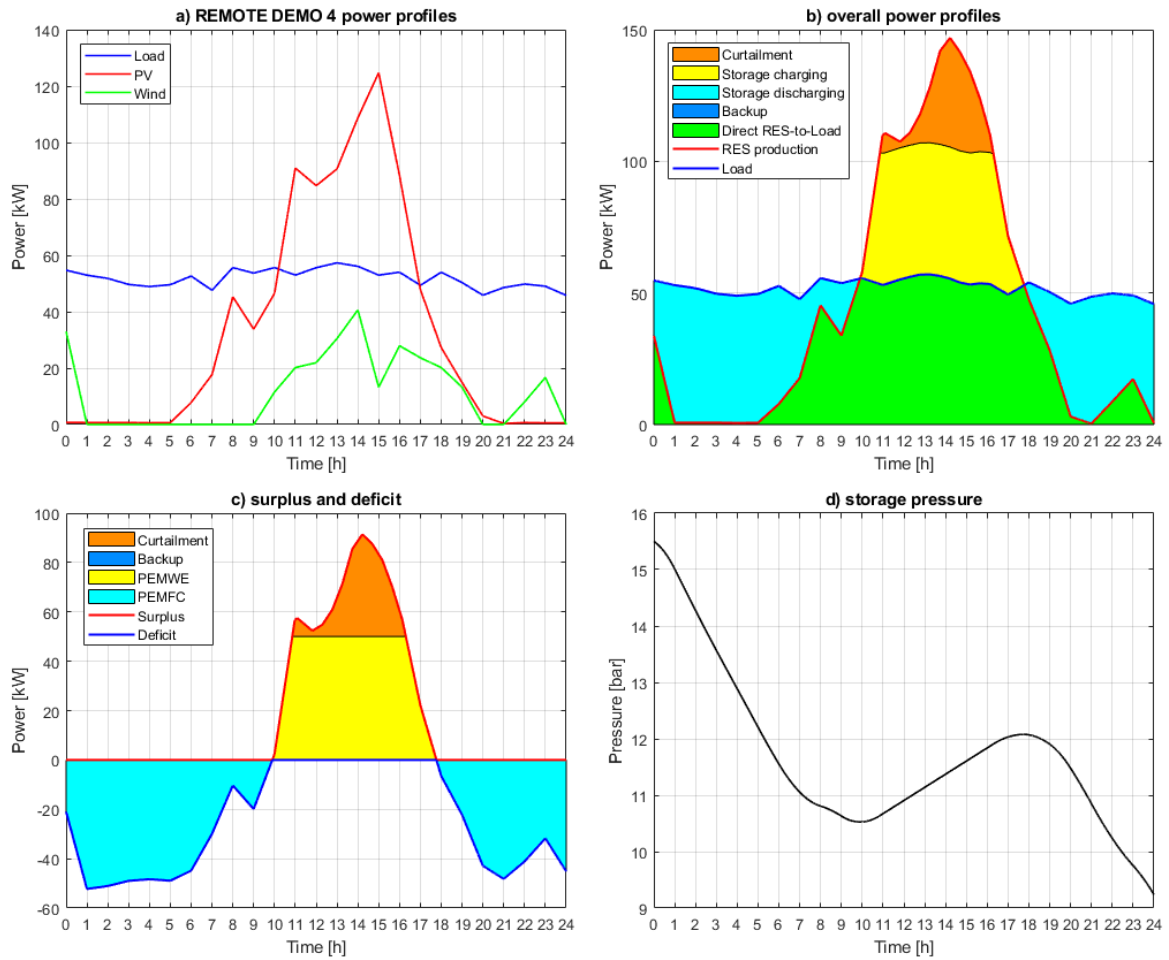


Figure 4.16 Simulation results on a non-working day in August: a) RES and load power profiles b) overall power profiles, c) surplus and deficit, d) storage pressure.

Table 4.18 KPI values on a non-working day in August

KPI	Description	Value
KPI 1	Load directly covered by RES	54%
KPI 2	Load covered by the fuel cell	46%
KPI 3	Load covered by the backup system	0%
KPI 4	RES directly sent to the load	61%
KPI 5	RES sent to the electrolyzer	30%
KPI 6	RES to curtailment	9%
KPI 7	Surplus RES to electrolyzer	76%
KPI 8	Surplus RES to curtailment	24%

4.1.17 Working day in September

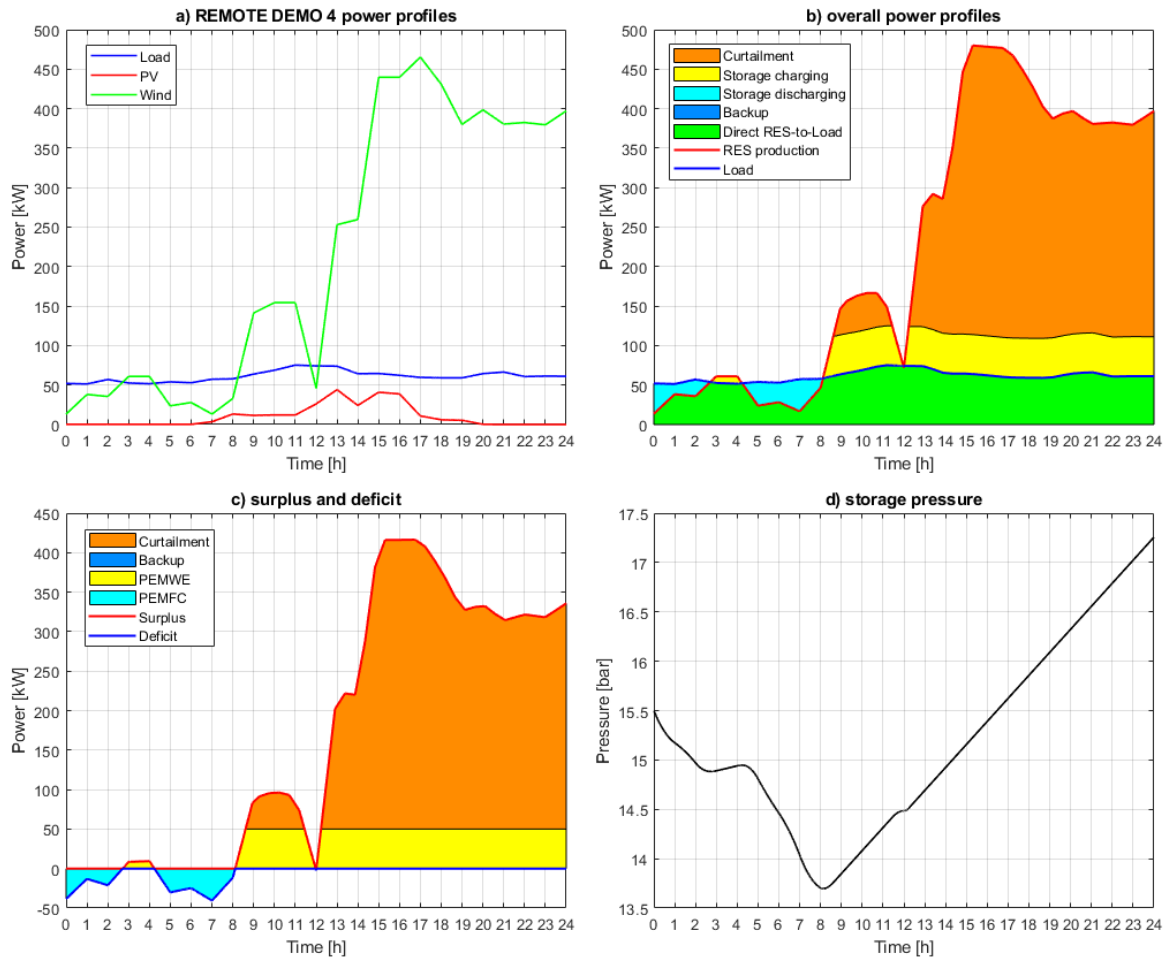


Figure 4.17 Simulation results on a working day in September: a) RES and load power profiles b) overall power profiles, c) surplus and deficit, d) storage pressure.

Table 4.19 KPI values on a working day in September

KPI	Description	Value
KPI 1	Load directly covered by RES	90%
KPI 2	Load covered by the fuel cell	10%
KPI 3	Load covered by the backup system	0%
KPI 4	RES directly sent to the load	24%
KPI 5	RES sent to the electrolyzer	14%
KPI 6	RES to curtailment	62%
KPI 7	Surplus RES to electrolyzer	19%
KPI 8	Surplus RES to curtailment	81%

4.1.18 Non-working day in September

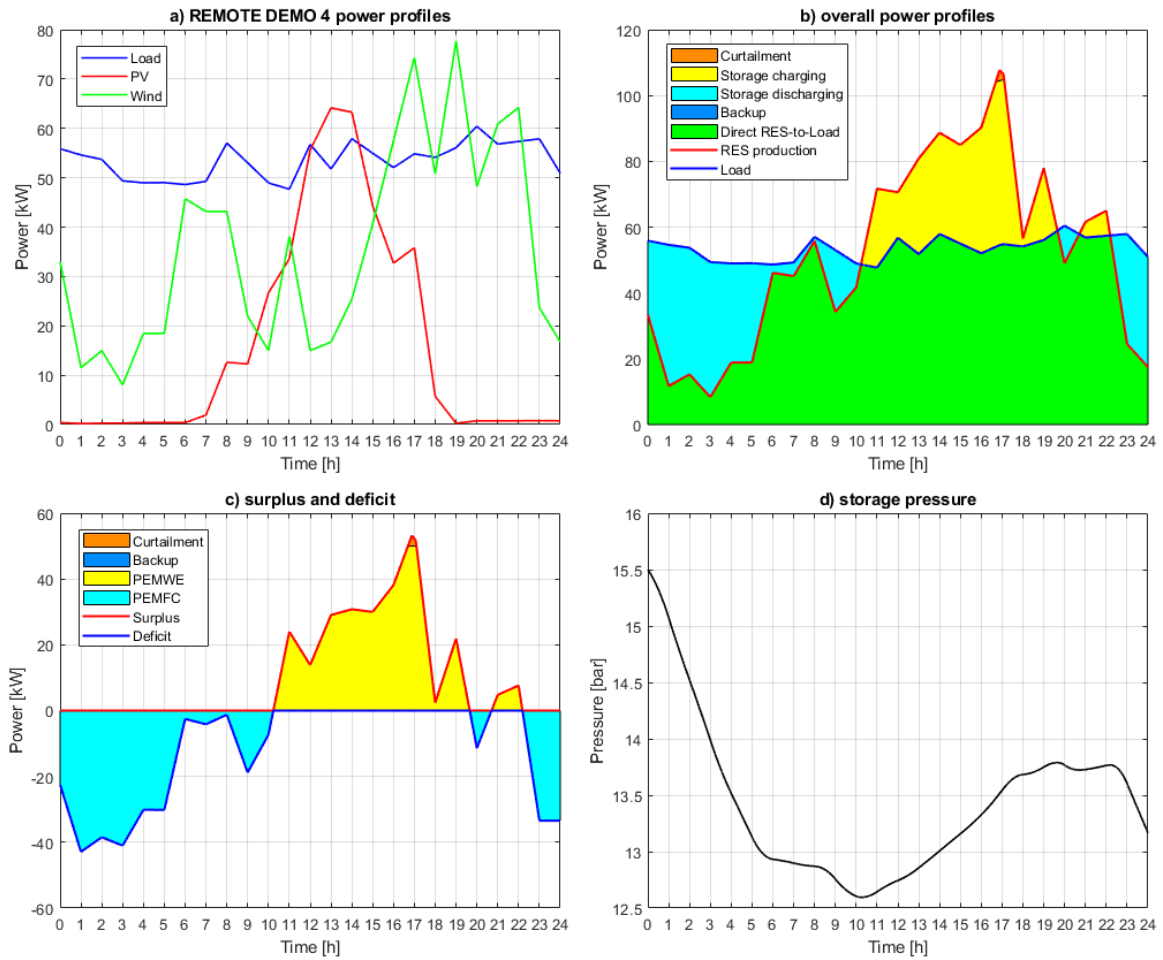


Figure 4.18 Simulation results on a non-working day in September: a) RES and load power profiles b) overall power profiles, c) surplus and deficit, d) storage pressure.

Table 4.20 KPI values on a non-working day in September

KPI	Description	Value
KPI 1	Load directly covered by RES	78%
KPI 2	Load covered by the fuel cell	22%
KPI 3	Load covered by the backup system	0%
KPI 4	RES directly sent to the load	80%
KPI 5	RES sent to the electrolyzer	20%
KPI 6	RES to curtailment	0%
KPI 7	Surplus RES to electrolyzer	100%
KPI 8	Surplus RES to curtailment	0%

4.1.19 Working day in October

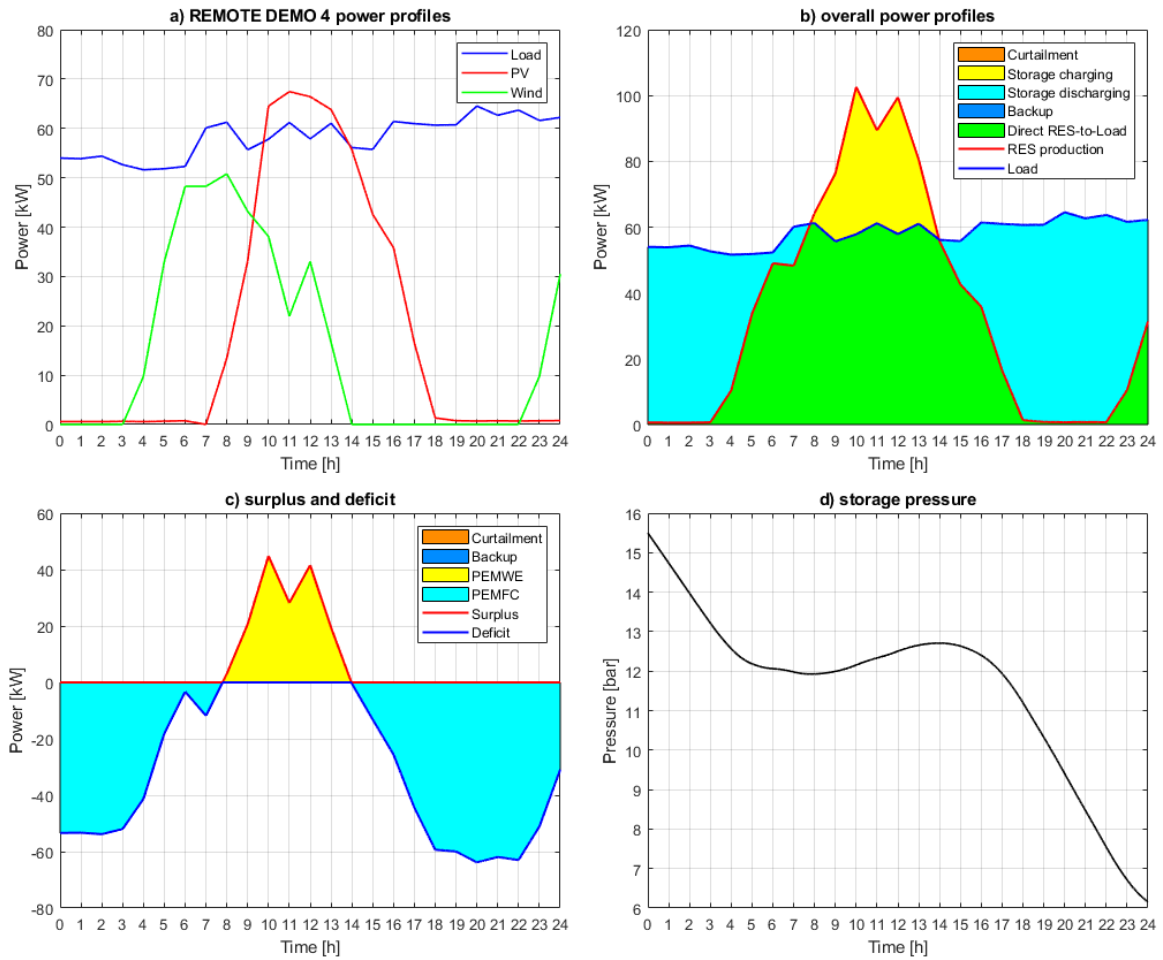


Figure 4.19 Simulation results on a working day in October: a) RES and load power profiles b) overall power profiles, c) surplus and deficit, d) storage pressure.

Table 4.21 KPI values on a working day in October

KPI	Description	Value
KPI 1	Load directly covered by RES	49%
KPI 2	Load covered by the fuel cell	51%
KPI 3	Load covered by the backup system	0%
KPI 4	RES directly sent to the load	81%
KPI 5	RES sent to the electrolyzer	19%
KPI 6	RES to curtailment	0%
KPI 7	Surplus RES to electrolyzer	100%
KPI 8	Surplus RES to curtailment	0%

4.1.20 Non-working day in October

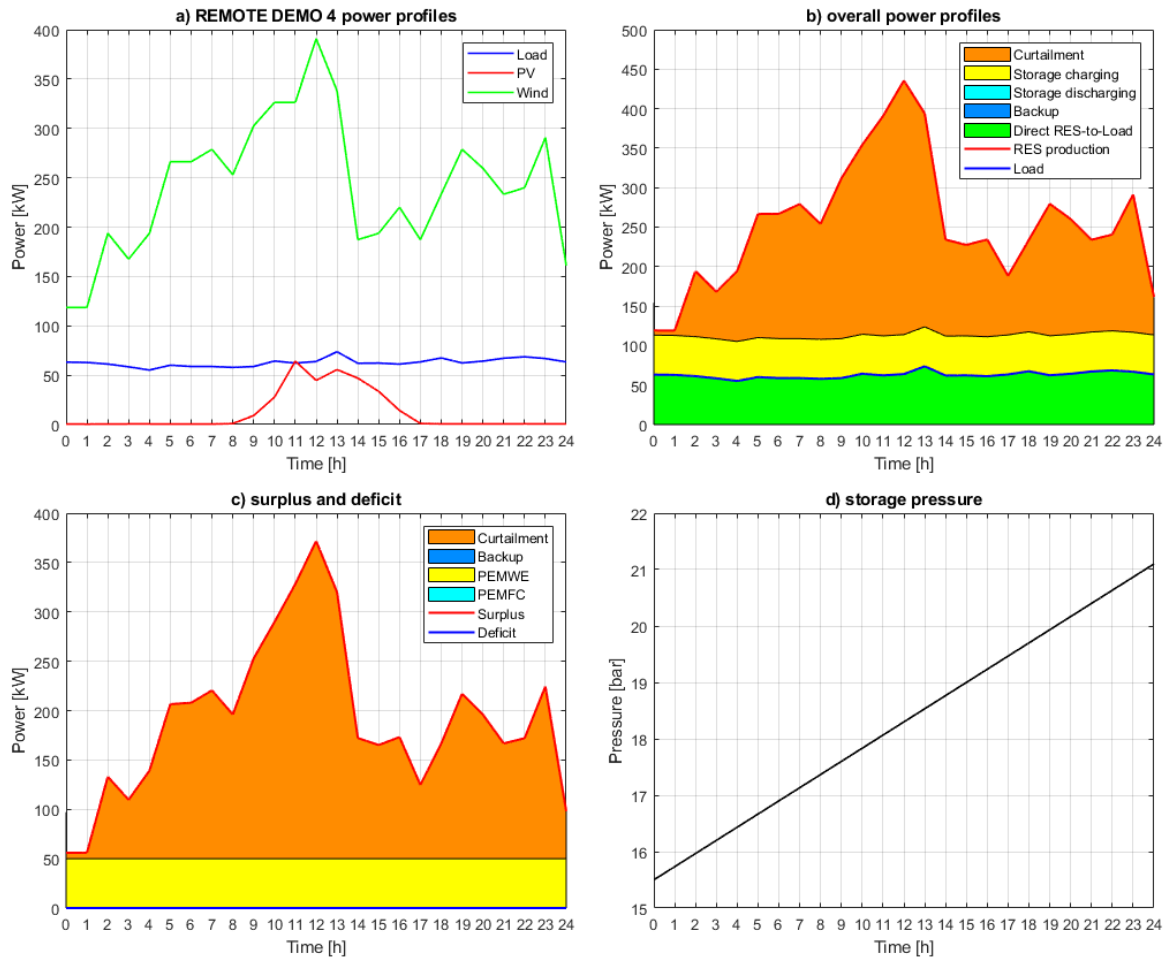


Figure 4.20 Simulation results on a non-working day in October: a) RES and load power profiles b) overall power profiles, c) surplus and deficit, d) storage pressure.

Table 4.22 KPI values on a non-working day in October

KPI	Description	Value
KPI 1	Load directly covered by RES	100%
KPI 2	Load covered by the fuel cell	0%
KPI 3	Load covered by the backup system	0%
KPI 4	RES directly sent to the load	24%
KPI 5	RES sent to the electrolyzer	20%
KPI 6	RES to curtailment	56%
KPI 7	Surplus RES to electrolyzer	26%
KPI 8	Surplus RES to curtailment	74%

4.1.21 Working day in November

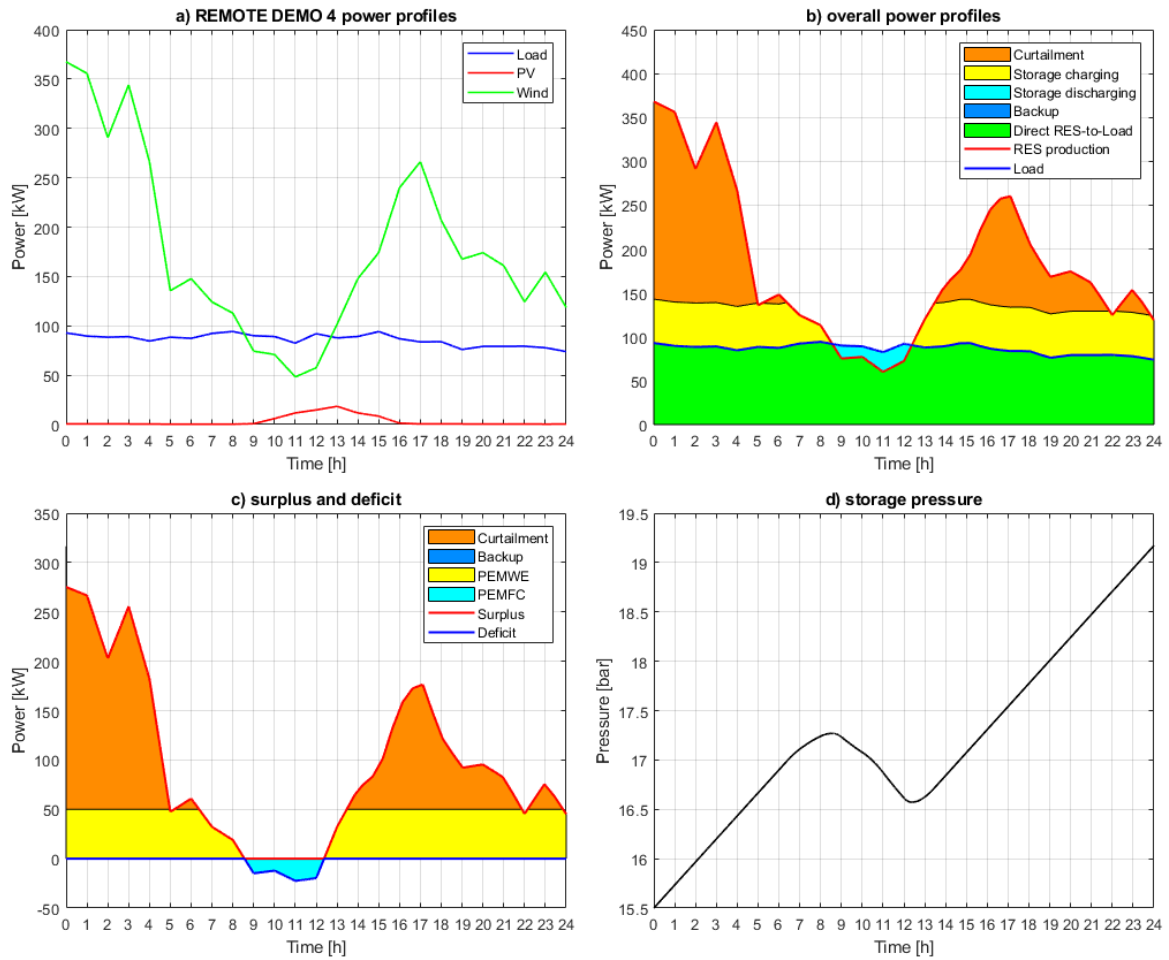


Figure 4.21 Simulation results on a working day in November: a) RES and load power profiles b) overall power profiles, c) surplus and deficit, d) storage pressure.

Table 4.23 KPI values on a working day in November

KPI	Description	Value
KPI 1	Load directly covered by RES	97%
KPI 2	Load covered by the fuel cell	3%
KPI 3	Load covered by the backup system	0%
KPI 4	RES directly sent to the load	47%
KPI 5	RES sent to the electrolyzer	22%
KPI 6	RES to curtailment	31%
KPI 7	Surplus RES to electrolyzer	41%
KPI 8	Surplus RES to curtailment	59%

4.1.22 Non-working day in November

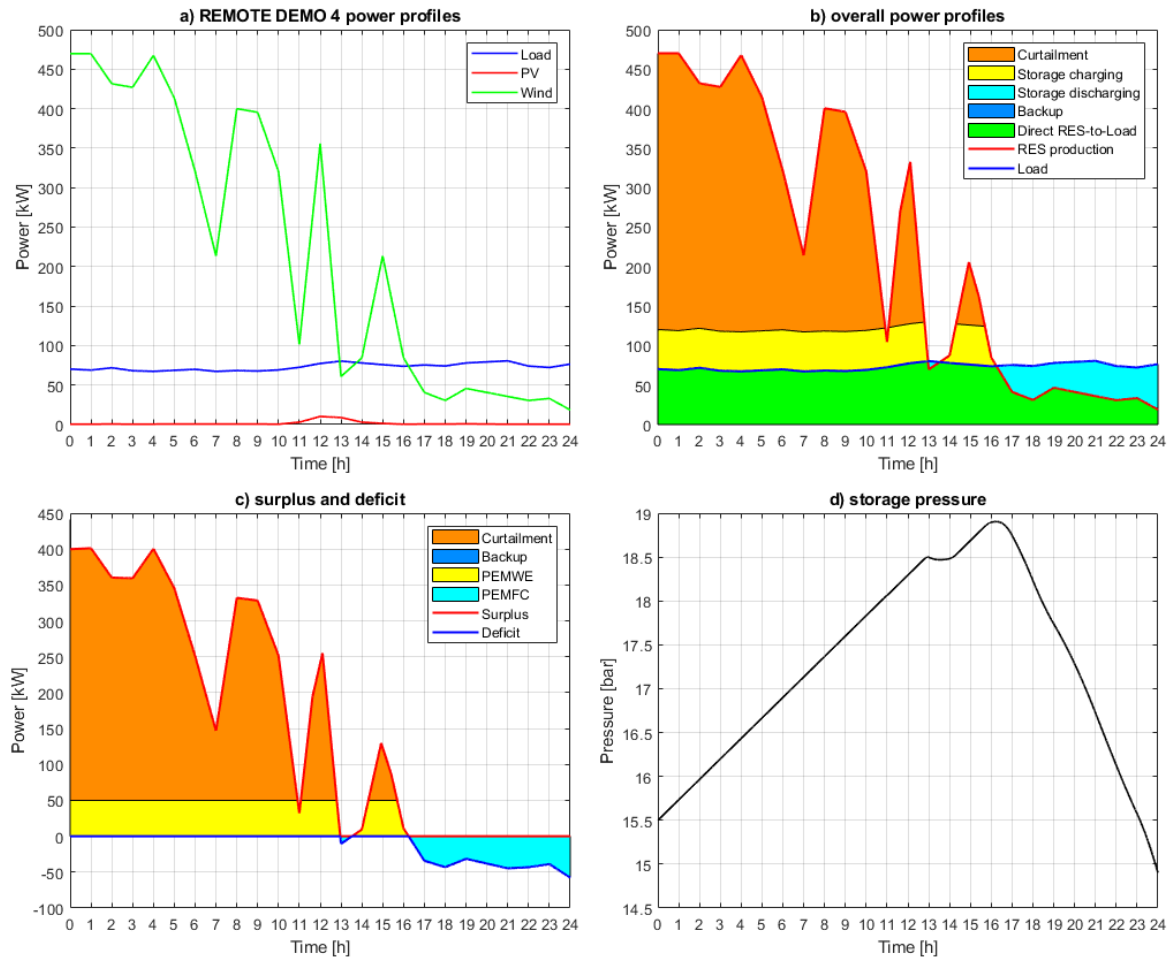


Figure 4.22 Simulation results on a non-working day in November: a) RES and load power profiles b) overall power profiles, c) surplus and deficit, d) storage pressure.

Table 4.24 KPI values on a non-working day in November

KPI	Description	Value
KPI 1	Load directly covered by RES	83%
KPI 2	Load covered by the fuel cell	17%
KPI 3	Load covered by the backup system	0%
KPI 4	RES directly sent to the load	27%
KPI 5	RES sent to the electrolyzer	14%
KPI 6	RES to curtailment	59%
KPI 7	Surplus RES to electrolyzer	19%
KPI 8	Surplus RES to curtailment	81%

4.1.23 Working day in December

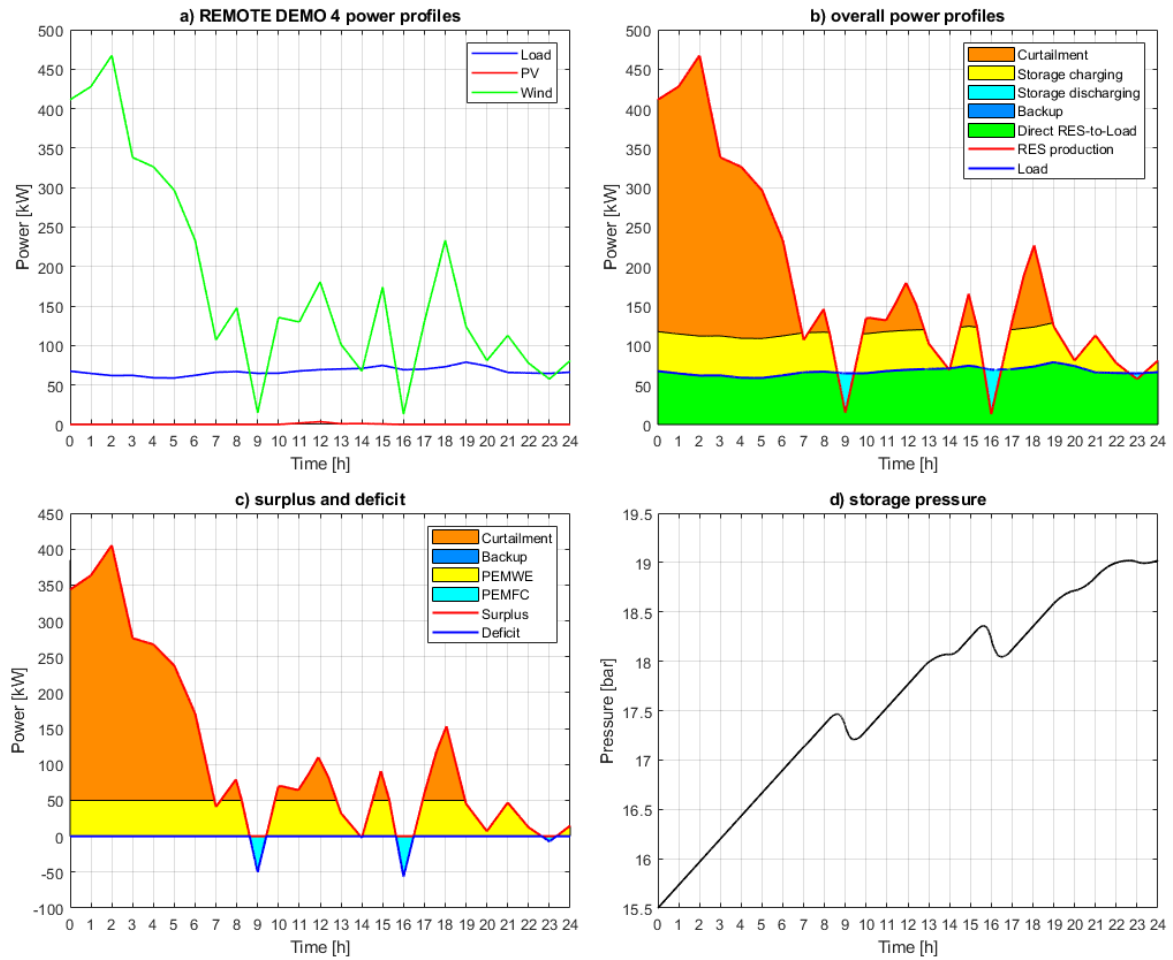


Figure 4.23 Simulation results on a working day in December: a) RES and load power profiles b) overall power profiles, c) surplus and deficit, d) storage pressure.

Table 4.25 KPI values on a working day in December

KPI	Description	Value
KPI 1	Load directly covered by RES	97%
KPI 2	Load covered by the fuel cell	3%
KPI 3	Load covered by the backup system	0%
KPI 4	RES directly sent to the load	37%
KPI 5	RES sent to the electrolyzer	21%
KPI 6	RES to curtailment	42%
KPI 7	Surplus RES to electrolyzer	33%
KPI 8	Surplus RES to curtailment	67%

4.1.24 Non-working day in December

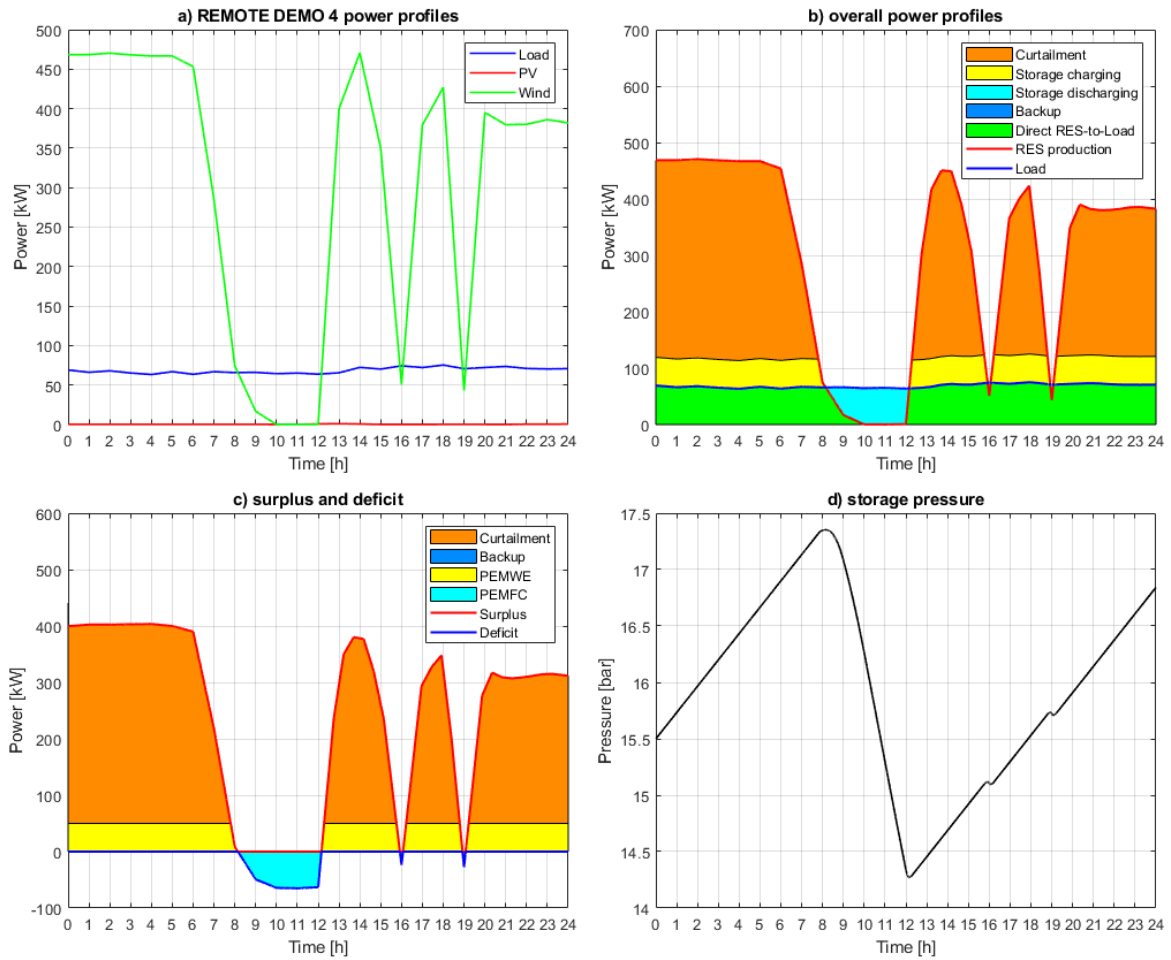


Figure 4.24 Simulation results on a non-working day in December: a) RES and load power profiles b) overall power profiles, c) surplus and deficit, d) storage pressure.

Table 4.26 KPI values on a non-working day in December

KPI	Description	Value
KPI 1	Load directly covered by RES	87%
KPI 2	Load covered by the fuel cell	13%
KPI 3	Load covered by the backup system	0%
KPI 4	RES directly sent to the load	20%
KPI 5	RES sent to the electrolyzer	13%
KPI 6	RES to curtailment	67%
KPI 7	Surplus RES to electrolyzer	17%
KPI 8	Surplus RES to curtailment	83%

4.2 Comments

As it can be seen in results in section 4.1, the P2P system allows to recover a not negligible amount of energy that would be otherwise curtailed. With a simulation time of one day and the assumption of an initial state of charge (SOC) equals to 50%, at which correspond a pressure in the tank of 15,5 bar, the P2P system does not need any contribution from the backup system, since the storage tank never reaches the minimum or maximum operating pressure. However, considering either different starting SOC or longer simulation times, the backup system is expected to give a contribution to the power profiles, even if it would be very small. Indeed, according to data from literature in previous work related to REMOTE [28], the site in DEMO 4 is characterized by a high RES exploitation, higher than 95% [2]. Furthermore, it is expected to have also larger amount of curtailed energy with longer simulation times, since in this site the production from RES is much larger than the demand in most periods of the year. Indeed, from results in section 4.1, the surplus of production from RES to curtailment is often higher than 50%, except for few days in which wind production is very low.

As told in the introduction, the DEMO 4 is characterized by RES production from wind and PV generators, which have different variability during the year. More in detail, power from PV generators is larger in summer and lower (or absent in some case) in winter, but daily power profiles of such source have about the same shape during the year. Instead, power produced by wind generators is more variable over the day according to availability or not of the wind source and, generally, it is higher during the winter season. These two different variabilities of these kind of sources can be observed looking at power profiles (i.e. RES production) in typical winter and summer days (e.g. December and June) in the main simulation results shown in section 4.1. For instance, during winter the shape of RES power profiles is much more variable due to wind, while in the summer it has a more regular shape, similar to the one of PV generators, except for particularly windy days.

In general, the load is mainly covered directly by RES production, while the contribution of the P2P (i.e. power from the PEMFC stack) is lower, but necessary to cover the demand as much as possible, even in case of low production from RES. Indeed, without the P2P system, there would be a much larger contribution of the backup system and therefore a larger consumption of fossil resources and consequently a larger amount of emissions.

Except for few cases in which power production from RES is very low, this power is mostly curtailed and directly used to cover the load, while the remaining part is sent to the P2P system (i.e. to the PEMWE stack) to charge the hydrogen storage tank. Thus, the P2P system allows a larger exploitation of power produced by RES that otherwise would be curtailed.

In conclusion, the P2P system allows to have larger exploitation of RES and to reduce GHG emissions.

Table 4.27 Average, minimum and maximum KPI values according to all simulations results

KPI	Description	average	min	max
KPI 1	Load directly covered by RES	79%	49%	100%
KPI 2	Load covered by the fuel cell	21%	0%	51%
KPI 3	Load covered by the backup system	0%	0%	0%
KPI 4	RES directly sent to the load	44%	20%	99%
KPI 5	RES sent to the electrolyzer	22%	1%	30%
KPI 6	RES to curtailment	34%	0%	67%
KPI 7	Surplus RES to electrolyzer	47%	16%	100%
KPI 8	Surplus RES to curtailment	53%	0%	83%

4.3 Further analyses

After having assessed the results of main simulations related to working and non-working days for each month of the year, other analyses have been carried out. First, an optimization of the sizes of RES generators has been performed in order to minimize the curtailment. After that, an alternative solution has been analysed considering the possibility to use the curtailed energy to produce additional hydrogen used for local mobility. Once the different relevant sizes of the RES systems associated with the different solutions have been defined, a comparison of the related costs have been carried out. Finally, a comparison between hydrogen and battery energy storage systems has been performed in terms of volumes, weights and costs.

4.3.1 Optimization of RES sizes

The optimization has been done reducing step-by-step the nominal size of RES systems to reduce the amount of curtailed energy and ensure the coverage of the load. Starting values of nominal power for wind and PV generators are respectively 675 kW (i.e. three wind turbines of 225 kW) and 250 kW [28], which are the sizes considered for the main simulations. The optimization has been done for the day which shows the lowest value of curtailed energy (i.e. the lowest KPI related to curtailment that is the KPI 8) to ensure the coverage of the load in the other days. Days in which the curtailed power is zero have not been considered in this first step of such analysis. Therefore, the day considered for this analysis has resulted to be the working day in March.

The optimization has been performed by iteration by assigning a reduced value for the rated power and calculating the resulting daily profile with the simplified assumption of a law of direct proportionality between rated power and actual power from daily profiles:

$$P_n^* : P^* = P_n : P \quad (4.2)$$

where, P is the power value at a specific time of the day and the superscript $*$ identifies the modified conditions. The result of such analysis has been shown in figure 4.25.

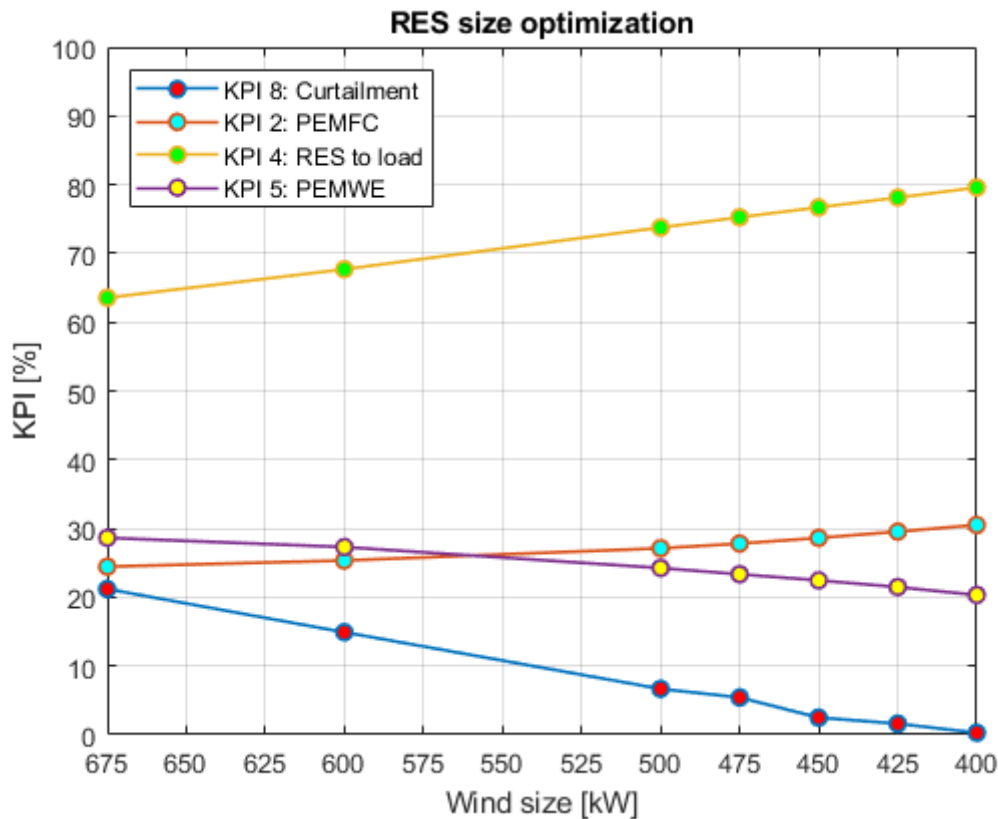


Figure 4.25 KPI values related to 250 kW PV system and different sizes of the wind system on the working day in March

The results show that is enough to keep the size of the PV plant (i.e. 250 kW) constant and reduce the size of wind generators to 400 kW to reach the aim of zero curtailment and ensure the coverage of the load on that day. It is noteworthy that the reduction of the curtailment leads to a higher contribution of the PEMFC stack to cover the load (i.e. KPI 2) and an increase of the power from RES directly sent to the load (i.e. KPI 4), against a reduction of the power from RES sent to the PEMWE stack (i.e. KPI 5).

However, in order to ensure the coverage of the load in all the simulated days, even the worst condition has been considered for this analysis. Such day is the working day in February that is characterized by the lowest value of power sent to the PEMWE (i.e. lowest KPI 5) and no curtailment. From the result shown in table 4.28, the size of 400 kW for the wind generators is too low to ensure the coverage of the load without the contribution of the backup system. Thus, the size of wind generators has to be increased to avoid the contribution of the backup generator even on working day in February. The size of the wind system which allows to both reduce the curtailment and ensure the coverage of the load in the worst scenario is 475 kW.

Table 4.28 Backup system contribution related to 250 kW PV system and different sizes of the wind system on the working day in February

Wind size kW	KPI 3 (Backup)
400	4%
425	3%
450	1%
475	0%

Another analysis has been carried out to evaluate the influence of the size of PV system. In such evaluation, the sizes of PV and wind generators have been chosen in order to ensure the coverage of the load even on the working day of February. In this case, reducing the size of the PV system and increasing the size of the wind system leads to a worse solution. Indeed, the higher is the size of the wind system, the higher would be the curtailment (see table 4.29).

Table 4.29 Curtailment related to different RES sizes on the working day in March

PV/Wind kW	KPI 8 (Curtailment)
250/475	5%
225/500	8%
200/525	11%

Therefore, the optimal sizes of RES systems which allow to both reduce the curtailment on the working day in March and ensure the coverage of the load in the worst scenario are 475 kW for the wind system and 250 kW for the PV system.

4.3.2 Curtailed power to hydrogen mobility

An alternative solution could consist of using the energy that would be curtailed to produce hydrogen for local mobility. In this way, there would be less waste of energy and the system would lead to more sustainable local mobility, reducing even further the GHG emissions. More in detail, the case study analysed concerns a route travelled by a ferry.

For each simulation, data related to the curtailed energy has been extracted and used to calculate the daily amount of hydrogen used for local mobility, calculated as:

$$m_{H_2} = \frac{E_{\text{Curtailed}}}{LHV_{H_2}} \quad (4.3)$$

where, LHV_{H_2} is the low heating value of the hydrogen, known to be equal to about 120 MJ/kg [4]. After that, the length of the daily route has been calculated starting from the consumption related to a given hydrogen powered ferry, whose data have been taken from literature [33]:

$$L = \frac{m_{H_2}}{c_s} \quad (4.4)$$

where, c_s is the specific consumption that has been set equal to 3,4 kg per nautical mile (i.e. about 1,84 kg/km), according to a study commissioned by the Fuel Cells and Hydrogen Joint Undertaking (FCH2 JU) [33].

Considering the Sistranda-Halten route [34] (i.e. a typical itinerary in this area of the Norway, also used for birdwatching), a distance travelled of about 120 km has been estimated for a round trip. Furthermore, one round trip per day has been assumed considering the type of activity, the hours of daylight in such area, possible stops along the route, the average speed of the ferry and so the travelling time, etc. Thus, the overall length of the daily route covered by the ferry has been considered equal to 120 km.

The result of such analysis is that the hydrogen produced with the curtailed power considering actual sizes of RES systems (i.e. 675 kW wind and 250 kW PV) is not enough to cover the demand associated to the hydrogen powered ferry for the daily local mobility (see figure 4.26). Indeed, the average length of the route covered by hydrogen produced from curtailed power is around 25 km (i.e. about 20% of the daily route).

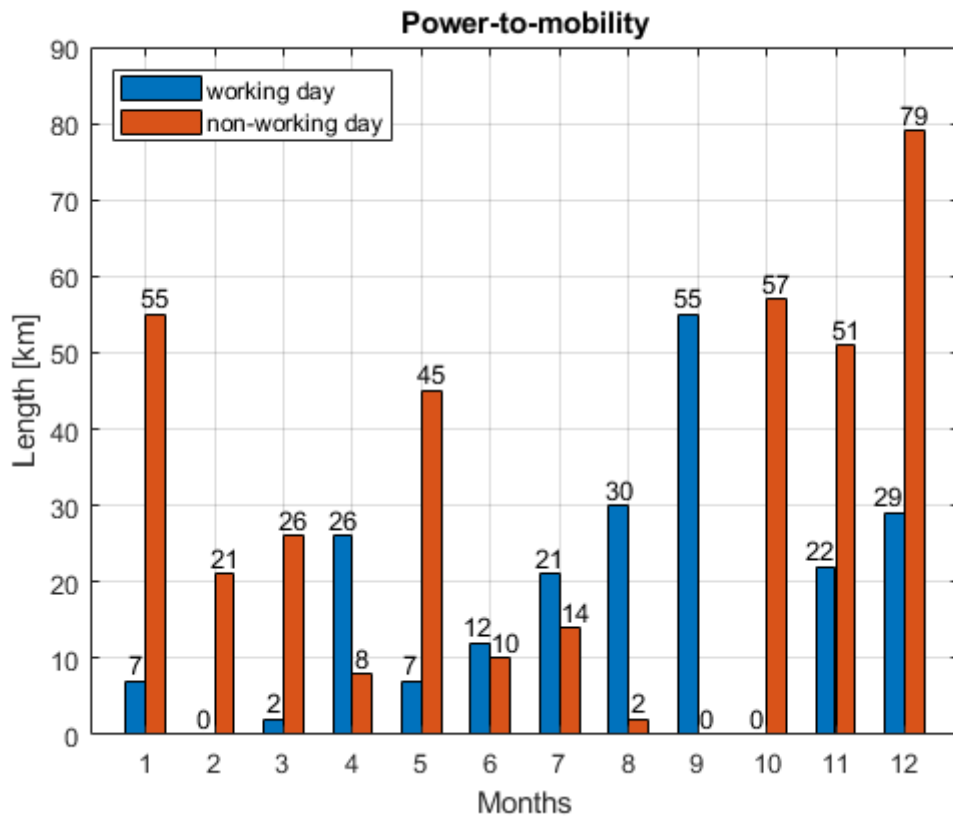


Figure 4.26 Daily length of the route covered by the system on all the simulated days

Since the amount of energy is not enough to sustain the demand for local mobility, the RES systems have been resized to cover both the electricity and mobility demands. Even in this case, it has been considered a day with no curtailment and characterized by the lowest value of power sent to the PEMWE stack (i.e. KPI 5). Thus, the working day in February has been chosen to ensure the coverage of global demand in all the other days.

The change in the size of the RES systems has been done by keeping the ratio between the rated powers of PV and wind generators as constant as possible (see table 4.30). The result is that the sizes of the RES systems need to be increased up to more than 10 times (i.e. about 11,8 times) compared to the starting values (i.e. 250/675 kW).

Table 4.30 Length of the daily route covered by the system according to different RES sizes on the working day in February

PV/Wind sizes	E_{Curtailed}	Covered length
kW	MWh	Km
250/675	0,000	0
400/1000	0,001	0
2000/5000	3,824	62
2750/7500	6,715	110
2950/8000	7,366	120

However, the amount of curtailed energy to ensure the ferry daily round trip is very high. Indeed, the KPI related to the amount of surplus energy that has to be curtailed would be equal to 86% (see table 4.31), which corresponds to the amount energy used to cover the daily round trip of the ferry.

Table 4.31 KPI related to the highest RES sizes on the working day in February

KPI	Description	Value
KPI 1	Load directly covered by RES	99%
KPI 2	Load covered by the fuel cell	1%
KPI 3	Load covered by the backup system	0%
KPI 4	RES directly sent to the load	16%
KPI 5	RES sent to the electrolyzer	12%
KPI 6	RES to curtailment	73%
KPI 7	Surplus RES to electrolyzer	14%
KPI 8	Surplus RES to curtailment	86%

4.3.3 Comparison between different RES sizes

In this section the comparison between the sizes of RES systems used for the main simulations in section 4.1 and the sizes evaluated in the further analyses in sections 4.3.1 and 4.3.2 has been performed. Overall power profiles related to the different sizes have been shown in figure 4.27.

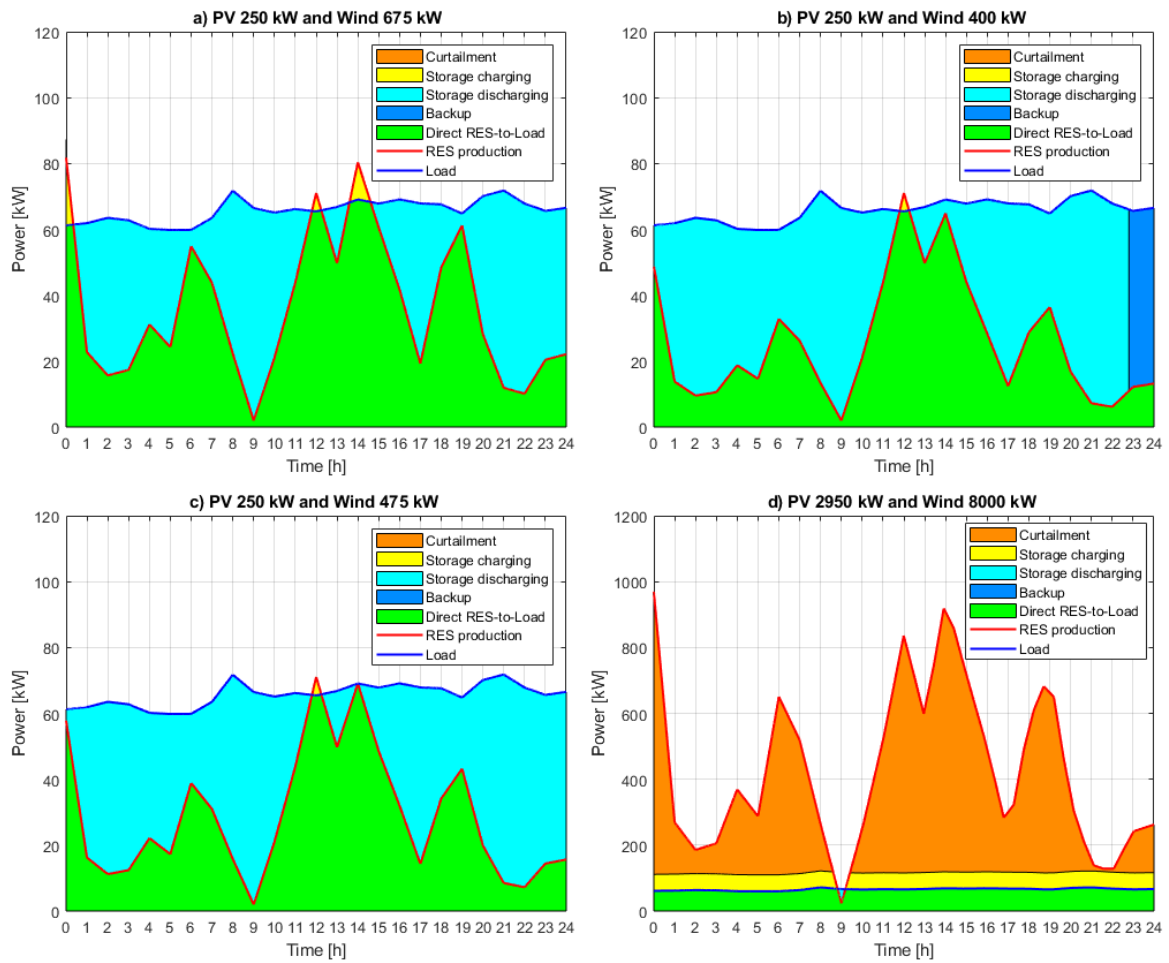


Figure 4.27 Overall power profiles on the working day in February for different PV/Wind sizes: a) 250/675 kW, b) 250/400 kW, c) 250/475 kW, d) 2950/8000 kW.

In order to make the comparative analysis more complete, a brief economic assessment has been carried out by using value of specific costs derived from literature [28], that have been defined in table 4.32.

Table 4.32 Specific costs for PV and wind plants [28]

Component	Investment	Replacement	O&M ^a
PV plant	1547 €/kW (ref. size 250 kW)	80 €/kW (10 y.)	24 €/kW
Wind plant	1175 €/kW (ref. size 675 kW)	-	3% inv.

^a Operational and maintenance cost per year.

Also, the correction related to the variation of the size of the different components compared to the reference size has been considered, according to literature [28]:

$$c = c_{\text{ref}} \cdot \frac{S_{\text{ref}}}{S} \cdot \left(\frac{S}{S_{\text{ref}}} \right)^n \quad (4.5)$$

where:

- c and c_{ref} are the specific costs respectively related to the actual and reference sizes;
- S and S_{ref} are the actual and reference sizes;
- n is the cost exponent which depends on the type of equipment. Considering the absence of further information, the exponent n has been assumed equal to 0,6 according to the six-tenths rule [35].

In order to compare the different sizes, a key factor has been evaluated. It is the net present cost (NPC), which has been calculated assuming different lifetimes of the plant. The NPC has been evaluated as follow [28]:

$$NPC = CAPEX + \sum_{i=1}^n \frac{OPEX_i + RC_i}{(1 + d)^i} \quad (4.6)$$

where:

- $CAPEX$ is the total investment at the beginning of the period (i.e. the first year);
- $OPEX_i$ is the total operational and maintenance cost (O&M) at the i -th year;
- RC_i is the total replacement cost at the i -th year;
- d is the real discount rate assumed equal to 4,9% [28].

In general, the higher is the lifetime the higher is the NPC, as shown in table 4.33. As expected, the highest NPC has been obtained in the last solution characterized by the highest values of the sizes of the RES systems to ensure the coverage of both the energy demand related to the load and the hydrogen demand related to the ferry. On the other hand, the lowest NPC is achieved in the second solution (i.e. 250/400 kW), according to the lowest sizes of the RES systems.

Table 4.33 NPC for different sizes and lifetimes

Lifetime	PV/Wind sizes			
	250/675 kW	250/400 kW	250/475 kW	2950/8000 kW
5 y.	1 214 309 €	1 000 560 €	1 063 506 €	5 349 032 €
10 y.	1 262 070 €	1 048 281 €	1 111 238 €	5 559 743 €
15 y.	1 290 765 €	1 076 937 €	1 139 904 €	5 686 628 €
20 y.	1 338 526 €	1 124 659 €	1 187 637 €	5 897 339 €
25 y.	1 367 222 €	1 153 315 €	1 216 303 €	6 024 223 €

The best solutions for the sizes of the RES systems could be either the second one (i.e. 250/400 kW) or the third one (i.e. 250/475 kW), depending on the priority given either to the NPC value or to the contribution of the backup generators respectively.

4.3.4 Comparison between hydrogen and battery energy storage systems

Another analysis has been carried out concerning the comparison of volumes, weights and costs related to hydrogen and battery energy storage systems. The comparative analysis has been performed considering the size of the battery system equals to the size of the hydrogen energy storage system (i.e. about 3,3 MWh [28]).

More in detail, the battery system considered for this study has been taken from datasheets available on the web [36]. The main data of the reference rack have been reported in table 4.34.

Table 4.34 Parameter of the reference battery rack [36]

Parameter	Value
Energy	110,9 kWh
Capacity	126 Ah
Nominal Voltage	881 V
Voltage Range	714 – 1 000 V
Width	520 mm
Height	2 200 mm
Depth	655 mm
Weight	912 kg

In order to reach the same size of the hydrogen energy storage system 30 racks have been considered for the battery system. Thus, the overall size of the battery system have been estimated assuming 30 racks in parallel configuration, placed in a typical container used for such purposes whose dimensions have been taken from the same datasheet of the battery rack [36] (see table 4.35). Considering a reference weight of 50 t associated to the 4,8 MWh reference battery system [36] and assuming that it consists of 43 battery racks of 110,9 kWh each, the actual total weight associated to the 3,3 MWh battery system has been calculated by introducing the following correction to the reference weight:

$$W = W_{\text{ref}} - W_{\text{rack}} \cdot (n_{\text{rack,ref}} - n_{\text{rack}}) \quad (4.7)$$

where:

- W_{ref} and W_{rack} are the weights of the reference battery system and the battery rack;
- $n_{\text{rack,ref}}$ and n_{rack} are the number of racks associated to the reference and the actual battery system.

Table 4.35 Estimated parameters, total volume and total weight of the battery system [36]

Parameter	Value
Energy	3,3 MWh
Capacity	3 780 Ah
Nominal Voltage	881 V
Voltage Range	714 – 1 000 V
Width	12,2 m
Height	2,9 m
Depth	2,5 m
Weight	38 t

Concerning volumes and weights of the hydrogen energy storage system (i.e. hydrogen storage tank and containers for PEMWE and PEMFC stacks), data from previous work [37] and available on the web [38, 39, 40] have been considered. The total volume of the containers for both PEMWE and PEMFC has been calculated by considering the dimensions of a 10 ft ISO container [38, 39] which have been reported in table 4.36. The type of container has been chosen according to the dimensions related to the PEMFC module and its subsystems (e.g. coolant and air subsystems) which have been taken from literature [40] and assuming similar dimensions also for the PEMWE. The total weight associated to both PEMWE and PEMFC systems (i.e. the containers including modules and subsystems) has been assumed equal to 2 t according to data available on the web [39, 40], while the weight of the hydrogen storage tank has been taken from previous work [37] (see table 4.37).

Table 4.36 Dimensions of a 10 ft ISO container [38, 39]

Parameter	Value
Length	3,048 m
Height	2,591 m
Width	2,438 m
Volume	19,254 m ³
Empty weight	1 450 kg

Table 4.37 Total volumes and total weights related to the hydrogen energy storage system [37, 38, 39, 40]

Parameter	PEMWE	PEMFC	H₂ storage
Volume	19,254 m ³	19,254 m ³	46,633 m ³
Weight	2 t	2 t	24 t

In table 4.38, a comparison of total volume and total weight of hydrogen and battery energy storage systems has been reported. Based on the assumptions and considerations set out in this section and on the choice of the type of containers, it has been resulted that the hydrogen energy storage system is lighter in terms of total weight, but in terms of total volume both energy storage systems are quite similar. Moreover, it is noteworthy the high contribution of the hydrogen storage tank to both total volume and total weight of the storage system (i.e. approximately 55% in terms of volume and 85% in terms of weight).

Table 4.38 Comparison of total volume and total weight related to hydrogen and battery energy storage system

Parameter	Hydrogen	Battery
Volume	85,1 m ³	88,5 m ³
Weight	28 t	38 t

Regarding the cost analysis, the values of the specific costs have been derived from previous work [28] as it has been done in section 4.3.3 and they have been defined in table 4.39. The value of the specific cost related to the PEMFC has been corrected as shown in equation (4.5). According to Marocco et al. [28], the cost exponent has been assumed equal to 0,7 for the PEMFC and the specific costs of the battery have been considered not dependent on the size.

Table 4.39 Specific costs for different components of the energy storage systems [28]

Component	Investment	Replacement	O&M
PEMFC	3947 €/kW (ref. size 10 kW)	46% inv. (5 y.)	3% inv.
PEMWE	4600 €/kW	35% inv. (5 y.)	3% inv.
H ₂ storage	470 €/kg	-	2% inv.
Li-ion	550 €/kWh	550 €/kWh (10 y.)	10 €/kWh

Considering the same assumptions that have been made in section 4.3.3 (e.g. real discount rate, lifetime, NPC, etc.), from the results shown in table 4.40 it is clear that the hydrogen based energy storage system is economically more advantageous than the battery energy storage system in each scenario considered for the different lifetimes of the plant.

Table 4.40 Comparison of NPC related to hydrogen and battery energy storage systems for different lifetimes

Lifetime	Hydrogen	Battery
5 y.	711 715 €	2 003 751 €
10 y.	936 376 €	3 891 263 €
15 y.	1 161 037 €	4 048 556 €
20 y.	1 385 697 €	5 936 068 €
25 y.	1 610 358 €	6 093 360 €

5 Conclusions

In this thesis, it has been studied the dynamic behaviour and performances of a P2P energy storage system by developing a lumped parameter dynamic model on Simulink® environment. The analysis has been carried out on different scenarios to evaluate the response of the modelled system to different power profiles. The results consist of daily power profiles and tables reporting KPI evaluated on a working day and a non-working day for each month of the year. In addition to the main results, further analyses have been performed concerning the optimal sizing of RES systems, the exploitation of curtailed energy to produce hydrogen for local mobility, the evaluation of the NPC related to different sizes of RES systems and the comparison between hydrogen and battery energy storage systems in terms of volumes, weights and costs.

The analysis of the main simulation results has shown that the P2P system allows to exploit larger amount of power from RES and to withstand the local demand without the contribution of the backup system, considering a starting SOC of 50% for the hydrogen storage tank and simulation time of one day. More in detail, the results show that power from RES is directly sent to the load whenever it is possible and, in case of surplus of production, it is mostly curtailed in most of the cases because it is much larger than the rated power of the PEMWE stack, while the remaining part is sent to charge the storage. In case of deficit of production from RES, the load is covered by the PEMFC without any contribution from the backup system. However, considering different assumptions for the simulations, such as initial conditions and simulation times, the results could change slightly.

As regards the further analyses carried out after the main simulations, the results have shown that the optimal sizes for RES systems could be either 250 kW for the PV plant and 475 kW for the wind plant by giving priority to the coverage of the load or 250 kW for the PV plant and 400 kW for the wind plant by giving priority to the NPC. The alternative solution of using hydrogen from curtailed energy for local mobility has resulted to be not convenient, since it would lead to an increase in the size of RES systems up to more than 10 times to both cover the energy demand and ensure local mobility. Regarding the comparison between hydrogen and battery energy storage systems and considering all the assumptions made in section 4.3.4, it has been resulted that both systems are quite similar in terms of volume, but the hydrogen system is lighter in terms of weight and economically more advantageous even considering different lifetimes of the plant.

The modelled system does not account for all auxiliaries, which can affect its dynamic response and performances. Further works could potentially be done in this direction, integrating auxiliary components and a battery system in the model, investigating their influence on system response and validating the dynamic model with experimental data from the real-scale installation, currently not available.

The model could be used, for instance, to investigate and predict the effect of different operating conditions on system performances and perform an optimization.

References

- [1] European Commission, “Climate strategies & targets,” [Online]. Available: https://ec.europa.eu/clima/policies/strategies/2030_en. [Accessed April 2020].
- [2] “REMOTE,” [Online]. Available: <https://www.remote-euproject.eu/>. [Accessed May 2020].
- [3] C. Bao, M. Ouyang and B. Yi, “Modeling and control of air stream and hydrogen flow with recirculation in a PEM fuel cell system—I. Control-oriented modeling,” *International journal of hydrogen energy*, vol. 31, no. 13, pp. 1879-1896, 2006.
- [4] M. Santarelli, *Notes from the course Polygeneration and Advanced Energy Systems*, Politecnico di Torino, 2019.
- [5] A. A.-M. D’Hérin Bytner, *Caratterizzazione sperimentale e modellazione dinamica di un elettrolizzatore alcalino per la produzione di idrogeno ed ossigeno*, tesi di laurea specialistica in Ingegneria Energetica e Nucleare, Politecnico di Torino, 2012.
- [6] A. Peticchia, *Thermodynamic and Degradation Models of a PEM Electrolyzer, Supported by EIS Analysis*, tesi di laurea specialistica in Ingegneria Energetica e Nucleare, Politecnico di Torino, 2016.
- [7] M. W. J. Chase, NIST-JANAF Thermochemical Tables, Fourth ed., Phys. Chem. Ref. Data, Monograph 9, 1998, pp. 1-1951.
- [8] F. Marangio, M. Santarelli and M. Cali, “Theoretical model and experimental analysis of a high pressure PEM water electrolyser for hydrogen production,” *International Journal of Hydrogen Energy*, vol. 34, no. 3, pp. 1143-1158, 2009.
- [9] A. Awasthi, K. Scott, S. Basu, “Dynamic modeling and simulation of a proton exchange membrane electrolyzer for hydrogen production,” *International Journal of Hydrogen Energy*, vol. 36, no. 22, pp. 14779-14786, November 2011.
- [10] R. García-Valverde, N. Espinosa and A. Urbina, “Simple PEM water electrolyser model and experimental validation,” *International Journal of Hydrogen Energy*, vol. v. 37, no. n. 2, pp. 1927-1938, January 2012.
- [11] M. Espinosa-López, C. Darras, P. Poggi, R. Glises, P. Baucour, A. Rakotondrainibe, S. Besse and P. Serre-Combe, “Modelling and experimental validation of a 46 kW PEM high pressure water electrolyzer,” *Renewable Energy*, vol. 119, pp. 160-173, April 2018.
- [12] L. Zhao, J. Brouwer and S. Samuelsen, “Dynamic analysis of a self-sustainable renewable hydrogen fueling station,” *ASME 2014 12th International Conference on Fuel Cell Science, Engineering and Technology collocated with the ASME 2014 8th International Conference on Energy Sustainability*, vol. 45882, p. V001T02A001, 2014.
- [13] H. Görgün, “Dynamic modelling of a proton exchange membrane (PEM) electrolyzer,” *International Journal of Hydrogen Energy*, vol. 31, no. 1, p. 29–38, 26 May 2006.

- [14] Y. Shan and S.-Y. Choe, "A high dynamic PEM fuel cell model with temperature effects," *Journal of power sources*, vol. 145, no. 1, pp. 30-39, 2005.
- [15] F. Musio, F. Tacchi, L. Omati, P. G. Stampino, G. Dotelli, S. Limonta, D. Brivio and P. Grassini, "PEMFC system simulation in MATLAB-Simulink® environment," *International Journal of Hydrogen Energy*, vol. 36, no. 13, pp. 8045-8052, 2011.
- [16] C. Wang, M. H. Nehrir and S. R. Shaw, "Dynamic models and model validation for PEM fuel cells using electrical circuits," *IEEE transactions on energy conversion*, vol. 20, no. 2, pp. 442-451, 2005.
- [17] L. Cantone, *Dynamic simulation and experimental analysis of integrated modules electrolyzer-fuel cell for aerospace applications*, degree thesis in Energetic and Nuclear engineering, Politecnico di Torino, 2014.
- [18] C. Tizzoni, *Analisi e simulazione dinamica di un sistema di propulsione basato su celle a combustibile PEM per utilizzo aeronautico*, tesi di laurea specialistica in Ingegneria Energetica e Nucleare, Politecnico di Torino, 2007.
- [19] D. Guilbert and G. Vitale, "Dynamic emulation of a pem electrolyzer by time constant based exponential model," *Energies*, vol. 12, no. 4, p. 750, 2019.
- [20] D. Guilbert, D. Sorbera and G. Vitale, "A stacked interleaved DC-DC buck converter for proton exchange membrane electrolyzer applications: Design and experimental validation," *International Journal of Hydrogen Energy*, vol. 45, no. 1, pp. 64-79, 2020.
- [21] S. C. McCutcheon, J. L. Martin, T. O. Barnwell and D. R. Maidment, *Handbook of hydrology*, New York: McGraw-Hill, 1993.
- [22] L. Valverde-Isorna, D. Ali, D. Hogg and M. Abdel-Wahab, "Modelling the performance of wind-hydrogen energy systems: Case study the Hydrogen Office in Scotland/UK," *Renewable and Sustainable Energy Reviews*, vol. 53, pp. 1313-1332, 2016.
- [23] S. Kang, L. Zhao and J. Brouwer, "Dynamic modeling and verification of a proton exchange membrane fuel cell-battery hybrid system to power servers in data centers," *Renewable Energy*, vol. 143, pp. 313-327, 2019.
- [24] P. Medina and M. Santarelli, "Analysis of water transport in a high pressure PEM electrolyzer," *International Journal of Hydrogen Energy*, vol. 35, no. 11, pp. 5173-5186, 2010.
- [25] P. T. Nguyen, T. Berning and N. Djilali, "Computational Model of a PEM Fuel Cell with Serpentine Gas Flow Channels," *Journal of Power Sources*, vol. 130, no. 1, pp. 149-157, 2004.
- [26] J. T. Pukrushpan, *Modeling and control of fuel cell systems and fuel processors*, PhD Thesis, University of Michigan, 2003.
- [27] A. J. Del Real, A. Arce and C. Bordons, "Development and experimental validation of a PEM fuel cell dynamic model," *Journal of power sources*, vol. 173, no. 1, pp. 310-324, 2007.

- [28] P. Marocco, D. Ferrero, M. Gandiglio, M. M. Ortiz, K. Sundseth, A. Lanzini and M. Santarelli, “A study of the techno-economic feasibility of H₂-based energy storage systems in remote areas,” *Energy Conversion and Management*, vol. 211, 2020.
- [29] T. E. Springer, T. A. Zawodzinski and S. Gottesfeld, “Polymer electrolyte fuel cell model,” *Journal of the electrochemical society*, vol. 138, no. 8, p. 2334, 1991.
- [30] B. Jiang, L. Wu, . L. Yu, X. Qiu and J. Xi, “A Comparative Study of Nafion Series Membranes for Vanadium Redox Flow Batteries,” *Journal of Membrane Science*, vol. 510, no. C, pp. 18-26, 2016.
- [31] S. H. Frensch, A. C. Olesen, S. S. Araya and S. K. Kær, “Model-supported characterization of a PEM water electrolysis cell for the effect of compression,” *Electrochimica Acta*, vol. 263, pp. 228-236, 2018.
- [32] Wikipedia, the free encyclopedia, “Residual sum of squares,” 2020. [Online]. Available: https://en.wikipedia.org/wiki/Residual_sum_of_squares. [Accessed July 2020].
- [33] FCH, Roland Berger, “FCH, Fuel Cells and Hydrogen Joint Undertaking,” 2017. [Online]. Available: <https://www.fch.europa.eu/>. [Accessed September 2020].
- [34] “VisitNorway, Birdwatching Froan (ferry landing Sistranda-Halten),” 2020. [Online]. Available: <https://www.visitnorway.it/>. [Accessed September 2020].
- [35] P. Leone, *Notes from the course Thermal Design and Optimization*, Politecnico di Torino, 2019.
- [36] LG Chem, “LG Chem,” 2018. [Online]. Available: <https://www.lgchem.com/>. [Accessed September 2020].
- [37] D. Bionaz, *Life cycle environmental analysis of a hydrogen-based P2P storage system for remote applications*, tesi di laurea magistrale in Ingegneria Energetica e Nucleare, Politecnico di Torino, 2019.
- [38] Wikipedia, the free encyclopedia, “Intermodal container,” 2020. [Online]. Available: https://en.wikipedia.org/wiki/Intermodal_container. [Accessed September 2020].
- [39] Containers Direct, “Shipping and Storage Container Dimension Charts,” 2020. [Online]. Available: <https://www.shippingcontainersuk.com/>. [Accessed September 2020].
- [40] Ballard Power, “Fuel Cell & Clean Energy Solutions,” 2020. [Online]. Available: <https://www.ballard.com/>. [Accessed September 2020].